



CASE FILE COPY  
FILE COPY  
NO. 4

# NATIONAL ADVISORY COMMITTEE FOR AERONAUTICS

TECHNICAL NOTE

No. 957

THE LIBRARY OF  
CONGRESS  
SERIAL RECORD  
DEC 21 1945  
Copy 2  
GOVT. SOURCE

THE STRENGTH OF SEMIELLIPTICAL CYLINDERS SUBJECTED TO  
COMBINED LOADINGS

By E. E. Sechler and J. L. Frederick  
California Institute of Technology

THIS DOCUMENT ON LOAN FROM THE FILES OF  
NATIONAL ADVISORY COMMITTEE FOR AERONAUTICS  
LANGLEY MEMORIAL AERONAUTICAL LABORATORY  
LANGLEY FIELD, HAMPTON, VIRGINIA

RETURN TO THE ABOVE ADDRESS  
IF REQUESTS FOR PUBLICATIONS SHOULD BE ADDRESSED  
AS FOLLOWS:

NATIONAL BUREAU OF STANDARDS  
ATTENTION: DOCUMENT SUPPLY CENTER  
WASHINGTON 25, D.C.



Washington  
February 1945

NATIONAL ADVISORY COMMITTEE FOR AERONAUTICS

TECHNICAL NOTE NO. 957

THE STRENGTH OF SEMIELLIPTICAL CYLINDERS SUBJECTED TO  
COMBINED LOADINGS

By E. E. Sechler and J. L. Frederick

SUMMARY

The present report covers tests made on elliptical cylinders with a center support which were subjected to various simple and combined loadings. The tests yielded a series of interaction curves for combined loadings on such cylinders which should be useful in wing nose section analysis.

INTRODUCTION

The primary object of this research project was the determination of design criteria for the nose sections of airplane wings. Since the nose portions of most wing sections can be approximated fairly closely by portions of ellipses, it was decided to use unstiffened elliptical cylinders for test specimens in this research. These cylinders were designed in such a way that the boundary restraints of the sheet simulated the boundary restraints present in the sheet covering of an actual wing nose section.

The physical parameters tested were:

1. The degree of ellipticity  $\epsilon$  - that is, the ratio of the semimajor to the semiminor axis of the ellipse
2. The length of the cylinder  $L$ , usually expressed as a suitable dimensionless parameter
3. The thickness of the sheet covering  $t$ , usually expressed as a suitable dimensionless parameter

The loading conditions to which the cylinders were subjected were as follows:

1. Pure torsion
2. Pure bending
3. Bending plus torsion
4. Bending plus vertical shear

In all cases, the bending moments and the shears were applied in the plane of the minor axis of the section.

This investigation, conducted in the Structures Laboratory of the Guggenheim Aeronautical Laboratory of the California Institute of Technology, was sponsored by and conducted with the financial assistance of the National Advisory Committee for Aeronautics.

#### SYMBOLS

- A area enclosed by cylindrical shell (Cylinder cross-sectional area), square inches
- $A_s$  cross-sectional area of sheet making up cylinder but neglecting cover plates, square inches
- a semimajor axis of elliptical part of specimen (Also used as radius of circular cylinders), inches
- b semiminor axis of elliptical part of specimen, inches
- E modulus of elasticity of material (Taken as  $10.3 \times 10^6$  psi throughout report)
- F shear load at buckling which, acting at lever arm  $l$ , causes bending moment  $m_b = Fl$ , pounds
- $I_c$  moment of inertia of cover plates about specimen neutral axis, inches<sup>4</sup>
- $I_s$  moment of inertia of sheet covering of specimens about specimen neutral axis, inches<sup>4</sup>

- $I_t = I_s + I_c$  total moment of inertia of specimen, inches<sup>4</sup>  
 $K$  a nondimensional bending stress defined as  $K = \frac{b\rho_0}{Et}$   
 $L$  length of cylindrical specimens between end supports, inches  
 $l$  lever arm for applied shear load, inches  
 $M$  bending moment carried by sheet only (excluding that carried by cover plates), inch-pounds  $\left(M = m \frac{I_s}{I_t}\right)$   
 $m$  bending moment applied to specimen, inch-pounds  
 $M_b$  bending moment carried by sheet only at buckling, inch pounds  $\left(M_b = m_b \frac{I_s}{I_t}\right)$   
 $m_b$  bending moment applied to specimen at buckling, inch-pounds  
 $M_t$  torsional moment carried by sheet only, inch-pounds (Assuming that the contribution of cover sheets is negligible,  $M_t = m_t$ .)  
 $m_t$  applied torsional moment, inch-pounds  
 $m_{tb}$  applied torsional moment at buckling, inch-pounds  
 $m_{tu}$  applied torsional moment at specimen failure, inch-pounds  
 $M_u$  bending moment carried by sheet only at failure, inch-pounds  $\left(M_u = m_u \frac{I_s}{I_t}\right)$   
 $m_u$  applied bending moment at specimen failure, inch-pounds  
 $t$  thickness of sheet covering, inches  
 $e$  degree of ellipticity of elliptical part of specimen - that is, ratio of semimajor to semiminor axis of ellipse ( $e = a/b$ )

$\rho_o$	maximum radius of curvature of elliptical part of specimen, inches
$\sigma_b$	maximum bending stress at buckling corresponding to $M_b$ , psi
$\sigma_b'$	maximum bending stress corresponding to moment supported by a cylindrical specimen immediately after buckling takes place, psi
$\sigma_{b_o}$	maximum bending stress at buckling due to pure bending -- that is, no other applied loads, psi
$\sigma_u$	maximum bending stress at failure of specimen, psi
$\sigma_{uts}$	ultimate tensile strength of material, psi
$\sigma_y$	yield stress of material (0.2-percent offset), psi
$\tau$	torsional shearing stress, psi
$\tau_b$	torsional shearing stress corresponding to $m_{t_b}$ , psi
$\tau_{b_o}$	torsional shearing stress corresponding to $m_{t_b}$ for pure torsion, psi
$\tau_{sb}$	direct average shearing stress at buckling corresponding to $F$ , psi
$\tau_u$	torsional shearing stress corresponding to $m_{t_u}$ , psi
$\tau_{u_o}$	torsional shearing stress corresponding to $m_{t_u}$ for case of pure torsion, psi

## EXPERIMENTAL TECHNIQUE

### Material and Material Tests

Since it is a very commonly used aircraft structural material, 24S-T aluminum alloy was chosen for the purposes of the experimental investigation. This material was obtained in nominal sheet thicknesses ranging from 0.010 to 0.040 inch. Despite the relatively large deviations from the nominal dimensions of the sheet supplied during the course of the research program, the individual sheets themselves were reasonably uniform.

Random samples were selected from the various shipments of material in an effort to obtain representative properties of the actual material used in the construction of the test specimens. The testing of these samples was limited to that of tension only\* since the most important property desired was that of the modulus of elasticity  $E$ , which was assumed to be the same in tension and compression.

These material tests were conducted in a standard Riehle testing machine having a maximum rated capacity of 3000 pounds. Strain measurements were made by means of Huggenberger type extensometers having a magnification of approximately 300 times. Typical tensile stress-strain curves are presented in figure 1 and a complete summary of test results is given in table I, from which figure 2 has been plotted. The scatter of experimental points in figure 2 may be attributed to variations in the material itself and to the limitations imposed upon the attainable accuracy by the experimental procedure used.

Inspection of figure 2 indicates that the modulus of elasticity  $E$  is substantially independent of the direction of loading relative to the sheet grain, and has an average value of  $10.3 \times 10^6$  psi. The ultimate tensile stress  $\sigma_{uts}$  is slightly less across the grain than with the grain; while the difference in the defined yield stress ( $\sigma_y \sim 0.2$  percent offset in the initial gage length) is more marked. The average values and variations of tensile properties with grain direction are in agreement with previously published results. (See references 1 and 2.) While of general interest, these variations are of secondary importance to the basic research project, since buckling of the test cylinders occurs at stresses considerably below the defined yield point.

#### Test Specimens

The specimens consisted of two semielliptical (or semi-circular) segments of sheet supported and clamped at the ends of the minor axis of the ellipse, thus simulating two wing nose sections mounted to a common spar and tested as a unit. (See fig. 3a.) It was at first thought possible to use a Wagner spar as a means of providing the required beam

---

\*Approximate compression properties may be obtained if desired by use of table I-1 of reference 1.

support and to subtract the effect of this spar in order to determine the net-load-carrying properties of the curved sheet alone. After several tests had been completed under different loading conditions, it was decided that the presence of a spar having relatively large bending and shear rigidities made it very difficult to obtain accurate and reliable results of the net strength of the sheet covering.

It was therefore decided to replace the Wagner type spar by the system of vertical spacer blocks illustrated in figure 3b. The spacer blocks were joined by a series of loose links in such a manner that relative motion in all directions was possible. This completely eliminated the difficulty of shear rigidities and reduced the problem of the bending rigidity to a minimum. In order to prevent buckling of the sheet covering between spacer blocks, cover plates were placed above and below the junctions of the two semielliptical sections of sheet. The thickness of these cover plates was so chosen that they would have a slightly higher buckling load than that of the curved sheets. It can be readily seen that this means of support would contribute only negligibly to the shear and torsional strength of the specimen, and would carry a definite, calculable amount of bending moment.

At the ends of the specimen were 1-inch-thick steel plates having the cross section of the desired ellipticity, with the addition of a 2-inch rectangular center section to which was attached the above-mentioned support and cover plate system. These end plates served a twofold purpose: namely,

1. They held the ends of the sheet covering to the correct contour.
2. They provided a convenient means of attaching the specimen to the testing machines.

With regard to the first item, the sheet was firmly held to the end plates by 1/4-inch bolts which screwed into tapped holes, spaced 1 inch apart around the circumference of the specimen. For specimens where the failing stresses were quite high, steel bands having the shape of the end plates were placed between the bolt heads and the sheet to distribute the clamping loads of the bolts and to prevent interbolt buckling. A photograph of the assembled specimens is shown in figure 3c.

In the actual assembly of the specimens, considerable care was taken to avoid soft spots or wrinkles in the sheet covering and to insure that each specimen was as accurately formed as possible. There were several unavoidable instances when compliance with the above conditions was not obtained and, therefore, the validity and the consistency of the results of such tests were critically considered and the test results discarded when that was deemed advisable.

All the specimens tested had a depth (equal to twice the length of the semiminor axis) of approximately 6 inches, the degree of ellipticity being obtained by variations in the length of the semimajor axis. The ellipticities were 1.0, 2.0, and 3.0; while the length of the specimens ranged from 1.0 inch to 34.0 inches. These variations, in conjunction with the three nominal sheet thicknesses tested, 0.010, 0.016, and 0.020 inch, reduced the program to a systematic investigation of the effect of the geometry of the test specimens on the load-carrying abilities of the specimens.

#### Test Apparatus and Testing Procedure

Because of the various loading conditions decided upon for investigation, it was necessary to use several different testing machines during the course of the experimental program. Each of these machines will be discussed separately in conjunction with the description of the loading conditions for which they were used.

The greater part of the pure torsion test program was conducted on a standard Olsen torsion-testing machine (see fig. 4) having a maximum rated capacity of 50,000 inch-pounds. As shown in this figure, a detachable loading jig consisting of a length of H-beam and a section of steel shafting was used to transmit the torsional moment from the jaws of the testing machine to the end plates of the test specimen. During the majority of these tests, angular deflection measurements were taken over a portion of the length of the specimen, and were used to obtain a check of the buckling load determined from visual observations, since the point of buckling was marked by a change in the slope of the load-deflection curve.

The remainder of the pure torsion, all the pure bending, and all the bending-plus-torsion tests were carried out in the bending-torsion machine shown in figure 5. In the cases of the pure torsion and bending-plus-torsion tests made in

this machine, angular deflection measurements were taken as before. In conjunction with the pure bending and bending-plus-torsion tests, extensometer readings were taken on both the tension and compression sides of each test specimen in order to obtain the stress distribution in the specimen, both before and after buckling of the sheet covering had taken place.

The requirements of testing with a wide range of ratios of bending moments to vertical shear forces in the bending-plus-shear tests necessitated a special testing machine. This machine is shown in figure 6 and the working parts consist of a fixed face plate, shown to the right in this figure, and a movable face plate, to which is attached the head of the loading arm. The specimen to be tested was placed between and bolted to this pair of face plates. In order to eliminate any tare loads from acting on the specimen during the testing operation, the loading arm and the movable face plate unit were counterweighted through a knife-edge lever system, which was so designed as to be independent of the amount of deflection of the loading arm. Thus, the loading arm was made floating with respect to the specimen. Portions of this counterweight system may be seen in the figure. The variation of the bending-to-shear ratio was accomplished merely by shifting the point of load application along the length of the central loading arm. During the bending-plus-vertical shear tests, extensometers were again mounted to the specimens in order to obtain an experimental value of the stresses in the specimen.

Sheet thicknesses were measured on a thickness gage reading to  $\pm 0.0002$  inch. These measurements were made at several points on the individual sheets used in each specimen, and since the variations were small for any one sheet, the average sheet thickness was recorded for the purpose of subsequent calculations. In some of the earlier tests, the sheet thickness that was used was the nominal thickness and, while this can have no marked effect on the validity of the results presented, it can be noticed in the tabular data and therefore has been mentioned.

#### EXPERIMENTAL RESULTS

In all discussions which follow, the cylinders referred to as semielliptical or semicircular were those having a fixed support, such as is shown in figure 3, at the ends of

the minor axis. Cylinders referred to as circular or elliptical are sheet structures with no support other than that applied at the ends of the specimen.

### Pure Torsion of Semicircular Cylinders

Since the problem of the strength of circular cylinders under pure torsion has been extensively covered both theoretically and experimentally (see references 3 and 4), it was decided to test first the semicircular and semielliptical cylinder in pure torsion. As in the case of the circular cylinders, the buckling load of the semicircular cylinders was very close to the ultimate load of the specimen. This is shown in table II, where it can be seen that the value of the torsional moment causing failure  $m_{tu}$  is seldom more than a few percent higher than the torsional moment causing buckling  $m_{tb}$ .

In order to express the torsional loads in terms of shearing stress, use has been made of the usual equation of torsional shearing stress in a thin-walled cylinder: namely,

$$\tau = \frac{m_t}{2At} \quad (1)$$

This equation is valid up to the point of buckling and, after buckling, gives a fictitious average shearing stress which, at failure, is analogous to the modulus of rupture in beams. Using equation (1), values for  $\tau_b$  and  $\tau_u$  have been calculated and are shown in table II.

In reference 3, Donnell derives a theoretical expression for the ultimate strength of short and moderately long cylinders of radius "a" and fixed ends subjected to a pure torsional moment. This equation is

$$\frac{\tau_u L^2}{Et^2} = 5.06 + \sqrt{9.42 + 1.88 \left( \frac{L}{2ta} \right)^{1.5}} \quad (2)$$

A plot of this curve is shown as the short dashed line in figure 7.

A curve faired through the experimental points for circular cylinders (360° of unsupported skin) is also shown in

In order to express the torsional loads in terms of shearing stress, use has been made of the usual equation of torsional shearing stress in a thin-walled cylinder: namely,

figure 7 as the long dashed curve, indicating that the experimental values are somewhat less than those predicted theoretically.

Using the same parameters for the semicircular cylinders ( $180^\circ$  of unsupported skin) the data from table II have been plotted in figure 7. A study of this figure brings out the following points:

1. For the longer specimens ( $L^2/2ta \doteq 10,000$ ) the ultimate strength of the semicircular cylinders is approximately twice that of the circular cylinders.
2. For the shorter cylinders ( $L^2/2ta \doteq 10$ ) the semicircular cylinders have an ultimate strength which is only about 10 percent greater than that of the circular cylinders.
3. That equation (2) could be used for designing semicircular cylinders and would be conservative for all specimens in which  $L^2/2ta$  was greater than 300 and would not become excessively nonconservative down to a value of  $L^2/2ta = 100$ . A little later a more exact empirical equation will be given for the case of the semicircular cylinders.

The large increase in the ultimate strength of the longer semicircular cylinders over that of the circular cylinders is explainable by a consideration of the buckle pattern of the two types of specimen. For moderately long specimens, the number of circumferential buckles is small (of the order of 2 in  $360^\circ$ ); hence the added restraint due to support at  $0^\circ$  and  $180^\circ$  is quite effective in delaying the buckling. However, as the length decreases, the number of waves increases, so that the presence of the added restraint begins to lose its effectiveness. For the lower limit of the experimental data under discussion, the number of circumferential buckles was of the order of 16 so that any restraint would have an effect on only a small percentage of the area going into the wave state. It is therefore probable that for very short specimens, the experimental curves for the circular and semicircular cylinders would join since the effect of the restraint would become negligible.

#### Pure Torsion of Semielliptical Cylinders

Considering now the semielliptical cylinders, it is immediately obvious that conditions are quite different from

what they are in the semicircular cylinders. The radius of curvature on the circumference of a semielliptical specimen varies between a maximum value at the ends of the minor axis to a minimum value at the ends of the major axis, the magnitude of these limits depending on the ellipticity and the depth of the cross section. Thus, it may be expected that the specimen would first buckle in the regions of maximum radius of curvature, and, under further increase in load, these buckles would extend diagonally towards the nose. At the same time, as each section of the circumference reached its critical load, depending on the local radius of curvature, new shear buckles would appear and propagate slowly. Owing to the fact that the minimum radius of curvature is located at the nose of the specimen, this nose portion would resist buckling in such a manner as to act as a stiffener. Consequently, a diagonal tension field would be formed in the remaining portions of the specimen. Under further increase of the applied load, the combined forces due to the induced tension field and the direct torsional loading would soon reach a magnitude sufficient to cause the collapse of the relatively stiff nose and therefore bring about the complete collapse of the cylinder.

Thus, it is seen that for semielliptical cylinders the buckling and ultimate loads are two separate and distinct points in the loading history and that the difference in the values of these two critical loads should increase with increasing ellipticity. It is apparent that this second statement must be true when the relative values of the maximum and minimum radii of curvature as a function of the ellipticity ratio are considered. Similar conclusions were reached by Lundquist and Burke in reference 5. Visual observations confirmed the above-mentioned conclusions as to buckle history, and the data given for these cylinders in tables III and IV show that the difference between the buckling and failure torsional moments increases as the ellipticity ratio increases.

In plotting these data, the same parameters were tried as were used in figure 7: namely,  $\tau L^2/Et^2$  against  $L^2/2ta$ ; where  $a$  is the semimajor axis of the ellipse. As can be seen from figures 8 and 9, these parameters were satisfactory and the experimental points had comparatively little scatter from a mean curve drawn through them. The solid lines in these figures correspond to equations (3) and (4). The curves of figures 7, 8, and 9 were then collected in figures 10 and 11.

Figure 10 gives the torsional buckling strength of semi-elliptical cylinders as a function of the dimensions of the cylinder and the ellipticity ratio. It is seen here that, as the ellipticity ratio increases, the buckling strength decreases, other items being kept equal. This is in line with the previous physical discussion since the cylinders with the larger ellipticities have a larger maximum radius of curvature and would thus buckle at lower loads than cylinders with smaller ellipticity ratios.

Figure 11, which gives the value of the ultimate load on such specimens, indicates that the cylinders with the larger ellipticities have somewhat better maximum-torsional-moment-carrying abilities. This is due to the fact that the section near the end of the major axis, having a small radius of curvature, acts as a stiffener, and that the larger the ellipticity, the greater the moment which can be developed before this effective stiffener collapses.

A cross plot of figures 10 and 11 led to empirical equations for the buckling and ultimate loads of such semielliptical and semicircular cylinders as follows:

1. For the buckling strength

$$\frac{\tau_b L^2}{Et^2} = 1.60 + \sqrt{14.80 + 1.13 \left( \frac{L^2 \epsilon^{1/3}}{2t\rho_0} \right)^{1.6}} \quad (3)$$

or

$$\frac{\tau_b L^2}{Et^2} = 1.60 + \sqrt{14.80 + 1.13 \left( \frac{L^2}{2ta\epsilon^{2/3}} \right)^{1.6}} \quad (3a)$$

2. For the ultimate strength

$$\frac{\tau_u L^2}{Et^2} = 1.60 + \sqrt{14.80 + 1.13 \left( \frac{L^2 \epsilon^{1/3}}{2ta} \right)^{1.6}} \quad (4)$$

in which  $a$  is the semimajor axis and  $\rho_0$  is the maximum radius of curvature of the cross section. It can be shown that, for an ellipse,

$$\rho_0 = \epsilon a$$

The foregoing equations are plotted in figures 12 and 13 with the experimental points and show good agreement and a reasonable amount of scatter. Thus, equations (3) and (4) and figures 12 and 13 can be considered to be design equations and design curves for semicircular and semielliptical cylinders subjected to a pure torsional moment.

On comparing the present results with those of reference 5 on complete elliptical cylinders, two important differences are noted. For the same sheet thickness and length, an elliptical cylinder buckles at a lower stress than a circular cylinder of radius  $\rho_0$ ; while for semicylinders a higher stress is reached. The reason for this lies in the fact that it was impossible to construct the elliptical cylinders without a slight looseness of the skin at the ends of the minor axis (cf., p. 2 of reference 5), thus introducing a rather large effect of initial irregularities into the buckling-test results. This was not the case in the semielliptical cylinders, since the construction technique used eliminated this difficulty. With regard to the ultimate strengths, the chief difference lies in the presence of the multiplicative  $\epsilon^{1/3}$  factor in the parameter for the semielliptical cylinders. An attempt to detect the presence of this same term in the results of reference 5 was unsuccessful, because of the narrow range of ellipticities tested coupled with the usual amount of experimental scatter.

#### Pure Bending of Semicircular Cylinders

The next series of specimens was made up of semicircular and semielliptical cylinders subjected to pure bending moments. The bending moment was applied in the plane of the minor axis of the cylinder.

As in the case of pure torsion, it is necessary to define the critical loads of pure bending in terms of suitable stresses. To accomplish this, use has been made of the normal beam equation,

$$\sigma = \frac{mb}{I_t} \quad (5)$$

The values of stress given by this equation should represent the true stress in the specimens tested up to the point of buckling. Beyond this point, the stresses given are of a fictitious nature, owing to the fact that the neutral axis

of the test specimens will shift toward the tension side of the specimens as the buckle deformations increase on the compression side. Extensometers mounted to the specimens during the testing procedure were used to check equation (5). In figure 14 are plotted sample curves of the experimentally determined stresses on the tension and the compression sides, prior to buckling, as a function of the applied bending moment. For comparison, stress values calculated from equation (5) are included. It can be seen that a linear and symmetrical stress distribution exists before buckling takes place for each of the three examples shown and that the agreement between the actual and calculated stresses is quite good. The fact that the calculated stresses are lower for each of the three cases plotted is merely a result of the selection of the examples and is not typical of the test data when considered as a whole, as can be seen in the upper curve of figure 15, where a comparative summary has been made. The scatter of the data about the line for unity in this figure can be attributed to the inherent difficulties in making stress measurements on curved, thin-walled sections by means of mechanical extensometers. The experimentally determined values of the bending stresses, after buckling has taken place, substantiate the shift in the neutral axis; however, the influence of the local buckle deformations is so great on these readings that they have little practical significance.

The first series of tests consisted of semicircular cylinders of various sheet thicknesses and lengths subjected to pure bending moments applied in the plane of the vertical spacer blocks (the plane of the minor axis for  $\epsilon = 1.0$ ). Prior to the specimens reaching their critical load, the skin covering remained unbuckled; however, at this point in the loading history, the compression side of the specimens would suddenly buckle into a large number of characteristic elliptical and diamond-shape patterns, all directed inward. Although this buckling phenomenon was quite violent at times, the applied bending loads had little tendency to drop off at this point. If the loads were increased, the buckle deformations would increase rapidly both in magnitude and scope, indicating that the sheet covering had already reached its ultimate stress and that the load was being supported by the cover-plate system alone. This conclusion appears to be well substantiated by the fact that the maximum load reached (at cover-plate failure) was independent of the geometric variables of the sheet covering and was solely a function of the cover plate thickness. For this reason, it has been assumed,

in the discussion that follows, that the buckling load was also the maximum load that could be carried by the semicircular shell.

The results of this series of tests on semicircular cylinders are presented in table VI and figure 16. The results have been correlated by using a reduced bending stress  $K$ , in which

$$K = \frac{\sigma_b a}{Et} = \frac{\sigma_b \rho_o}{Et} \quad (6)$$

This nondimensional stress coefficient is analogous to that used in reference 6 for axial compression stresses.

A study of figure 16 indicates that the reduced bending stress coefficient  $K$  gives a satisfactory parameter for plotting the data for a generalized curve for semicircular cylinders under pure bending. The scatter of the experimental points is not only reasonably small but is random in nature.

The oscillatory nature of the curve in figure 16 was at first questioned, but a study of reference 6 indicated that such a length effect might be expected. Reference 6 contains a linearized theory on the length effect of cylinders under axial compression, and the final results show a length effect that is qualitatively similar to that shown in figure 16. The necessary condition for such an effect was that the number of buckles in the complete circumference of the specimen must remain independent of the length of the cylinder. A careful check of the data on the number of buckles at buckling of the semicircular specimens showed that they varied only from 8 to 10 in range of  $L/\rho_o$ 's from 0.33 to 11.30 and  $\rho_o/t$ 's from 147 to 313, and that the variation was random in nature. On this basis, it is thought that the shape of the curve in figure 16 is at least tentatively justified.

In comparing the failing stress of semicircular cylinders under pure bending with the failing stress in circular cylinders under the same loading condition (see reference 7 and p. 466 of reference 8) it is found that the value of  $K$  is much smaller for the semicircular cylinders than it is for the full circular cylinders for the same value of  $\rho_o/t$ . Part of this difference is explainable by the fact that, for

the full cylinders, any seams in the cylinders were placed on the neutral axis of the specimen; while, in the case of the semicircular cylinders, the seams were located in regions of maximum tension and compression stress.

In an effort to determine experimentally the effect of seam location it was decided to construct and test a series of circular cylinders in pure bending under conditions similar to those of the semicircular cylinders. These specimens consisted of circular end plates approximately 6 inches in diameter, to which were attached the thin sheet covering in exactly the same manner as previously described. The seam or seams were formed by lapping the edges of the sheet and fastening them together by means of two rows of closely spaced, carefully fitted machine screws. These screws were not tightened excessively, in order to keep the deformations of the sheet covering across the seam to a minimum. To obtain the complete effect of the seams, four arrangements were selected:

1. One seam located on the neutral axis
2. One seam located on the tension side
3. One seam located on the compression side
4. Two seams located on the tension and compression sides

All these specimens were tested in the testing machine shown in figure 5, and the results are presented in table V and figure 17. The reduced buckling stress shown for the circular specimens with the single seam on the neutral axis, when compared to the similar specimens of reference 7, shows rather good agreement. With the seam on the tension side, a small reduction in stress is obtained; while, for the single seam on the compression side, the buckling stress is lowered still further. For the specimens with seams on both top and bottom, the reduction in stress is greater than the sum of the second and third configuration. All these buckling stresses are considerably lower than the value given by the classical theory and show clearly the influence of discontinuities in the specimen.

The dotted curve in figure 17 indicates the load carried by these specimens immediately after buckling and shows that all specimens tend to fall on the same curve. This

last phenomenon is explained by the recent work of Kármán and Tsien (reference 9) on the nonlinear buckling problem. In this paper, it was shown that there exist two buckling equilibrium points, one of which is closely given by the classical linearized theory, the other by the nonlinear theory. This latter equilibrium point was shown to exist at a much lower stress than the former point, and buckling could occur at stresses anywhere between these two limits, depending on initial imperfections and eccentricities in the shell and on the presence of external disturbances such as vibrations. Generally, buckling would be characterized by a sudden jump in the applied load to the value corresponding to the lower equilibrium point. This dotted curve then corresponds to the lower equilibrium point of full circular cylinders under bending.

The lower curve of figure 17 gives the values for the semicircular cylinders tested, and it can be seen that the  $K$  value for these specimens is still lower than the minimum point for the circular cylinders. The buckling of these semicircular cylinders was characterized by the fact that the applied load had little tendency to jump at the buckling load. This would imply that the specimens had buckled at a stress corresponding to the lowest possible equilibrium stress and never exceeded this value at any previous time in their loading history. The cause of such a condition's existing is undoubtedly the fact that the presence of the support system, including the cover plates, introduced small but sufficient amounts of initial eccentricity and irregularity into the sheet covering to cause failure to occur at the minimum point. This can be understood when it is considered that the cover plates were necessarily located at the most highly stressed point on the circumference of the specimen.

In view of the foregoing discussion, it is thought that figure 16 gives a satisfactory design curve for semicircular cylinders subjected to pure bending. The values obtained, while considerably lower than those obtained for full circular cylinders, probably will give a better approximation to the actual case of the nose section of a wing and therefore should be used for nose-section design where applicable.

#### Pure Bending of Semielliptical Cylinders

During the testing of the semielliptical cylinders subjected to pure bending loads, several experimental observations were made which will be discussed before presenting

the quantitative results. These specimens, upon reaching their buckling load, deformed into a type of wave pattern in the large radius of curvature regions that was entirely different from that of the semicircular cylinders. The buckles that appeared were definitely of the characteristic flat-plate type for both ellipticities tested. These large shallow circular or elliptical buckles covered the major portion of the compression sides of the curved sheet covering and were different from the flat-plate type only in that they were all directed inward. In a manner similar to that described under the pure torsion tests, the small radius nose portions of the specimen behaved as if they were stiffeners, and actually formed the lower boundaries for the buckle pattern. The formation of the buckles was characterized by the facts that the buckling was not of a particularly violent nature and that there was no noticeable decrease in the load-carrying ability at the point of buckling.

As the load was increased beyond the buckling load, these same buckles increased in amplitude and scope until they approached quite close to the boundaries formed by the plates, the cover-plate system, and the nose of the section. Upon further application of load, these buckles created much smaller induced buckles, particularly in the four corners of the affected region. In no case, however, did the nose portion fail first since the point of collapse was always dictated by the strength of the cover plates. This is as would be expected, since the loading was pure bending and increasing the amount of material in the cover plates would have the same effect as increasing the size of the spar caps in a wing. The data obtained are therefore directly applicable to wing nose section design.

The results of this series of tests are given in table VII and table VIII, and these data have been combined with the test results in table VI on semicircular cylinders to give the curve shown in figure 18. This curve shows considerable scatter, but retesting and rechecking points indicated that the scatter was random and was inherent in the specimens. For that reason, the suggested design curve shown in the figure is placed near the lower limit of the points rather than through the mean of the experimental points tested.

This suggested design curve can be represented by the equation

$$\frac{\sigma_b}{E} \left( \frac{a}{t} \right)^{1.5} = 1.70 + 0.15 \left( \frac{a}{L} \right)^{1.5} \quad (7)$$

or

$$\frac{\sigma_b}{E} \left( \frac{\rho_o}{\epsilon t} \right)^{1.5} = 1.70 + 0.15 \left( \frac{\rho_o}{L\epsilon} \right)^{1.5} \quad (8)$$

This can be written as

$$\frac{\sigma_b}{E} = 1.70 \left( \frac{t}{a} \right)^{1.5} + 0.15 \left( \frac{t}{L} \right)^{1.5} \quad (9)$$

or

$$\frac{\sigma_b}{E} = 1.70 \left( \frac{\epsilon t}{\rho_o} \right)^{1.5} + 0.15 \left( \frac{t}{L} \right)^{1.5} \quad (10)$$

Equation (9) is plotted in figure 19.

There is some indication that the number of buckles in the buckle pattern of the specimens accounted in part for the wide scattering in figure 18. Further theoretical study may justify this presumption, but until more data are available it is thought that equation (9) or (10) will give a sufficiently conservative value of the critical buckling stress of semicircular or semielliptical cylinders under the action of pure bending.

#### Bending-Plus-Torsion Tests

The bending-plus-torsion tests were made on the machine illustrated in figure 5. The loading was so arranged that a constant ratio of bending moment to torsional moment was applied to the specimen up to the failing point. Buckling was noted both visually and with the aid of stress-strain measurements taken in the specimen during loading. The bending and shearing stresses were calculated from the equations

$$\sigma = \frac{mb}{I_t} = \frac{Mb}{I_s} \quad (11)$$

and

$$\tau = \frac{m_t}{2At} \quad (12)$$

Subscripts b and u in the tables correspond to buckling and ultimate stresses, respectively. The values for  $\sigma_{b_0}$ ,  $\tau_{b_0}$ , and  $\tau_{u_0}$  were taken from figures 18, 10, and 11, respectively.

The test data for these specimens are tabulated in tables IX, X, and XI for ellipticity ratios of 1.0, 2.0, and 3.0, respectively. These data have been plotted in figures 20 to 25, in which figures each ellipticity is considered separately. A study of these figures led to the conclusion that single curves would satisfactorily represent the relationships between  $\sigma_b/\sigma_{b_0}$  and  $M_b/m_t b$ ,  $\tau_b/\tau_{b_0}$  and  $M_b/m_t b$ , and  $\tau_u/\tau_{u_0}$  and  $M_u/m_t u$  and that the introduction of the ellipticity ratio into the ultimate bending-stress ratio gave one curve for all ellipticities of the form  $\sigma_u/\epsilon\sigma_{b_0}$  as a function of  $M_u/m_t u$ . It was necessary to use the ratio of the ultimate compressive stress to the buckling compression stress (with no torsion) since, as was discussed under Pure Bending, the failure bending stress for pure bending was solely a function of the size of the cover plates, corresponding to the size of the spar caps in a normal wing.

The combined curves are shown in figures 26 to 29, and it can be seen that, although considerable scatter is present, a consistent trend of the stress ratios with a variation in the  $M/m_t$  ratios is indicated. For the values of  $\sigma_{b_0}$  in tables IX, X, and XI, the mean curve of figure 18 was used throughout. For the ultimate values, design curves have been indicated which approximate to the lower limits of the experimental data.

If these suggested design curves are cross-plotted, plotting  $\frac{1}{\epsilon} \frac{\sigma_u}{\sigma_{b_0}}$  as a function of  $\frac{\tau_u}{\tau_{u_0}}$  for constant values of  $M_u/m_t u$ , it is found that a curve expressed by the following equation is obtained:

$$\frac{1}{\epsilon} \frac{\sigma_u}{\sigma_{b_0}} + \left( \frac{\tau_u}{\tau_{u_0}} \right)^2 = 1 \quad (13)$$

This equation will give conservative results for all values of  $M_u/m_{tu}$  and therefore can be used for design purposes.

A cross plot of the buckling curves (figs. 26 and 27) indicates that a similar equation will give a satisfactory first approximation with considerable scatter (as indicated in figs. 26 and 27). Thus,

$$\frac{\sigma_b}{\sigma_{b_u}} + \left( \frac{\tau_b}{\tau_{b_0}} \right)^2 = 1 \quad (14)$$

The buckling and failure wave patterns of these specimens depended largely upon the  $M/m_t$  ratio. For large values of this ratio, typical diamond-shape compression waves appeared when the buckling stress was reached and for small values of this ratio diagonal shear waves appeared. Intermediate values led to wave patterns which were combinations of these two types. Failure of the cylinders occurred across the nose (minimum radius section) of the specimen for the cases when the torsional shearing moment was high and in the cover plates when the bending moment was high. This fact explains the reason for the relatively large scatter in the experimental data for the larger values of the  $M/m_t$  ratios. The higher values of the experimental stresses correspond to specimens in which the cover plates were strong enough to permit the development of the full torsional shearing strength of the section so that failure finally occurred across the nose section.

Comparison between measured and calculated stresses in the regions below buckling are shown in the second curve in figure 15 and also in the upper curve of figure 30. It is seen that the scatter is random in nature and is of the order of magnitude that would be expected when measuring thin sheet stresses with mechanical extensometers.

The last four lines of tables IX, X, and XI are for specimens with lengths shorter than the standard length of 12.5 inches, which was held throughout the other tests. It can be seen that the test data for these specimens plot satisfactorily on the curves for the other specimens, indicating that there is no new length effect which appears for this combined loading.

## Bonding-Plus-Shear Tests

The bending-plus-shear tests were conducted on the testing machine shown in figure 6. Two lengths of specimens were tested, 6.5 and 16.0 inches, and the usual three skin thicknesses and three ellipticity ratios were covered. The moment-to-shear ratio was varied by the position of the jack on the extended loading arm. As previously described, the weight of the extended loading arm is separately balanced out and no tare readings entered the loading force.

The data for these specimens are tabulated in tables XII, XIII, and XIV. The equations used in reducing the data were:

$$\sigma_b = \frac{mb}{I_t} = \frac{Flb}{I_t} \quad (15)$$

$$\tau_{sb} = \frac{F}{A_s} \quad (16)$$

$$\frac{M}{Fb} = \frac{l}{b} \frac{I_s}{I_t} = \frac{m}{Fb} \frac{I_s}{I_t} \quad (17)$$

Only the buckling data have been recorded and reduced, since ultimate failure was, in nearly every case, caused by cover-plate failure. Thus, ultimate failure could be delayed indefinitely by increasing the cover-plate size (corresponding to an increase in spar-cap size). A few cases in which the  $M_b/Fb$  ratio was very low (small moment but large shear) actually failed across the nose section, but the number of these specimens was not sufficiently great to allow the drawing of any general conclusions.

The value of  $\sigma_{b_0}$  in the tables was obtained, using the mean curve of figure 18. The resulting values of  $\sigma_b/\sigma_{b_0}$  show a scatter which is generally no more than that shown in figure 18, which indicates that very little additional scatter has been put into the points by the addition of direct

shear to the pure bending load. Scatter was particularly bad for the ellipticity ratio of 3. However, this was to be expected, since these specimens were very hard to make without initial deformations near the ends of the minor axis. Also, loads for these specimens were quite light and the accuracy of measuring these light loads had a tendency to decrease.

The data in tables XII, XIII, and XIV have all been plotted in figures 31 to 45. Figures 31, 36, and 41 give the variation of  $\sigma_b/\sigma_{b_0}$  as a function of the  $M_b/Fb$  ratio and, as mentioned before, the scatter tends to increase as the ellipticity ratio increases.

The results for the shear stress at buckling are plotted in the remaining curves. This shear stress is taken as the average shearing stress distribution. Each set of curves for a given ellipticity ratio has been collected and re-plotted in figures 35, 40, and 45. The scatter on these curves is not so high as that indicated for the bending stresses, which would tend to indicate that the distribution of the bending stress between the cylindrical sheet and the cover plates may not have been accurately given by the  $I_s/I_t$  ratio, as was assumed.

No attempt was made to determine a  $\tau_{sb}/\tau_{sb_0}$  ratio, since it was impossible to obtain a value for  $\tau_{sb_0}$ . Therefore the value of  $\tau_{sb}$  has been presented simply as a function of the  $M_b/Fb$  ratio.

Again, extensometer readings were taken below buckling to check the calculated value of the bending stresses, and the results are shown in figures 15 and 30. The scatter shown is random and is of the order of magnitude expected when using mechanical extensometers to measure stresses in thin sheet structures.

## CONCLUSIONS

The data contained in this report are intended to serve as a guide to the possible buckling and ultimate load-carrying abilities of wing nose sections. In most cases these

nose sections can be approximated by ellipses, and for this reason the elliptical section has been used for test purposes. The data and curves presented should give the designer a considerable insight into the behavior of such sections under pure loading conditions as well as conditions of combined bending and shear and combined bending and torsion. The problem of combined bending, torsion, and shear has not been studied in this investigation and future investigations should study the effect of all three loading conditions and should, if possible, make an attempt actually to measure skin stress distributions by means of electric strain gages in order to obtain a more complete stress distribution pattern.

A summary of the design equations and curves for the conditions studied is given as follows:

### 1. Pure Torsion

#### a. Buckling

$$\frac{\tau_b L^2}{Et^2} = 1.60 + \sqrt{14.80 + 1.13 \left( \frac{L^2}{2ta \epsilon^{2/3}} \right)^{1.6}}$$

(See fig. 12.)

#### b. Ultimate

$$\frac{\tau_u L^2}{Et^2} = 1.60 + \sqrt{14.80 + 1.13 \left( \frac{L^2 \epsilon^{1/3}}{2ta} \right)^{1.6}}$$

(See fig. 13.)

### 2. Pure Bending

#### a. Buckling

$$\frac{\sigma_b}{E} = 1.70 \left( \frac{t}{a} \right)^{1.5} + 0.15 \left( \frac{t}{L} \right)^{1.5}$$

(See fig. 19.)

b. Ultimate

No ultimate curve since ultimate load is a function of the cover-plate strength.

3. Bending Plus Torsiona. Buckling

$$\frac{\sigma_b}{\sigma_{b_0}} + \left( \frac{\tau_b}{\tau_{b_0}} \right)^2 = 1$$

(See figs. 26 and 27.)

b. Ultimate

$$\frac{1}{\epsilon} \frac{\sigma_u}{\sigma_{b_0}} + \left( \frac{\tau_u}{\tau_{u_0}} \right)^2 = 1$$

(See figs. 28 and 29.)

4. Bending Plus Direct Sheara. Buckling

Bending stresses - Figures 31, 36, and 41 for ellipticities 1, 2, and 3, respectively.

Shear stresses - Figures 35, 40, and 45 for ellipticities 1, 2, and 3, respectively.

b. Ultimate

No ultimate values, since the ultimate stress is largely dependent upon cover-plate strength.

## REFERENCES

1. Anon.: ANC-5, Strength of Aircraft Elements. U. S. Government Printing Office, 1942.
2. Anon.: Alcoa Aluminum and Its Alloys. Aluminum Co. of Am., 1941.
3. Donnell, L. H.: Stability of Thin-Walled Tubes under Torsion. NACA Rep. No. 479, 1933.
4. Lundquist, Eugene E.: Strength Tests on Thin-Walled Duralumin Cylinders in Torsion. NACA TN No. 427, 1932.
5. Lundquist, Eugene E., and Burke, Walter F.: Strength Tests on Thin-Walled Duralumin Cylinders of Elliptical Section. NACA TN No. 527, 1935.
6. Flügge, Wilhelm: Statik und Dynamik Der Schalen. Julius Springer (Berlin), 1934.
7. Lundquist, Eugene E.: Strength Tests of Thin-Walled Duralumin Cylinders in Pure Bending. NACA TN No. 479, 1933.
8. Timoshenko, S.: Theory of Elastic Stability. McGraw-Hill Book Co., Inc. (New York), 1936.
9. von Kármán, Theodore, and Tsien, Hsue-Shen: The Buckling of Thin Cylindrical Shells under Axial Compression. Jour. Aero. Sci., vol 8, no. 8, June 1941, pp. 303-312.

## BIBLIOGRAPHY

- Cox, H. L.: Stress Analysis of Thin Metal Construction. Jour. R.A.S., vol. 44, no. 3, March 1940, pp. 231-272.
- Kanemitsu, Sunao, and Nojima, Noble M.: Axial Compression Tests of Thin Circular Cylinders. Thesis, C.I.T., 1939. (unpublished)
- Lundquist, Eugene E.: Strength Tests of Thin-Walled Duralumin Cylinders in Compression. NACA Rep. No. 473, 1933.

TABLE I

## Tensile Properties of 24S-T Aluminum Alloy

## Sheet Used in Specimens Tested

Specimen No.	t (in.)	Loading direction relative to grain	$E \times 10^{-6}$ (lb./in. <sup>2</sup> )	$\sigma_{yp}$ (lb./in. <sup>2</sup> )	$\sigma_u$ (lb./in. <sup>2</sup> )
MT-1	0.0101	With	10.85	—	69100
MT-2	0.0102	"	10.71	51000	66300
MT-3	0.0099	Across	9.94	44600	65500
MT-4	0.0098	"	10.05	45500	66100
MT-5	0.0175	With	10.46	52800	68700
MT-6	0.0174	"	10.49	51200	69800
MT-7	0.0174	Across	10.44	44900	68100
MT-8	0.0175	"	10.43	44800	66900
MT-9	0.0209	With	9.44	49500	69300
MT-10	0.0205	"	10.02	52500	70300
MT-11	0.0204	Across	9.76	45800	67600
MT-12	0.0204	"	10.24	44800	66900
MT-13	0.0319	With	11.18	55500	72800
MT-14	0.0320	"	10.80	56300	72100
MT-15	0.0315	Across	11.20	47100	71200
MT-16	0.0315	"	10.51	47500	70300
MT-17	0.0383	With	10.65	52300	70800
MT-19	0.0387	Across	10.47	45800	69400
MT-20	0.0386	"	10.01	43800	69900
MT-A	0.0210	With	10.00	54000	--
MT-B	0.0210	Across	10.00	46300	--
MT-C	0.0165	"	9.80	45500	--
MT-D	0.0165	"	10.00	45100	--

TABLE II

Torsional Strength of Semi-Circular Cylinders,  $\epsilon = 1.0$ 24S-T  $\mu = 0.3$   $E = 10.3 \times 10^6$  lb./in.<sup>2</sup>  $b = 3.01$  in.

Spec. No.	t (in.)	L (in.)	Mt <sub>b</sub> (in.-lb.)	Mt <sub>u</sub> (in.-lb.)	$\tau_b$ (in./in. <sup>2</sup> )	$\tau_u$ (lb./in. <sup>2</sup> )	$\frac{\tau_b L^2}{Et^2}$	$\frac{\tau_u L^2}{Et^2}$	$\frac{L^2}{2ta}$	$\frac{L^2 \epsilon^{2/3}}{2tp_0}$	$\frac{L^2 \epsilon^{1/3}}{2ta}$
PT-9	0.0190	34.0	8840	9090	5740	5910	1790	1840	10110	10110	10110
PT-10	"	"	8850	8850	5750	5750	1790	1790	"	"	"
PT-11	"	"	8830	9000	5740	5850	1780	1820	"	"	"
PT-12	"	"	8220	8220	5340	5340	1660	1660	"	"	"
PT-13	"	"	8230	8290	5350	5390	1660	1660	"	"	"
PT-14	0.0160	"	6060	6060	4680	4680	2050	2050	12010	12010	12010
PT-15	"	"	5430	5720	4190	4410	1840	1940	"	"	"
PT-26	0.0200	16.0	12380	12380	7640	7640	475	475	2130	2130	2130
PT-27	"	"	13240	13240	8170	8170	508	508	"	"	"
PT-28	0.0160	"	7900	7900	6100	6100	593	593	2660	2660	2660
PT-29	"	"	7830	7830	6050	6050	587	587	"	"	"
PT-73	0.0104	"	2980	2980	3540	3540	814	814	4100	4100	4100
PT-74	0.0102	"	2800	2900	3400	3520	812	841	4180	4180	4180
PT-20	0.0200	6.5	18040	18040	11140	11140	114	114	351	351	351
PT-21	0.0200	"	19450	19450	12010	12010	123	123	"	"	"
PT-23	0.0160	"	12840	12840	9920	9920	159	159	439	439	439
PT-24	0.0160	"	11930	12160	9210	9390	147	150	"	"	"
PT-58	0.0108	"	4000	4500	4590	5160	162	182	651	651	651
PT-32	0.0200	2.5	23760	23760	14660	14660	22.2	22.2	51.9	51.9	51.9
PT-33	0.0200	"	24700	24700	15250	15250	23.2	23.2	"	"	"
PT-30	0.0160	"	15000	17140	11580	13230	27.3	31.3	64.9	64.9	64.9
PT-31	"	"	18390	18390	14200	14200	33.3	33.3	"	"	"

TABLE III

Torsional Strength of Semi-Elliptical Cylinders,  $\epsilon = 2.0$

24S-T  $\mu = 0.3$   $E = 10.3 \times 10^6$  lb./in.<sup>2</sup>  $b = 3.01$  in.

Spec. No.	t (in.)	L (in.)	Mt <sub>b</sub> (in.-lb.)	Mt <sub>u</sub> (in.-lb.)	$\tau_b$ (lb./in. <sup>2</sup> )	$\tau_u$ (lb./in. <sup>2</sup> )	$\frac{\tau_b L^2}{Et^2}$	$\frac{\tau_u L^2}{Et^2}$	$\frac{L^2}{2ta}$	$\frac{L^2 \epsilon^{1/3}}{2t\rho_0}$	$\frac{L^2 \epsilon^{1/3}}{2ta}$
PT-16	0.210	34.0	9260	10500	3190	3620	812	920	4570	2880	5750
PT-48	0.0200	16.0	10390	13580	3760	4920	234	306	1110	700	1400
PT-49	"	"	10240	13850	3710	5020	231	312	"	"	"
PT-65	0.0170	"	5400	9850	2300	4200	198	362	1250	788	1570
PT-71	0.0167	"	5500	10490	2390	4560	213	406	1280	806	1610
PT-72	0.0106	"	2000	4240	1370	2900	254	536	2010	1270	2530
PT-66	0.0104	"	1800	3670	1260	2570	290	590	2050	1290	2580
PT-22	0.0200	6.5	18000	23500	6530	8520	67.0	87.4	183	115	230
PT-47	"	"	18550	19650	6000	7125	61.5	73.1	"	"	"
PT-59	0.0177	"	10400	14100	4260	5780	55.7	75.5	198	125	250
PT-25	0.0160	"	10500	14000	4760	6350	76.4	102	219	138	276
PT-60	0.0104	"	3000	4750	2100	3330	79.7	126	338	213	426
PT-62	0.0101	"	2800	5060	2020	3640	81.2	146	348	220	439
PT-35	0.0200	2.5	23650	28760	8570	10430	13.0	15.8	27.1	17.1	34.2
PT-36	0.0200	"	24380	35640	8830	12930	13.4	19.6	"	"	"
PT-34	0.0160	"	13930	24640	6320	11180	15.0	26.5	32.5	20.5	41.0
PT-37	"	"	16270	23090	7370	10480	17.5	24.8	"	"	"
PT-51	0.0103	"	4000	6790	2820	4790	16.2	27.4	50.5	31.8	63.6
PT-54	0.0101	"	--	6450	--	4640	--	26.6	51.5	32.5	65.0

TABLE IV

Torsional Strength of Semi-Elliptical Cylinders,  $\epsilon = 3.0$

24S-T  $\mu = 0.3$   $E = 10.3 \times 10^6$  lb./in.<sup>2</sup>  $b = 3.01$  in.

Spec. No.	t (in.)	L (in.)	M <sub>tb</sub> (in.-lb.)	M <sub>tu</sub> (in.-lb.)	$\tau_b$ (lb./in. <sup>2</sup> )	$\tau_u$ (lb./in. <sup>2</sup> )	$\frac{\tau_b L^2}{Et^2}$	$\frac{\tau_u L^2}{Et^2}$	$\frac{L^2}{2ta}$	$\frac{L^2 \epsilon^{1/3}}{2t\rho_0}$	$\frac{L^2 \epsilon^{1/3}}{2ta}$
PT-17	0.0200	34.0	6080	12240	1560	3140	439	883	3200	1540	4610
PT-18	"	16.0	7000	17640	1800	4520	112	281	709	340	1020
PT-19	"	"	6800	15960	1750	4080	109	254	"	"	"
PT-44	"	"	6800	15400	1750	3950	"	246	"	"	"
PT-68	0.0176	"	5500	12160	1610	3550	129	284	806	387	1160
PT-69	0.0174	"	--	12300	--	3630	--	298	816	392	1180
PT-70	0.0103	"	--	4600	--	2300	--	539	1380	663	1990
PT-45	0.0200	6.5	14420	20030	3700	5140	38.0	52.8	117	56.2	169
PT-46	"	"	9200	17850	2360	4580	24.2	47.0	"	"	"
PT-50	"	"	13000	25200	3330	6460	34.2	66.4	"	"	"
PT-63	0.0175	"	7000	17310	2050	5080	27.5	68.2	134	64.4	193
PT-61	0.0173	"	5500	15390	1630	4570	22.4	62.8	135	64.9	195
PT-67	0.0103	"	2600	6020	1300	3010	50.3	116	228	110	329
PT-64	0.0102	"	3000	6630	1510	3340	59.8	132	240	115	346
PT-40	0.0200	2.5	25900	45800	6550	11750	9.95	17.8	17.3	8.31	25.0
PT-41	"	"	26000	--	6670	--	10.1	--	"	"	"
PT-42	"	"	24400	41000	6260	10510	9.50	15.9	"	"	"
PT-38	0.0160	"	12880	22900	4140	7360	9.81	17.5	21.8	10.5	31.4
PT-39	"	"	11580	23560	3620	7570	8.59	18.0	"	"	"
PT-56	0.0103	"	3500	7900	1750	3950	10.0	22.6	33.7	16.2	48.6
PT-55	0.0099	"	4000	8920	2080	4640	13.1	29.2	35.0	16.8	50.5

TABLE V

Bending Strength of Circular Cylinders

$a = 3.0$  in.  $L = 6.5$  in.  $L/a = 2.16$

24S-T  $\mu = 0.3$   $E = 10.3 \times 10^6$  lb./in.<sup>2</sup>

Spec No.	t (in.)	a/t	M <sub>b</sub> (in.-lb.)	$\sigma_b$ (lb./in. <sup>2</sup> )	$\frac{\sigma_{ba}}{Et}$	$\frac{\sigma'_{ba}}{Et}$	Remarks
PB-103	0.0206	146	18050	30800	0.436	0.250	Seam on N.A.
PB-104	0.0205	147	16200	27800	0.396	0.214	" " "
PB-102	0.0162	186	11600	25200	0.454	0.240	" " "
PB-101	0.0160	188	11820	26000	0.475	0.286	" " "
PB-110	0.0102	295	5000	17300	0.494	0.279	" " "
PB-109	0.0094	320	3060	11500	0.356	0.264	" " "
PB-106	0.0199	151	16190	28600	0.420	0.219	" " T. side
PB-105	"	"	15530	27400	0.403	0.262	" " C. side
PB-112	0.0194	155	13410	24300	0.365	0.251	" " " "
PB-107	0.0205	147	13470	23100	0.329	0.220	" " T. and C. Sides
PB-108	0.0203	148	13480	23300	0.335	0.261	" " " " " "
PB-115	0.0160	188	9310	20500	0.374	0.262	" " " " " "
PB-117	0.0155	194	9460	21500	0.405	0.310	" " " " " "
PB-119	0.0104	289	3370	11400	0.324	0.284	" " " " " "
PB-121	0.0100	300	3600	12700	0.369	0.287	" " " " " "

TABLE VI

Bending Strength of Semi-Circular Cylinders,  $\epsilon = 1.0$   
 24S-T  $\mu = 0.3$   $E = 10.3 \times 10^6$  lb./in.<sup>2</sup>  $b = 3.01$  in.

Spec. No.	t (in.)	L (in.)	$I_s$ (in. <sup>4</sup> )	$I_{t4}$ (in. <sup>4</sup> )	$\rho_0/t$	$L/\rho_0$	$M_b$ (in.-lb.)	$\sigma_b$ (lb./in. <sup>2</sup> )	$\frac{\sigma_b}{E} \left(\frac{\rho_0}{\epsilon t}\right)^{1.5}$	$\frac{L}{\rho_0}$
PB-33	0.0212	34.0	1.818	4.785	142.0	11.30	19450	12250	2.01	11.30
PB-33B	"	"	"	"	"	"	19475	12270	2.01	"
PB-14	0.0203	16.0	1.739	4.620	148.2	5.31	19950	13000	2.28	5.31
PB-14B	"	"	"	"	"	"	18200	11860	2.08	"
PB-56	0.0160	"	1.369	4.168	188.1	"	15750	11370	2.85	"
PB-56B	"	"	"	"	"	"	15860	11440	2.87	"
PB-58	0.0098	"	0.835	2.545	307.0	"	5330	6290	3.29	"
PB-58B	"	"	"	"	"	"	4800	5660	2.96	"
PB-24	0.0204	12.5	1.749	4.712	147.5	4.15	23300	14880	2.58	4.15
PB-24B	"	"	"	"	"	"	22650	14470	2.51	"
PB-37	0.0164	"	1.402	4.201	183.4	"	16430	11770	2.84	"
PB-37B	"	"	"	"	"	"	16700	11960	2.88	"
PB-39	0.0095	"	0.810	2.509	316.2	"	5850	7010	3.83	"
PB-39B	"	"	"	"	"	"	5775	6920	3.78	"
PB-5	0.0200	6.5	1.714	4.550	150.5	2.16	24000	15900	2.85	2.16
PB-5B	"	"	"	"	"	"	23000	15200	2.73	"
PB-6	"	"	"	"	"	"	21800	14400	2.58	"
PB-6B	"	"	"	"	"	"	23000	15200	2.73	"
PB-18	0.0207	"	1.773	4.693	145.3	"	26150	16800	2.85	"
PB-18B	"	"	"	"	"	"	24200	15500	2.63	"
PB-11	0.0175	"	1.498	4.331	172.0	"	17870	12400	2.72	"
PB-11B	"	"	"	"	"	"	20500	14200	3.11	"
PB-17	0.0106	"	0.904	2.667	283.7	"	7000	7890	3.66	"
PB-17B	"	"	"	"	"	"	7250	8170	3.79	"
PB-21	"	"	"	2.716	"	"	8370	9280	4.31	"
PB-21B	"	"	"	"	"	"	7250	8040	3.73	"
PB-9	0.0198	2.5	1.969	4.591	152.0	0.83	16600	10900	1.99	0.83
PB-27	0.0200	"	1.714	4.649	150.5	"	18750	12130	2.17	"
PB-52	0.0161	2.5	1.378	4.163	187.0	"	16360	11800	2.93	"
PB-49	0.0095	"	0.810	2.497	316.1	"	4110	4950	2.70	"
PB-34	0.0205	1.0	1.788	4.705	146.9	0.33	22550	14420	2.49	0.33
PB-34B	"	"	"	"	"	"	22750	14550	2.52	"
PB-43	0.0163	"	1.395	4.176	184.6	"	18260	13140	3.20	"
PB-46	0.0096	"	0.818	2.508	313.0	"	4250	5090	2.74	"

TABLE VII

Bending Strength of Semi-Elliptical Cylinders,  $\epsilon = 2.0$   
 24S-T  $\mu = 0.3$   $E = 10.3 \times 10^6$  lb/in<sup>2</sup>  $b = 3.01$  in.

Spec. No.	t (in.)	L (in.)	I <sub>s</sub> (in. <sup>4</sup> )	I <sub>t</sub> (in. <sup>4</sup> )	$\rho_o/t$	L/ $\rho_o$	L/a	t/a	M <sub>b</sub> (in.-lb.)	$\sigma_b$ (lb./in. <sup>2</sup> )	$\frac{\sigma_b}{E} \left( \frac{\rho_o}{\epsilon t} \right)^{1.5}$	$\frac{L}{\rho_o}$
PB-16	0.0208	16.0	3.119	6.029	579	1.33	2.66	0.00346	8000	3990	1.91	2.66
PB-16B	"	"	"	"	"	"	"	"	10000	4990	2.38	"
PB-59	0.0165	"	2.468	5.249	730	"	"	0.00274	5940	3400	2.30	"
PB-59B	"	"	"	"	"	"	"	"	5820	3340	2.26	"
PB-25	0.0198	12.5	2.967	5.902	609	1.04	2.08	0.00328	9900	5050	2.60	2.08
PB-25B	"	"	"	"	"	"	"	"	10500	5350	2.75	"
PB-40	0.0165	"	2.460	5.261	729	"	"	0.00274	7300	4160	2.80	"
PB-40B	"	"	"	"	"	"	"	"	6680	3820	2.58	"
PB-38	0.0095	"	1.418	3.112	1266	"	"	0.00158	1500	1450	2.24	"
PB-38B	"	"	"	"	"	"	"	"	1410	1360	2.10	"
PB-3	0.0210	6.5	3.152	6.019	573	0.540	1.08	0.00350	17700	8850	4.15	1.08
PB-3B	"	"	"	"	"	"	"	"	15700	7850	3.69	"
PB-19	0.0205	"	3.070	6.047	587	"	"	0.00340	13050	6500	3.17	"
PB-19B	"	"	"	"	"	"	"	"	15300	7630	3.72	"
PB-10	0.0173	"	2.591	5.367	696	"	"	0.00287	10700	6000	3.77	"
PB-15	0.0106	"	1.581	3.359	1133	"	"	0.00176	2000	1790	2.34	"
PB-15B	"	"	"	"	"	"	"	"	2350	2100	2.74	"
PB-7	0.0205	2.5	3.074	6.040	588	0.208	0.42	0.00340	9800	4880	2.38	0.42
PB-7B	"	"	"	"	"	"	"	"	12400	6190	3.02	"
PB-28	"	"	"	6.007	"	"	"	"	10250	5140	2.51	"
PB-28B	"	"	"	"	"	"	"	"	9400	4710	2.30	"
PB-53	0.0166	"	2.474	5.276	725	"	"	0.00276	8840	5040	3.37	"
PB-53B	"	"	"	"	"	"	"	"	8410	4800	3.21	"
PB-54	0.0100	"	1.492	3.230	1202	"	"	0.00169	1410	1310	1.87	"
PB-54B	"	"	"	"	"	"	"	"	1340	1250	1.79	"
PB-35	0.0210	1.0	3.155	6.117	574	0.083	0.17	0.00349	19750	9760	4.60	0.17
PB-35B	"	"	"	"	"	"	"	"	21300	10520	4.96	"
PB-44	0.0165	"	2.468	5.288	729	"	"	0.00274	14000	7950	5.36	"
PB-48	0.0094	"	1.402	3.078	1280	"	"	0.00156	3140	3080	4.83	"

**TABLE VIII**

Bending Strength of Semi-Elliptical Cylinders,  $\epsilon = 3.0$   
 24S-T  $\mu = 0.3$   $E = 10.3 \times 10^6$  lbs/in.<sup>2</sup>  $b = 3.01$  in.

Spec. No.	t (in.)	L (in.)	$I_s$ (in. <sup>4</sup> )	$I_t$ (in. <sup>4</sup> )	$\rho_0/t$	$L/\rho_0$	L/a	t/a	$M_b$ (in.-lb.)	$\sigma_b$ (lb./in. <sup>2</sup> )	$\frac{\sigma_b}{E} \left( \frac{\rho_0}{\epsilon t} \right)^{1.5}$	$\frac{L}{\rho_0}$
PB-26	0.0199	16.0	4.256	7.169	1361	0.590	1.77	0.00220	5400	2270	2.13	1.77
PB-57B	0.0158	"	3.375	6.177	1715	"	"	0.00175	2430	1180	1.57	"
PB-55B	0.0098	"	2.089	3.812	2760	"	"	0.00109	910	718	1.95	"
PB-23	0.0206	12.5	4.410	7.285	1315	0.461	1.38	0.00231	6000	2480	2.21	1.38
PB-23B	"	"	"	"	"	"	"	"	4570	1890	1.69	"
PB-42	0.0166	"	3.541	6.343	1632	"	"	0.00184	5390	2560	3.16	"
PB-42B	"	"	"	"	"	"	"	"	5000	3280	2.94	"
PB-41	0.0093	"	1.982	3.675	2910	"	"	0.00103	1000	818	2.40	"
PB-41B	"	"	"	"	"	"	"	"	"	"	2.40	"
PB-2	0.0200	6.5	4.284	7.120	1354	0.240	0.72	0.00221	7630	3230	3.01	0.72
PB-2B	"	"	"	"	"	"	"	"	8000	3480	3.24	"
PB-20	0.0207	"	4.430	7.370	1309	"	"	0.00229	8800	3600	3.19	"
PB-20B	"	"	"	"	"	"	"	"	10400	4250	3.76	"
PB-13	0.0175	"	3.745	6.549	1549	"	"	0.00194	3900	1750	2.00	"
PB-13B	"	"	"	"	"	"	"	"	4800	2210	2.52	"
PB-22	0.0179	"	3.830	6.724	1513	"	"	0.00198	3800	1700	1.87	"
PB-22B	"	"	"	"	"	"	"	"	5900	2640	2.91	"
PB-12	0.0103	"	2.195	3.978	2625	"	"	0.00114	1350	1020	2.57	"
PB-12B	"	"	"	"	"	"	"	"	1200	907	2.29	"
PB-8	0.0199	2.5	4.262	7.298	1361	0.092	0.28	0.00220	7400	3050	2.87	0.28
PB-8B	"	"	"	"	"	"	"	"	8450	3480	3.27	"
PB-29	0.0200	"	4.284	7.200	1355	"	"	0.00221	7650	3210	2.99	"
PB-29B	"	"	"	"	"	"	"	"	7250	3040	2.83	"
PB-51	0.0158	"	3.375	6.154	1714	"	"	0.00175	3110	1520	2.02	"
PB-51B	"	"	"	"	"	"	"	"	2890	1410	1.87	"
PB-50	0.0095	2.5	2.025	3.733	2848	0.092	0.28	0.00105	2170	1750	4.97	"
PB-50B	"	"	"	"	"	"	"	"	1430	1150	3.27	"
PB-36	0.0212	1.0	4.544	7.532	1279	0.037	0.11	0.00235	16550	6620	5.66	0.11
PB-36B	"	"	"	"	"	"	"	"	16880	6750	5.78	"
PB-45	0.0159	"	3.395	6.295	1703	"	"	0.00176	13000	6220	8.18	"
PB-47	0.0092	"	1.961	3.661	2940	"	"	0.00102	2700	2220	6.63	"

TABLE IX  
 Bending Plus Torsion Tests  
 $\xi = 1.0$   $E = 10.3 \times 10^6$  psi  
 $A = 40.5$  sq.in.,  $L = 12.5$  in.

Spec. No.	$t_s$ in.	$t_c$ in.	$I_s$ in. <sup>4</sup>	$I_t$ in. <sup>4</sup>	$m_b$ in.lb.	$m_{tb}$ in.lb.	$m_u$ in.lb.	$m_{tu}$ in.lb.	$\sigma_b$ psi.	$\tau_b$ psi.	$\sigma_u$ psi.	$\tau_u$ psi.	$\sigma_{bo}$ psi.	$\sigma_b/\sigma_{bo}$	$\tau_u/\tau_{bo}$	$\tau_{bo}$ psi.	$\tau_{u_0}$ psi.	$\tau_b/\tau_{bo}$	$\tau_u/\tau_{u_0}$	$M_b$ in.lb.	$M_u$ in.lb.	$M_b/m_{tb}$	$M_u/m_{tu}$
BT-1	0.0196	0.0322	1.679	4.590	10800	11100	10800	11100	7080	6990	7080	6990	14030	0.504	0.504	8360	8360	0.836	0.836	3960	3960	0.332	0.332
-3	0.0193	0.0321	1.654	4.548	9600	9850	10600	10100	6350	6300	7020	6460	13750	0.462	0.462	8100	8100	0.778	0.798	3490	3860	0.354	0.382
-5	0.0193	0.0321	1.653	4.548	18000	9000	19350	9850	11920	5760	12800	6290	13750	0.866	0.931	8100	8100	0.711	0.777	6540	7030	0.727	0.714
-7	0.0174	0.0319	1.489	4.312	9200	9200	9200	9200	6420	6520	6420	6520	11700	0.549	0.549	7580	7580	0.855	0.855	3170	3170	0.345	0.345
-9	0.0173	0.0317	1.481	4.286	9000	9000	9850	9800	6320	6420	6920	7000	11650	0.542	0.594	7490	7490	0.857	0.934	3100	3410	0.346	0.348
-9B	0.0172	0.0316	1.472	4.267	8600	8650	10000	10000	6060	6210	7050	7180	11600	0.522	0.608	7410	7410	0.838	0.969	2970	3450	0.344	0.345
-26	0.0206	0.0321	1.765	4.698	18000	9000	18000	9000	11540	5390	11540	5390	15230	0.757	0.757	8940	8940	0.603	0.603	6760	6760	0.753	0.753
-28	0.0205	0.0321	1.756	4.686	6800	13300	6800	13300	4370	8000	4370	8000	14970	0.292	0.292	8860	8860	0.903	0.903	2550	2550	0.192	0.192
-28B	0.0200	0.0320	1.714	4.622	6100	12300	6100	12300	3980	7560	3980	7560	14570	0.273	0.273	8430	8430	0.897	0.897	2260	2260	0.184	0.184
-30	0.0206	0.0320	1.765	4.691	6600	13200	6600	13200	4250	7850	4250	7850	15230	0.279	0.279	8940	8940	0.931	0.931	2480	2480	0.188	0.188
-32	0.0165	0.0321	1.411	4.219	4000	7600	5000	10000	2850	5720	3560	7540	10900	0.261	0.327	7180	7180	0.797	1.050	1340	1670	0.176	0.167
-34	0.0168	0.0317	1.436	4.225	4400	8500	4600	9200	3140	6250	3280	6780	11160	0.281	0.294	7440	7440	0.840	0.911	1500	1500	0.176	0.169
-36	0.0169	0.0318	1.445	4.244	13000	6400	13900	6850	9210	4670	9900	5000	11240	0.820	0.881	7520	7520	0.622	0.666	4430	4730	0.693	0.690
-37	0.0166	0.0318	1.419	4.209	14300	7200	16450	8400	10280	5360	11750	6260	11060	0.929	1.061	7260	7260	0.738	0.862	4820	5550	0.669	0.661
-38	0.0100	0.0196	0.852	2.562	1100	2270	1600	3200	1290	2810	1880	3960	5120	0.252	0.367	3950	3950	0.712	1.001	336	532	0.161	0.166
-40	0.0099	0.0206	0.844	2.623	2800	2730	3000	3000	3210	3410	3450	3750	5060	0.635	0.682	3870	3870	0.882	0.969	900	965	0.330	0.321
-42	0.0099	0.0208	0.844	2.637	2400	1200	4590	2300	2740	1500	5240	2880	5060	0.542	1.035	3870	3870	0.388	0.744	768	1470	0.640	0.640
-49	0.0212	0.0329	1.819	4.859	2800	13500	2800	13500	1740	7850	1740	7850	15840	0.110	0.110	8880	8880	0.884	0.884	1040	1040	0.077	0.077
-51	0.0210	0.0322	1.801	4.761	21600	5500	22850	5900	13660	3220	14400	3490	16650	0.873	0.920	8710	8710	0.370	0.401	8180	8640	1.487	1.465
-53	0.0210	0.0326	1.801	4.782	21000	3500	28900	4960	13230	2050	18110	2910	15650	0.844	1.156	8710	8710	0.235	0.334	7910	10890	2.260	2.198
-55	0.0204	0.0324	1.750	4.703	18000	1800	27700	2780	11520	1080	17750	1660	14880	0.774	1.192	8780	8780	0.123	0.189	6690	10300	3.715	3.708
-57	0.0170	0.0320	1.456	4.278	1885	9400	1895	9400	1330	6830	1375	6830	11290	0.118	0.122	7620	7620	0.896	0.896	646	649	0.069	0.069
-59	0.0169	0.0316	1.448	4.243	14000	3500	14980	3620	9940	2560	10640	2640	11200	0.887	0.949	7530	7530	0.340	0.351	4780	5110	1.366	1.411
-72	0.0168	0.0314	1.438	4.205	13000	2240	19450	3050	9300	1650	13850	2240	11200	0.831	1.240	7440	7440	0.222	0.301	4440	6650	1.982	2.180
-74	0.0167	0.0310	1.429	4.164	15190	3550	17850	4800	10980	2630	12930	3550	11120	0.986	1.161	7350	7350	0.358	0.483	5200	6120	1.465	1.275
-76	0.0104	0.0195	0.887	2.599	4800	1460	6510	1670	5560	1740	7550	2010	5470	1.016	1.380	4210	4210	0.413	0.477	1640	2220	1.124	1.328
-78	0.0099	0.0196	0.845	2.554	500	2500	900	4500	590	3130	1060	5930	5210	0.113	0.204	3880	3880	0.806	1.450	165	298	0.066	0.066
-80	0.0105	0.0202	0.895	2.663	4800	800	6320	1170	5420	940	7130	1380	5530	0.980	1.290	4290	4290	0.219	0.322	1610	2120	2.013	1.810
-82	0.0106	0.0206	0.904	2.704	4800	510	6290	600	5330	600	6990	700	5610	0.950	1.245	4370	4370	0.137	0.160	1600	2100	3.16	3.50
-84	0.0193	0.0316	1.653	4.513	13550	14000	13550	14000	9040	8950	9040	8950	13750	0.658	0.658	6820	6820	1.311	1.311	4960	4960	0.354	0.354 *
-84B	0.0193	0.0316	1.653	4.513	10670	10700	10910	10000	7140	6840	7310	6840	13750	0.519	0.532	6820	6820	1.004	1.004	3910	3910	0.399	0.399 *
-87	0.0195	0.0315	1.672	4.532	15470	15550	15470	15550	10290	9840	10290	9840	14040	0.733	0.733	6580	6580	1.495	2.131	5710	5710	0.367	0.367 **
-87B	0.0195	0.0315	1.672	4.532	14180	14400	14180	14400	9920	9100	9420	9100	14040	0.671	0.671	6580	6580	1.382	1.382	5230	5230	0.363	0.363 **

\* L = 6.5"

\*\* L = 2.5"

**TABLE X**  
 Bending Plus Torsion Tests  
 $E = 2.0 \times 10^6$  psi  
 $A = 68.9$   $L = 12.5$  in.

Spec. No.	$t_s$ in.	$t_c$ in.	$I_s$ in. <sup>4</sup>	$I_t$ in. <sup>4</sup>	$m_b$ in. lb.	$m_{t_b}$ in. lb.	$m_u$ in. lb.	$m_{t_u}$ in. lb.	$\sigma_b$ psi.	$\tau_b$ psi.	$\sigma_u$ psi.	$\tau_u$ psi.	$\sigma_{b_0}$ psi.	$\tau_{b_0}$ psi.	$\tau_{u_0}$ psi.	$\sigma_b/\sigma_{b_0}$	$\tau_b/\tau_{b_0}$	$\tau_b/\tau_{u_0}$	$\tau_u/\tau_{u_0}$	$M_b$ in. lb.	$M_u$ in. lb.	$M_b/m_{t_b}$	$M_u/m_{t_u}$	$\frac{1}{E} \frac{\tau_u}{\sigma_b}$
BT-2	0.0196	0.0321	2.939	5.842	6400	6500	13000	13000	3300	2420	6890	4840	5300	3540	5560	0.622	1.300	0.684	0.869	3220	6530	0.495	0.502	0.650
-4	0.0195	0.0319	2.924	5.810	6000	6000	12000	11820	3100	2120	6250	4250	5290	3510	5510	0.586	1.181	0.604	0.772	3020	6040	0.504	0.590	0.590
-6	0.0194	0.0319	2.909	5.792	7200	3700	15700	8000	3740	1380	8160	3000	5250	3470	5460	0.712	1.554	0.398	0.549	3620	7880	0.979	0.984	0.777
-8	0.0175	0.0320	2.621	5.454	6800	6700	10300	10450	3750	2780	5680	4340	4270	2930	5040	0.878	1.330	0.950	0.862	3270	4960	0.488	0.475	0.665
-10	0.0178	0.0319	2.666	5.501	6600	7000	11000	11000	3610	2860	6020	4460	4400	3030	5220	0.820	1.367	0.945	0.854	3190	5330	0.456	0.484	0.684
-12	0.0209	0.0320	3.134	6.068	6000	5000	19800	9700	2980	1740	9850	3390	5590	3900	6040	0.533	1.761	0.446	0.561	3100	10230	0.620	1.054	0.880
-14	0.0208	0.0321	3.119	6.057	4000	8000	7400	15400	1990	2800	3680	5400	5560	3850	5980	0.356	0.662	0.729	0.904	2060	3810	0.258	0.333	0.331
-16	0.0206	0.0316	3.089	5.986	4000	8000	7700	15100	2010	2840	3880	5320	5470	3780	5860	0.367	0.709	0.751	0.909	2060	3970	0.258	0.263	0.354
-18	0.0169	0.0317	2.531	5.325	4000	2000	16000	8000	2280	860	9040	3440	4070	2810	4890	0.555	2.220	0.306	0.704	1900	7600	0.950	0.950	1.110
-20	0.0169	0.0319	2.531	5.339	6000	3000	15600	7650	3380	1300	8800	3310	4070	2810	4890	0.830	2.160	0.463	0.676	2850	7400	0.950	0.966	1.080
-22	0.0167	0.0313	2.501	5.260	2800	5850	5850	10950	1605	2480	3240	4790	4000	2750	4780	0.401	0.810	0.903	1.001	1330	2690	0.235	0.246	0.405
-24	0.0172	0.0318	2.576	5.386	3000	6000	6200	12600	1680	2520	3480	5320	4170	2920	4880	0.403	0.835	0.862	1.090	1430	2960	0.238	0.235	0.418
-39	0.0099	0.0209	1.477	3.278	600	1200	2000	3890	550	880	1840	2860	1880	1480	2580	0.328	1.095	0.595	1.109	270	900	0.225	0.231	0.547
-43	0.0101	0.0209	1.507	3.313	1800	860	5900	2860	1640	610	5360	2060	1870	1540	2600	0.877	2.869	0.396	0.793	820	2680	0.954	0.938	1.434
-45	0.0101	0.0204	1.507	3.277	1710	860	6020	3070	1580	620	5540	2200	1870	1540	2600	0.845	2.962	0.403	0.846	790	2770	0.918	0.902	1.481
-61	0.0207	0.0320	3.100	6.035	1600	8000	3400	16250	800	2800	1700	5700	5480	3800	6360	0.146	0.310	0.737	0.898	820	1750	0.102	0.108	0.155
-63	0.0207	0.0321	3.100	6.038	10150	2110	24000	6100	5060	740	12020	2140	5480	3800	6360	0.924	2.193	0.194	0.336	5210	12310	2.465	2.020	1.096
-65	0.0207	0.0322	3.100	6.042	9000	1500	24950	4340	4500	530	12450	1520	5480	3800	6360	0.821	2.271	0.139	0.239	4620	12810	3.082	2.955	1.136
-66	0.0207	0.0323	3.100	6.058	7000	700	27600	2780	3480	240	13700	970	5480	3800	6360	0.635	2.500	0.063	0.152	3580	14100	5.110	5.070	1.250
-69	0.0169	0.0311	2.523	5.273	1600	8000	2600	13200	920	4310	1480	5580	4070	2810	4890	0.226	0.364	1.532	1.160	770	1240	0.096	0.094	0.182
-71	0.0101	0.0205	1.509	3.288	500	2500	1000	4700	460	1810	920	3400	1870	1540	2600	0.225	0.492	1.175	1.309	230	460	0.092	0.098	0.246
-73	0.0103	0.0205	1.538	3.321	1600	400	7510	1870	1460	280	6800	1180	1920	1570	2720	0.760	3.540	0.178	0.434	740	3480	1.850	2.080	1.770
-77	0.0170	0.0315	2.543	5.325	8140	1120	21000	3500	4620	490	11860	1490	4100	2850	4760	1.126	2.892	0.172	0.313	3890	10030	3.470	2.865	1.446
-83	0.0170	0.0312	2.543	5.305	5000	500	23020	2270	2850	210	13100	970	4110	2850	4760	0.694	3.189	0.074	0.024	2400	11050	4.800	4.865	1.594
-85	0.0196	0.0321	2.935	5.840	8000	8000	12000	12000	4140	2960	6200	4440	5120	6550	8060	0.768	1.150	0.452	0.551	4020	6030	0.503	0.502	0.575 *
-85A	0.0190	0.0321	2.935	5.840	7680	8000	16100	16050	3960	2960	8340	5960	4890	6240	7740	0.810	1.705	0.474	0.770	3860	8090	0.483	0.504	0.852 *
-88	0.0194	0.0318	2.905	5.785	10000	10000	16000	16000	5220	3740	8370	5950	5420	7440	11150	0.963	1.555	0.503	0.534	5020	8040	0.502	0.502	0.778 **
-88A	0.0194	0.0318	2.905	5.785	8980	8850	19380	19500	4640	3300	10150	7250	5420	8050	12390	0.868	1.873	0.411	0.585	4510	9740	0.510	0.499	0.936 **

\* L = 6.5"

\*\* L = 2.5"

TABLE XI  
 Bending Plus Torsion Tests  
 $\epsilon = 3.0$   $E = 10.3 \times 10^6$  psi  
 $A = 97.4$  sq.in.,  $L = 12.5$  in.

Spec. No.	$t_s$ in.	$t_c$ in.	$I_s$ in. <sup>4</sup>	$I_t$ in. <sup>4</sup>	$m_b$ in.lb.	$m_{tb}$ in.lb.	$m_u$ in.lb.	$m_{tu}$ in.lb.	$\sigma_b$ psi.	$\tau_b$ psi.	$\sigma_u$ psi.	$\tau_u$ psi.	$\sigma_{b0}$ psi.	$\tau_{b0}$ psi.	$\sigma_{u0}$ psi.	$\tau_{u0}$ psi.	$M_b$ in.lb.	$M_u$ in.lb.	$M_b/M_{tb}$	$M_u/M_{tu}$	$\frac{1}{E} \frac{\sigma_u}{\sigma_b}$			
BT-11	0.0197	0.0318	4.219	7.104	4650	4900	15700	15600	1970	1280	6650	4040	2820	0.699	2.353	1920	4600	0.666	0.878	2760	9330	0.564	0.598	0.786
-13	0.0193	0.0318	4.134	7.007	5000	4850	15700	15650	2150	1280	6750	4150	2730	0.788	2.472	1890	4540	0.677	0.914	2940	9250	0.606	0.591	0.824
-15	0.0202	0.0318	4.327	7.212	5350	3000	22000	11000	2450	760	9190	2790	2920	0.839	3.147	1960	4700	0.388	0.594	3510	13200	1.170	1.200	1.049
-17	0.0206	0.0317	4.412	7.316	4200	2100	20000	10000	1740	530	8230	2480	3010	0.578	2.734	2010	4750	0.264	0.522	2530	12080	1.204	1.208	0.911
-19	0.0206	0.0319	4.412	7.331	3600	7850	9000	17700	1480	1950	3700	4400	3010	0.493	1.229	2010	4750	0.970	0.926	2160	5430	0.276	0.307	0.410
-19A	0.0204	0.0322	4.369	7.304	3400	7100	8650	17100	1400	1780	3550	4280	2960	0.473	1.199	1970	4660	0.904	0.918	2030	5170	0.286	0.303	0.400
-21	0.0198	0.0317	4.241	7.122	3000	6000	8250	16850	1270	1510	3480	4260	2830	0.449	1.230	1940	4650	0.778	0.916	1790	4910	0.298	0.292	0.410
-23	0.0178	0.0317	3.809	6.629	2500	1600	13200	13200	1140	460	6020	3820	2420	0.471	2.488	2220	5490	0.207	0.696	1440	7590	0.900	0.575	0.829
-25	0.0166	0.0308	3.548	6.266	2000	4000	7400	15000	960	1240	3560	4650	2180	0.440	1.633	1560	3810	0.795	1.220	1130	4180	0.283	0.279	0.544
-27	0.0174	0.0318	3.723	6.538	2000	4000	7650	15050	920	1180	3540	4450	2330	0.395	1.519	1680	4090	0.702	1.088	1140	4360	0.285	0.289	0.506
-29	0.0173	0.0315	3.702	6.492	2800	2900	12650	12600	1300	860	5900	3750	2310	0.563	2.554	1660	4040	0.518	0.928	1600	7210	0.561	0.572	0.851
-31	0.0175	0.0319	3.744	6.570	4000	2000	17700	8800	1840	590	8120	2580	2350	0.783	3.455	1700	4140	0.347	0.623	2280	10090	1.140	1.146	1.152
-33	0.0170	0.0321	3.638	6.463	2000	1030	18400	9200	930	310	8510	2790	2260	0.412	3.765	1620	4000	0.191	0.698	1120	10340	1.089	1.126	1.255
-44	0.0099	0.0206	2.110	3.890	700	1400	2370	4720	540	730	1840	2440	1000	0.540	1.840	840	2070	0.869	1.179	380	1290	0.272	0.273	0.613
-46	0.0100	0.0202	2.131	3.884	900	900	3800	3800	710	460	2960	1960	1020	0.696	2.902	860	2110	0.535	0.929	490	2080	0.545	0.548	0.967
-47	0.0098	0.0203	2.089	3.843	1260	640	4320	2220	990	340	3370	1150	990	1.000	3.404	820	2020	0.415	0.569	690	2350	1.079	1.069	1.135
-48	0.0212	0.0316	4.550	7.469	1700	8500	3730	18100	690	2050	1510	4360	3140	0.220	0.481	2100	5040	0.976	0.865	1040	2280	0.123	0.126	0.160
-50	0.0211	0.0318	4.526	7.461	4000	1000	20000	5000	1620	240	8110	1220	3120	0.519	2.599	2080	4990	0.115	0.244	2430	12130	2.430	2.430	0.866
-52	0.0211	0.0326	4.526	7.509	7240	1190	20500	3500	2890	290	8080	850	3120	0.926	2.589	2080	4990	0.058	0.194	4360	12350	3.661	3.530	0.863
-54	0.0202	0.0327	4.330	7.295	3000	300	19040	2000	1240	80	7900	510	2920	0.425	2.705	1960	4700	0.041	0.108	1780	11310	5.940	5.660	0.902
-54A	0.0202	0.0327	4.330	7.295	8000	800	24950	2500	3320	200	10310	640	2920	1.137	3.531	1960	4700	0.102	0.136	4750	14810	5.940	5.940	1.177
-55	0.0171	0.0319	3.657	6.477	1100	5300	2850	14200	510	1680	1520	4260	2270	0.225	0.591	1640	4050	1.024	1.052	620	1610	0.111	0.113	0.194
-58	0.0170	0.0312	3.633	6.393	1540	400	17800	4370	730	120	8410	1320	2260	0.323	3.721	1620	4000	0.074	0.330	870	10110	2.175	2.314	1.240
-60	0.0170	0.0319	3.633	6.452	3580	600	18600	3260	1870	180	8650	990	2260	0.739	3.827	1620	4000	0.111	0.248	2020	10480	3.365	3.215	1.276
-62	0.0168	0.0320	3.583	6.400	1340	250	20900	2200	630	80	9850	670	2210	0.285	4.457	1580	3900	0.051	0.172	750	11700	3.000	5.320	1.486
-64	0.0100	0.0205	2.131	3.906	450	2250	1000	5000	350	1160	770	2570	1020	0.343	0.755	860	2110	1.345	1.218	250	550	0.111	0.110	0.252
-67	0.0100	0.0203	2.131	3.890	1200	300	6160	1730	930	160	4780	890	1020	0.912	4.686	860	2110	0.168	0.422	660	3380	2.200	1.952	1.562
-68	0.0099	0.0200	2.110	3.865	1500	250	7240	1230	1170	130	5640	640	1000	1.170	5.640	840	2070	0.155	0.309	820	3950	3.280	3.210	1.880
-70	0.0100	0.0100	2.131	3.870	1500	250	6690	900	1160	130	5180	460	1020	1.137	5.078	860	2110	0.151	0.218	1380	3680	5.520	4.090	1.693
-86	0.0193	0.0319	4.140	7.023	4000	4000	12000	12000	1720	1060	5180	3200	2730	0.630	1.896	2540	6000	0.417	0.534	2360	7070	0.590	0.589	0.632 *
-86A	0.0193	0.0319	4.140	7.023	6000	5200	17020	17300	2560	1390	7300	4620	2730	0.937	2.671	2540	6000	0.547	0.771	3500	10030	0.679	0.580	0.890 *
-89	0.0195	0.0317	4.180	7.055	8000	8000	18000	18000	3440	2100	7730	4750	3510	0.980	2.200	5330	10020	0.394	0.474	4740	10660	0.593	0.593	0.733 **
-89A	0.0195	0.0317	4.180	7.055	7000	7000	18410	24300	3000	1840	7900	6420	3510	0.855	2.249	5330	10020	0.346	0.640	4150	10890	0.593	0.592	0.750 **

\* L = 6.5"

\*\* L = 2.5"

TABLE XII

## Bending Plus Direct Shear Tests

$\epsilon = 1.0$        $E = 10.3 \times 10^6$  psi  
 $b = 3.01'' = a$ ,  $L = 6.5''$  except where noted

Spec. No.	$t_s$ in.	$I_s$ in <sup>4</sup>	$I_t$ in <sup>4</sup>	$A_g$ sq.in.	$l$ in.	F lb.	$\frac{M}{Fb}$	$\tau_b$ psi	$\sigma_b$ psi	$\sigma_{b0}$ psi	$\frac{\sigma_b}{\sigma_{b0}}$
BS-10	0.0215	1.844	5.161	0.407	14.6	1570	1.737	3850	13390	16430	0.814
-11	"	"	"	"	80.0	310	9.496	760	14410	"	0.877
-11B	"	"	"	"	80.0	270	9.496	660	12590	"	0.760
-12	"	"	5.406	"	29.1	750	3.292	1840	12120	"	0.738
-12B	"	"	5.650	"	29.1	1170	3.150	3870	18140	"	1.104
-13	"	"	"	"	38.3	640	4.153	1570	13050	"	0.784
-13B	"	"	"	"	38.3	820	4.153	2010	16710	"	1.019
-15B	"	"	5.650	"	53.1	610	5.752	1500	17230	"	1.049
-16	"	"	"	"	4.9	2350	0.529	5760	6140	"	0.374
-17	0.0165	1.411	5.089	0.312	4.9	960	0.451	3080	2780	11130	0.250
-18	"	"	"	"	10.1	1140	0.931	3650	6810	"	0.611
-19	"	"	"	"	14.6	1040	1.346	3330	8990	"	0.807
-20	0.0220	1.887	5.204	0.416	10.1	2620	1.210	6300	15210	17050	0.891
-21	0.0215	1.844	5.161	0.407	64.8	350	7.700	860	13220	16430	0.805
-21B	"	"	"	"	32.5	1050	3.865	2580	19900	16430	1.211
-22	0.0165	1.411	5.089	0.312	10.1	1330	0.931	4260	7950	11130	0.714
-23	"	"	"	"	79.8	300	7.360	960	14150	"	1.270
-23B	"	"	"	"	59.2	260	5.460	830	9100	"	0.816
-24	"	"	"	"	38.4	380	3.540	1220	8630	"	0.774
-24B	"	"	"	"	38.4	340	3.540	1090	7730	"	0.694
-25	"	"	"	"	36.1	690	3.330	2210	14710	"	1.320
-64	0.0101	0.861	2.167	0.191	79.8	62	10.52	320	6870	5350	1.282
-64B	"	"	"	"	"	64	10.52	340	7100	"	1.327
-65	"	"	2.624	"	59.4	98	6.47	510	6690	"	1.250
-65B	"	"	"	"	"	75	6.47	390	5110	"	0.955
-66	0.0100	0.852	2.554	0.189	41.0	130	4.060	690	6290	5150	1.221
-66B	"	"	"	"	"	114	"	600	5510	5150	1.070
-67	0.0103	0.878	2.611	0.194	29.6	200	3.250	1000	6830	5750	1.187
-67B	"	"	"	"	"	160	"	820	5460	5750	0.950
-68	0.0100	0.852	2.583	0.189	19.8	310	2.170	1640	7150	5150	1.388
-68B	"	"	"	"	"	260	"	1370	5990	5150	1.162
-69	"	"	2.590	"	9.9	310	1.081	1640	3570	5150	0.692
-70	0.0101	0.861	2.617	0.191	"	350	1.084	1830	3990	5350	0.776
* -57B	0.0196	1.679	4.456	0.371	79.9	310	9.800	840	16420	14510	1.131
* -58B	0.0205	1.758	4.607	0.388	14.2	1690	1.790	4350	15650	15250	1.027
* -59	0.0100	0.852	2.583	0.189	41.4	120	4.540	630	5790	5150	1.125
* -59B	"	"	"	"	19.9	300	2.185	1590	6950	5150	1.350

\* L = 16.0 in.

TABLE XIII

Bending Plus Shear Tests

$\epsilon = 2.0$   $E = 10.3 \times 10^6$  psi

$b = 3.01$  in.  $a = 6.02$  in.

$L = 6.5$  in. except where noted

Spec. No.	$t_s$ in.	$I_s$ in <sup>4</sup>	$I_t$ in <sup>4</sup>	$A_s$ sq.in.	$l$ in.	F lb.	$\frac{M}{Fb}$	$\tau_b$ psi	$\sigma_b$ psi	$\sigma_{b_0}$ psi	$\frac{\sigma_b}{\sigma_{b_0}}$
BS-37	0.0200	2.999	5.835	0.583	79.8	150	13.32	260	6180	5260	1.172
-37B	"	"	"	"	"	230	"	400	9360	"	1.780
-38	0.0210	3.152	6.019	0.613	10.1	1510	1.76	2470	7670	5670	1.355
-39	"	"	"	"	23.0	590	4.00	960	6710	"	1.183
-39B	"	"	"	"	"	780	"	1270	8870	"	1.565
-40	"	"	"	"	35.6	400	6.18	650	7120	"	1.255
-40B	"	"	"	"	"	370	"	600	6590	"	1.161
-41	"	"	"	"	50.4	340	8.76	560	8560	"	1.510
-41B	"	"	"	"	64.8	220	11.26	360	7140	"	1.529
-41C	"	"	"	"	4.9	1510	0.85	2460	3700	"	0.652
-71	0.0104	1.552	3.266	0.303	8.0	370	1.26	1220	2760	1970	1.401
-71B	"	"	"	"	8.2	280	1.30	920	2140	"	1.087
-73	0.0103	1.537	3.262	0.300	14.4	150	2.26	500	1990	1950	1.020
-73B	"	"	"	"	"	170	"	570	2020	"	1.035
-74	0.0104	1.552	3.273	0.303	19.5	120	3.08	400	2150	1970	1.091
-74B	"	"	"	"	"	140	"	460	2510	"	1.272
-76	"	"	"	"	28.9	140	4.53	460	3720	"	1.889
-76B	"	"	"	"	"	140	"	460	3720	"	1.889
-78	0.0102	1.522	3.281	0.297	41.2	75	6.37	250	2830	1920	1.472
-78B	"	"	"	"	"	75	"	250	2830	"	1.472
-80	0.0100	1.492	3.223	0.291	59.1	32	9.10	110	1770	1860	0.951
-80B	"	"	"	"	"	47	"	165	2590	"	1.391
-82	"	"	"	"	79.8	35	12.26	120	2610	"	1.402
-82B	"	"	"	"	"	38	"	130	2830	"	1.510
-84	0.0175	2.621	5.490	0.510	79.8	170	12.65	330	7440	4310	1.725
-84B	"	"	"	"	"	170	"	330	7440	"	1.725
-86	0.0174	2.606	5.472	0.507	59.4	220	9.41	430	7190	4270	1.681
-86B	"	"	"	"	"	210	"	410	6860	"	1.605
-87	0.0173	2.591	5.396	0.504	38.5	250	6.15	500	5380	4240	1.269
-87B	"	"	"	"	"	320	"	640	6880	"	1.621
-89	0.0170	2.546	5.313	0.496	23.4	390	3.73	790	5160	4130	1.220
-89B	"	"	"	"	"	440	"	890	5830	"	1.578
-91	0.0172	2.576	5.356	0.501	19.5	440	3.12	880	4820	4200	1.148
-91B	"	"	"	"	"	620	"	1240	6800	"	1.619
-93	"	"	"	"	14.4	710	2.29	1420	5740	"	1.366
-93B	"	"	"	"	"	770	"	1540	6240	"	1.485
-95	"	"	"	"	4.9	1080	0.77	2160	2970	"	0.707
* -60	0.0199	2.984	5.889	0.580	24.6	620	4.14	1070	7790	5220	1.491
* -60B	"	"	"	"	14.5	880	2.44	1520	6530	"	1.250
* -61	0.0099	1.477	3.205	0.288	29.0	95	4.44	370	2590	1830	1.415
* -61B	"	"	"	"	14.5	200	2.22	770	2720	"	1.486

\* L = 16.0 in.

TABLE XIV

## Bending Plus Direct Shear Tests

 $\epsilon = 3.0$ ,  $E = 10.3 \times 10^6$  psi $b = 3.01$  in.,  $a = 9.03$  in. $L = 6.5$  in. except where noted

Spec. No.	$t_s$ in.	$I_s$ in <sup>4</sup>	$I_t$ in <sup>4</sup>	$A_s$ sq.in.	$l$ in.	F lb.	$\frac{M}{Fb}$	$\tau_b$ psi	$\sigma_b$ psi	$\sigma_{b0}$ psi	$\frac{\sigma_b}{\sigma_{b0}}$
BS-34	0.0200	4.284	7.120	0.804	19.6	480	3.294	600	3970	2920	1.360
-34B	"	"	"	"	"	920	"	1150	7620	"	2.605
-35	"	"	"	"	35.6	260	7.122	325	3920	"	1.341
-35B	"	"	"	"	68.9	110	13.78	135	3210	"	1.099
-36	"	"	"	"	10.1	970	2.025	1210	4140	"	1.418
-36B	"	"	"	"	"	1520	"	1890	6490	"	2.220
-56	0.0197	4.219	7.089	0.792	53.1	150	10.50	190	3380	2820	1.199
-56B	"	"	"	"	77.5	120	15.33	150	3920	"	1.390
-72	0.0101	2.152	3.879	0.405	10.1	130	1.870	320	1020	1040	0.981
-75	0.0105	2.238	3.955	0.421	19.5	110	3.670	260	1630	1100	1.469
-75B	"	"	"	"	"	100	"	240	1480	"	1.333
-77	0.0104	2.216	3.952	0.417	23.4	100	4.363	240	1780	1090	1.631
-77B	"	"	"	"	"	74	"	175	1320	"	1.211
-79	"	"	"	"	29.6	120	5.505	290	2710	"	2.485
-79B	"	"	"	"	"	81	"	195	1830	"	1.679
-81	0.0101	2.152	3.886	0.405	47.4	48	8.732	120	1720	1040	1.652
-81B	"	"	"	"	"	41	"	100	1470	"	1.413
-83	0.0100	2.131	3.891	0.401	59.4	87	10.84	215	4000	1030	2.880
-83B	"	"	"	"	"	53	"	130	2440	"	2.370
-85	0.0104	2.216	3.980	0.417	79.8	97	14.79	230	5850	1090	5.360
-85B	"	"	"	"	"	46	"	110	2780	"	2.550
-88	0.0178	3.809	6.636	0.715	79.8	90	15.22	125	3260	2480	1.312
-88B	"	"	"	"	"	90	"	125	3260	"	1.312
-90	0.0170	3.638	6.405	0.683	59.3	120	11.20	175	3330	2270	1.466
-90B	"	"	"	"	"	100	"	145	2780	"	1.223
-92	0.0175	3.745	6.549	0.703	38.5	145	7.315	205	2570	2370	1.083
-92B	"	"	"	"	"	185	"	265	3270	"	1.380
-94	0.0179	3.830	6.660	0.719	29.6	215	5.662	300	2910	2460	1.181
-94B	"	"	"	"	"	295	"	410	3990	"	1.621
-96	0.0175	3.745	6.572	0.703	19.5	385	3.694	550	3440	3280	1.445
-96B	"	"	"	"	"	370	"	530	3310	"	1.432
-97	0.0173	3.702	6.485	0.695	14.3	470	2.715	680	3130	2340	1.338
-97B	"	"	"	"	"	370	"	530	2440	"	1.041
-98	"	"	"	"	9.8	620	1.859	890	2820	"	1.203
-98B	"	"	"	"	"	680	"	980	3100	"	1.324
* -28	0.0200	4.284	7.120	0.804	89.4	110	17.87	135	4160	2850	1.459
* -28B	"	"	"	"	"	95	"	120	3590	"	1.260
* -29	"	"	"	"	19.6	670	3.924	840	5550	"	1.948
* -29B	"	"	"	"	"	430	"	540	3570	"	1.252
* -30	"	"	"	"	35.6	330	7.122	410	4960	"	1.740
* -30B	"	"	"	"	"	330	"	410	4960	"	1.740
* -31	"	"	"	"	47.9	230	9.583	290	4650	"	1.631
* -32	"	"	"	"	68.9	145	13.77	180	4230	"	1.482
* -33	"	"	"	"	53.8	115	10.74	145	2620	"	0.912
* -33B	"	"	"	"	"	195	"	245	4440	"	1.558
* -62	0.0197	4.219	7.133	0.792	15.4	620	3.034	770	4030	2790	1.443
* -63	0.0100	2.121	3.884	0.401	24.0	85	4.376	210	1580	1010	1.564

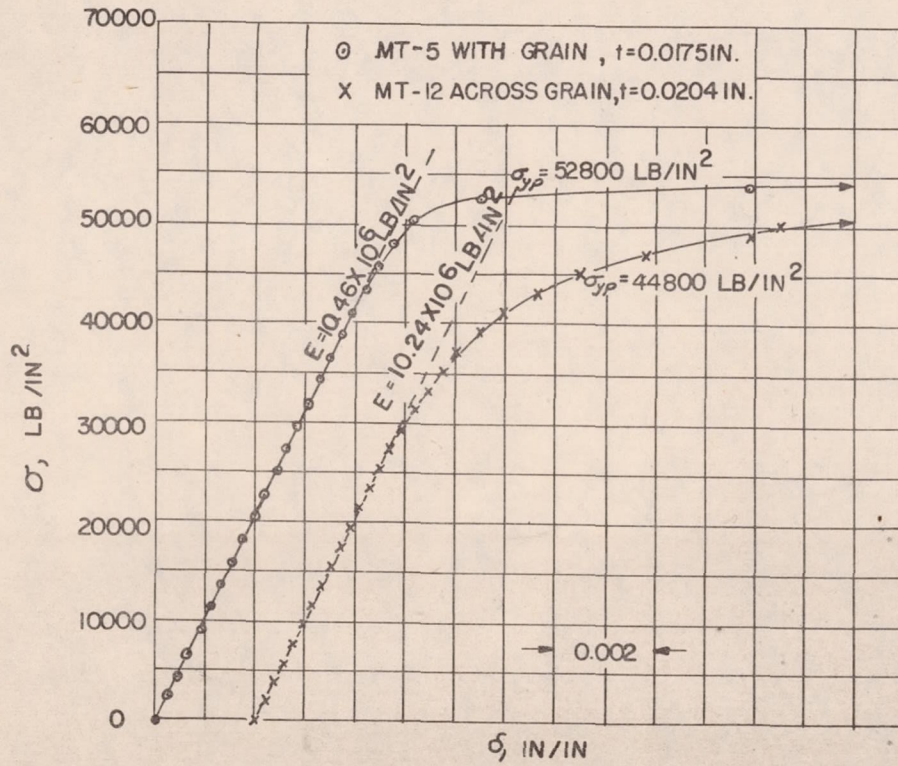


Figure 1.- Typical tensile stress-strain curves for 24S-T aluminum alloy sheet used in specimens.

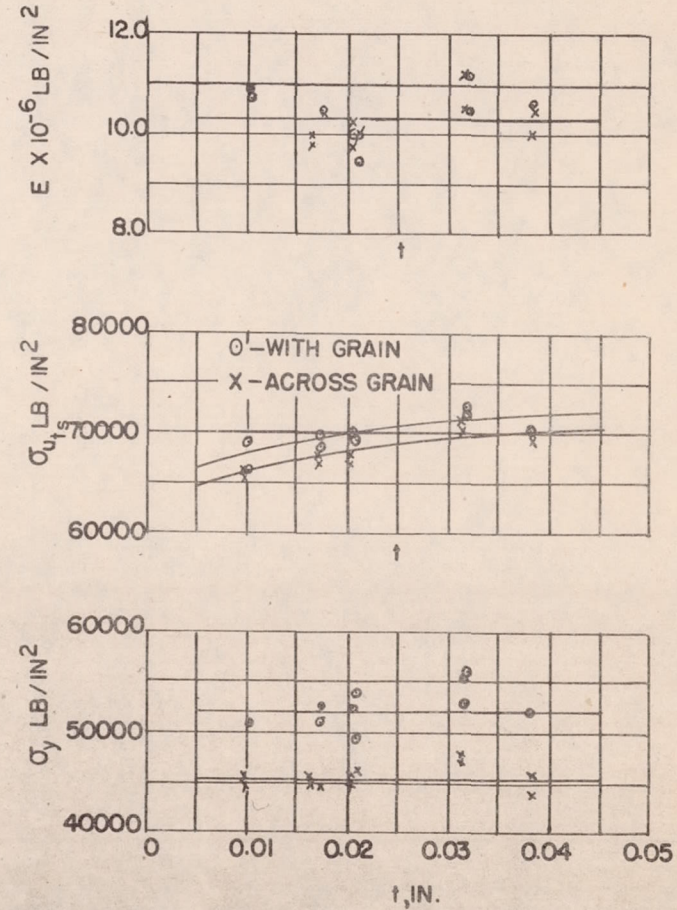


Figure 2.- Tensile properties of 24S-T aluminum alloy sheet used in specimens.

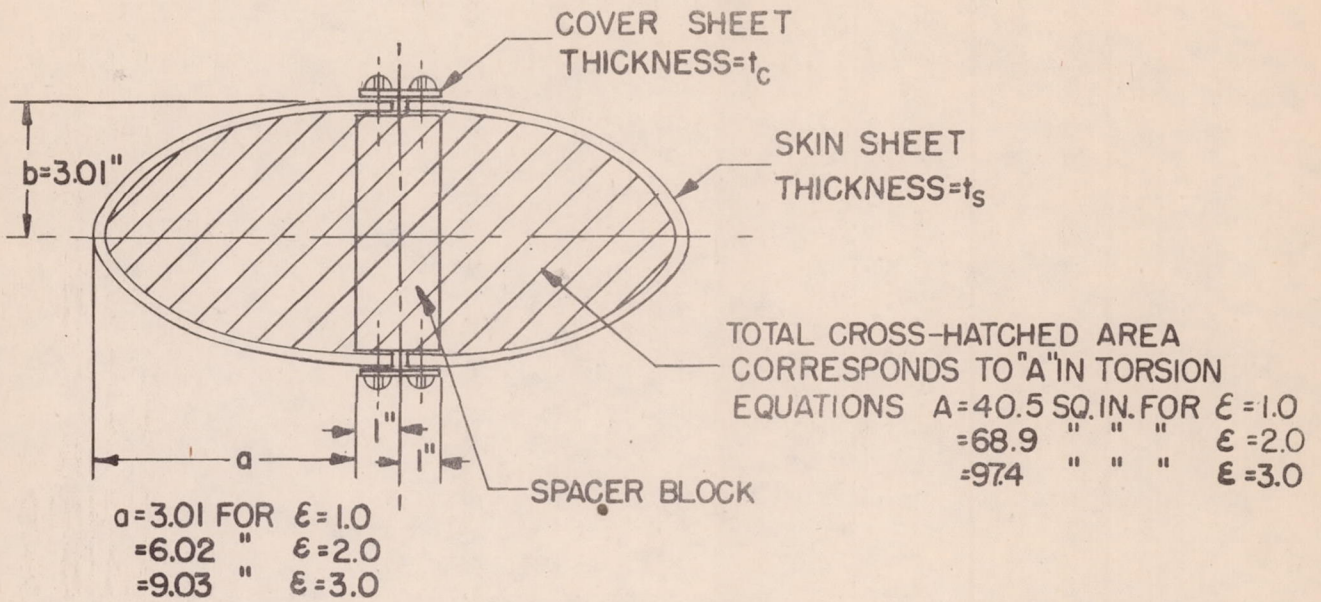


Figure 3a.- Cross section of specimen.

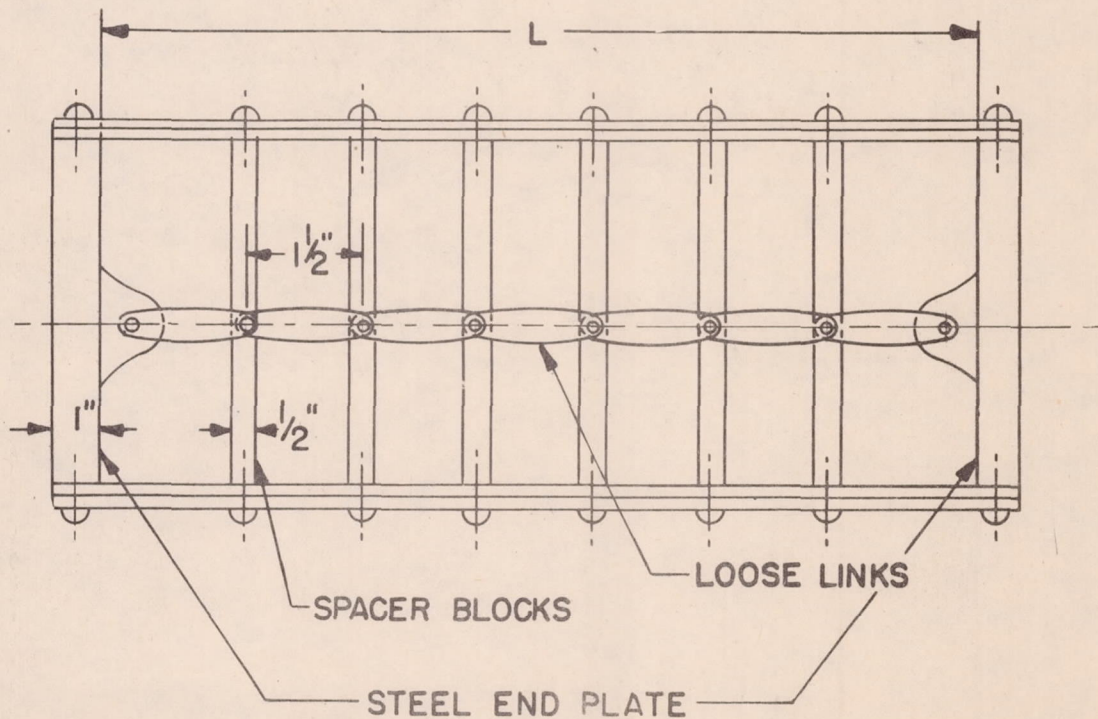


Figure 3b.- Longitudinal section of specimen showing spacer blocks.

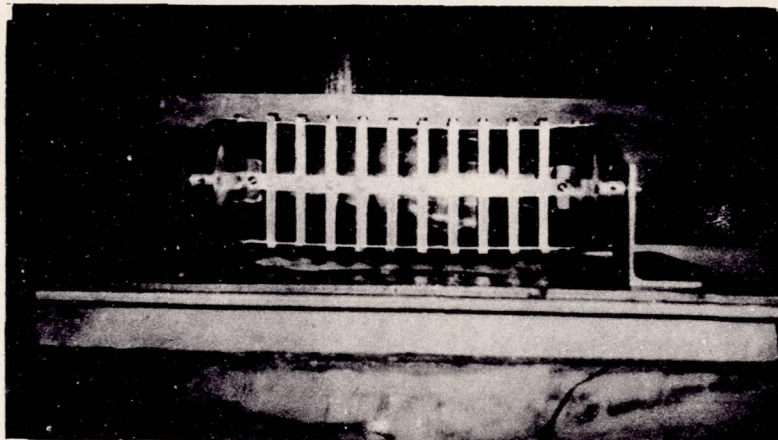


Figure 3c.- Exposed section of test specimen showing details of construction.

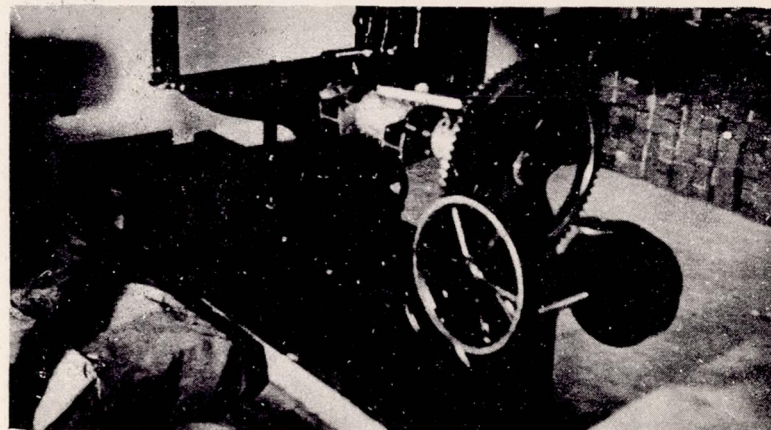


Figure 4.- Testing machine and apparatus used for pure torsion tests.

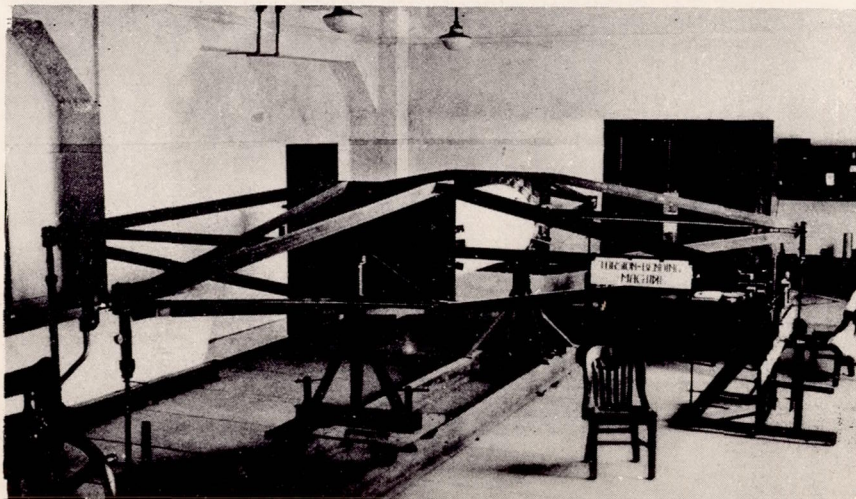


Figure 5.- Testing machine used for pure bending and bending plus torsion tests.

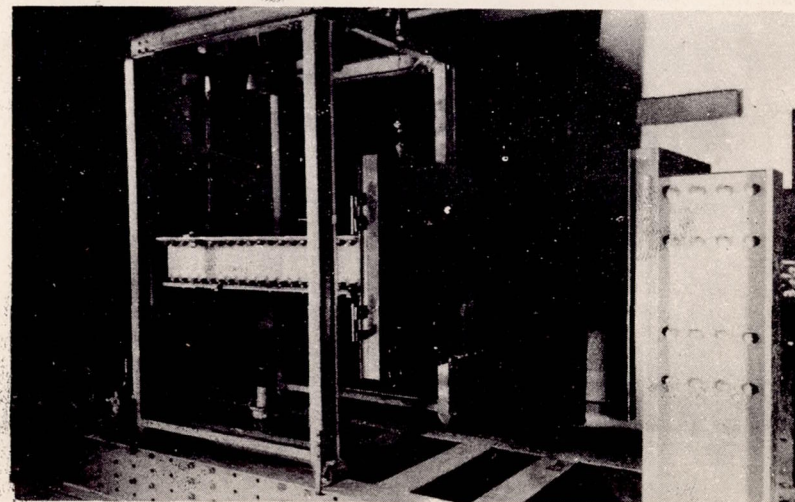
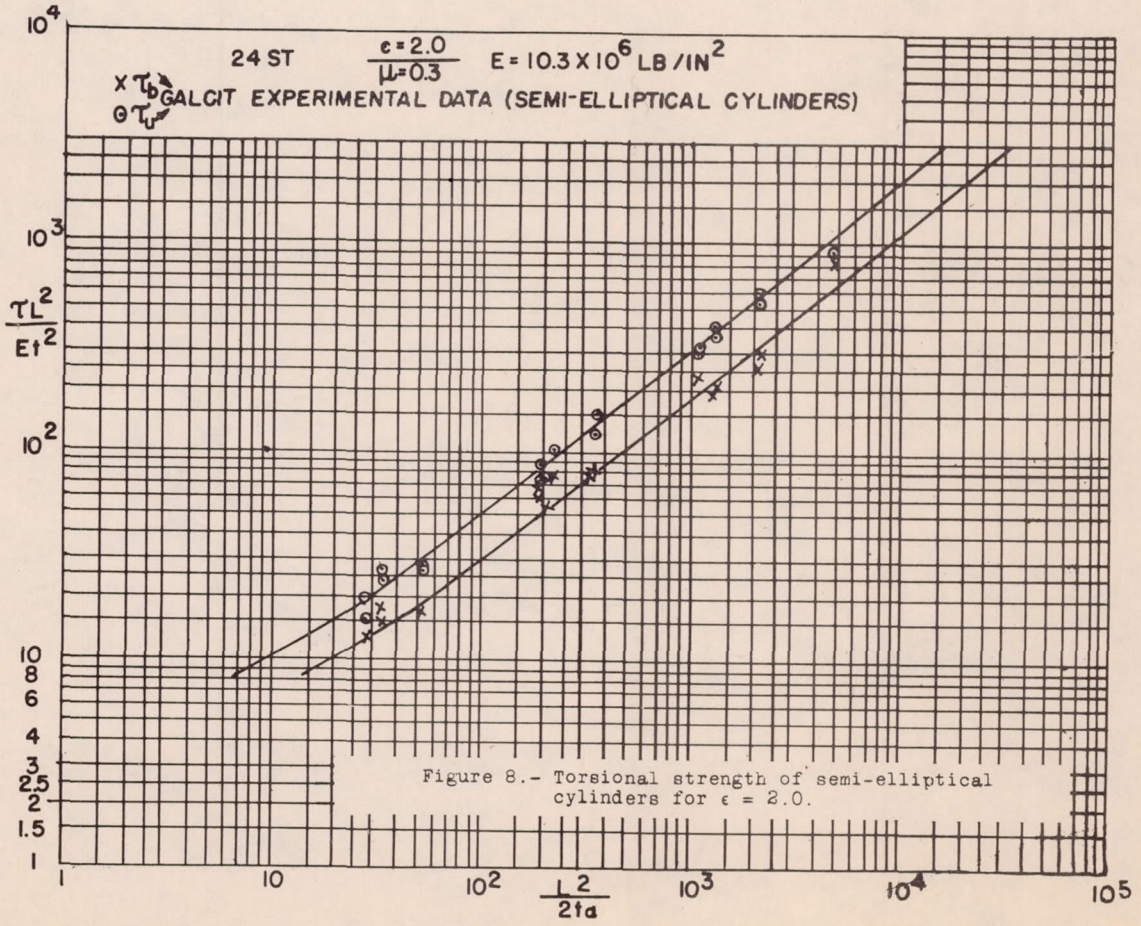
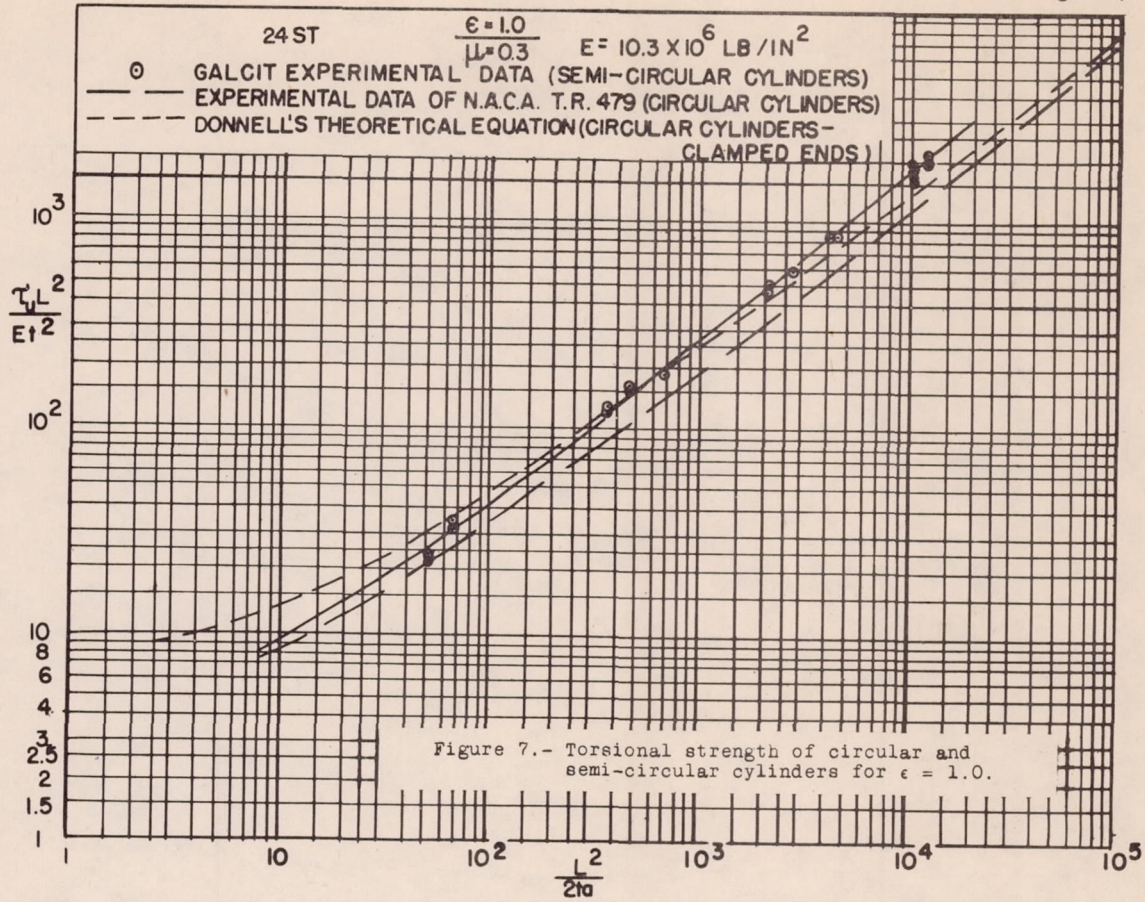
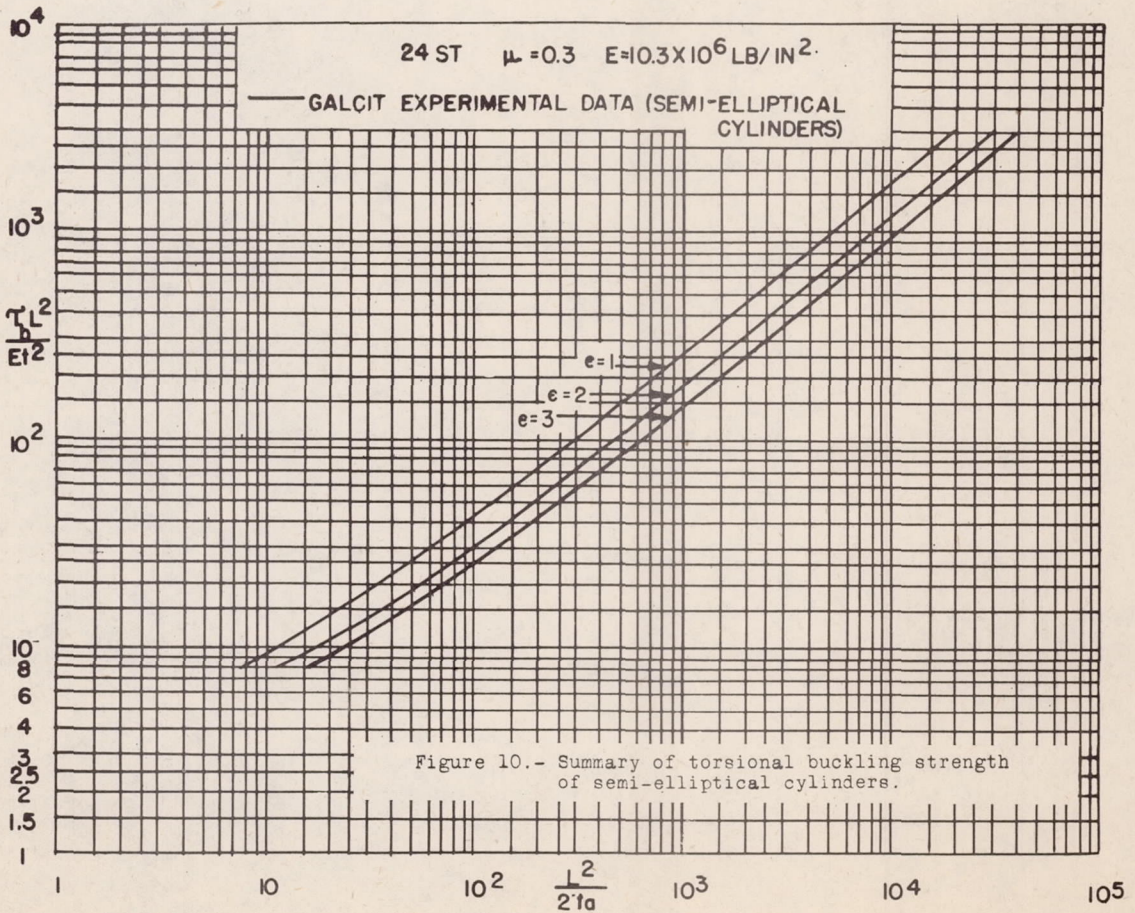
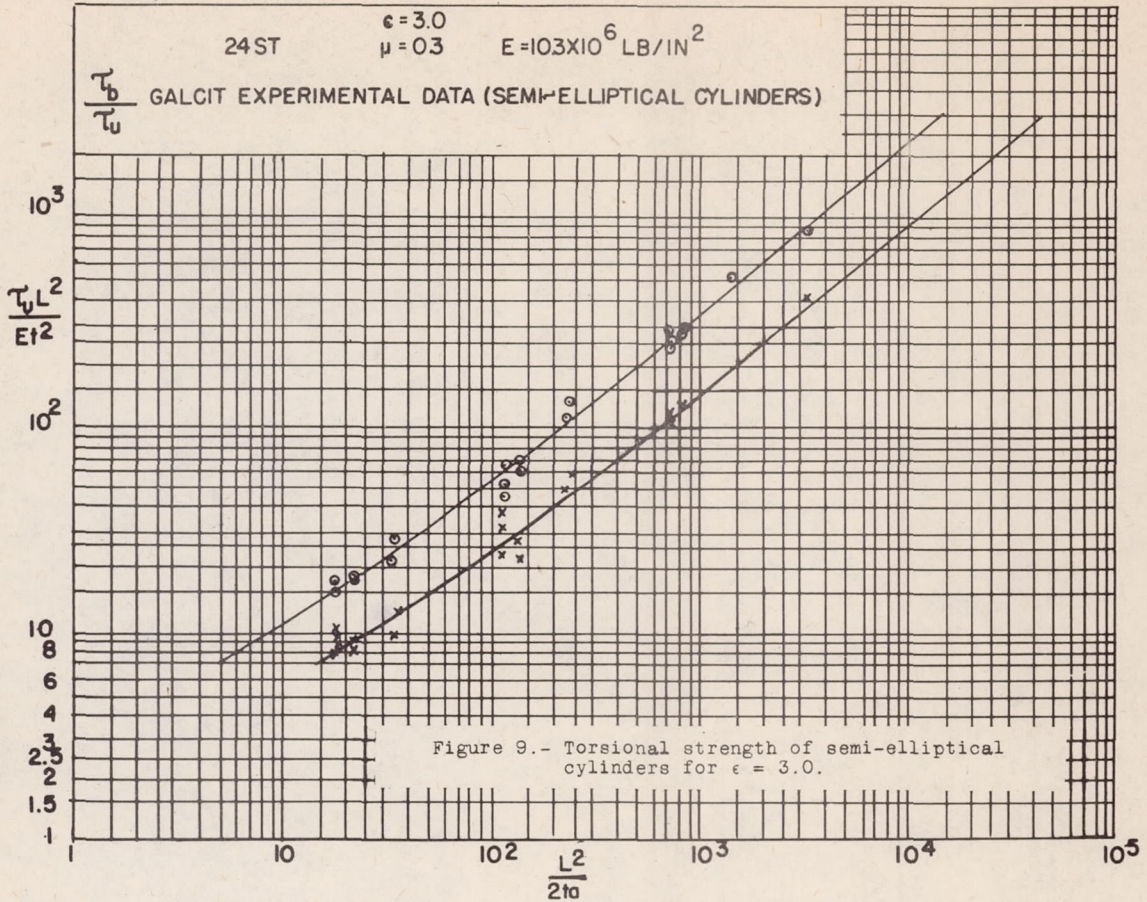
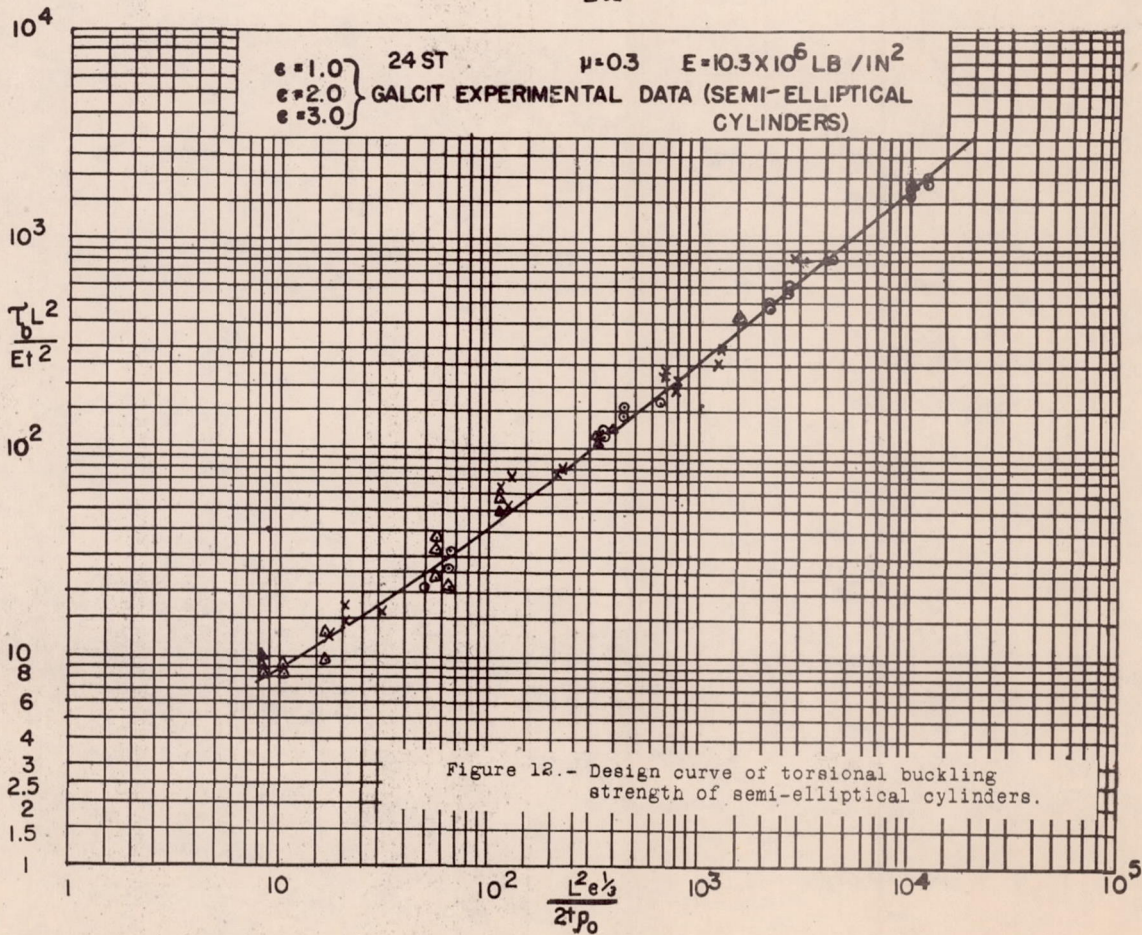
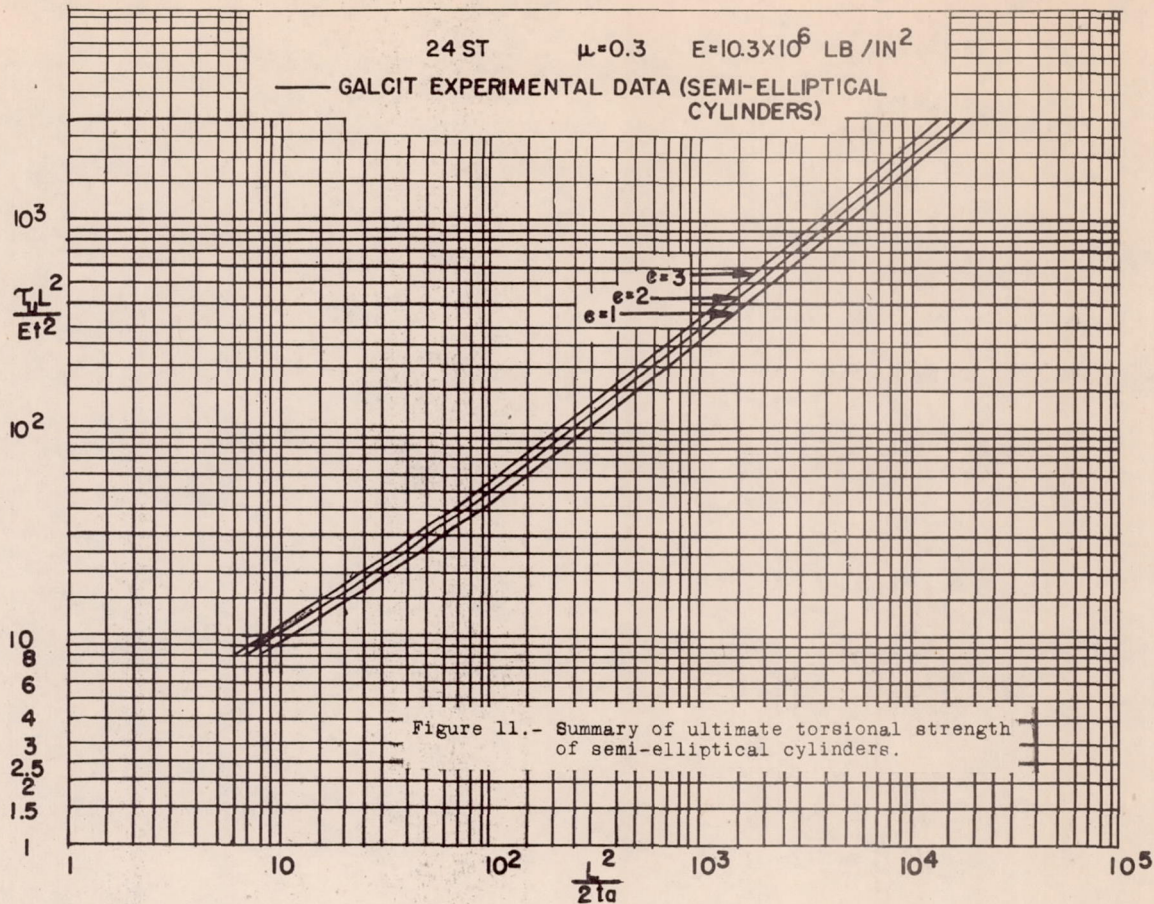


Figure 6.- Testing machine used for bending plus shear tests.







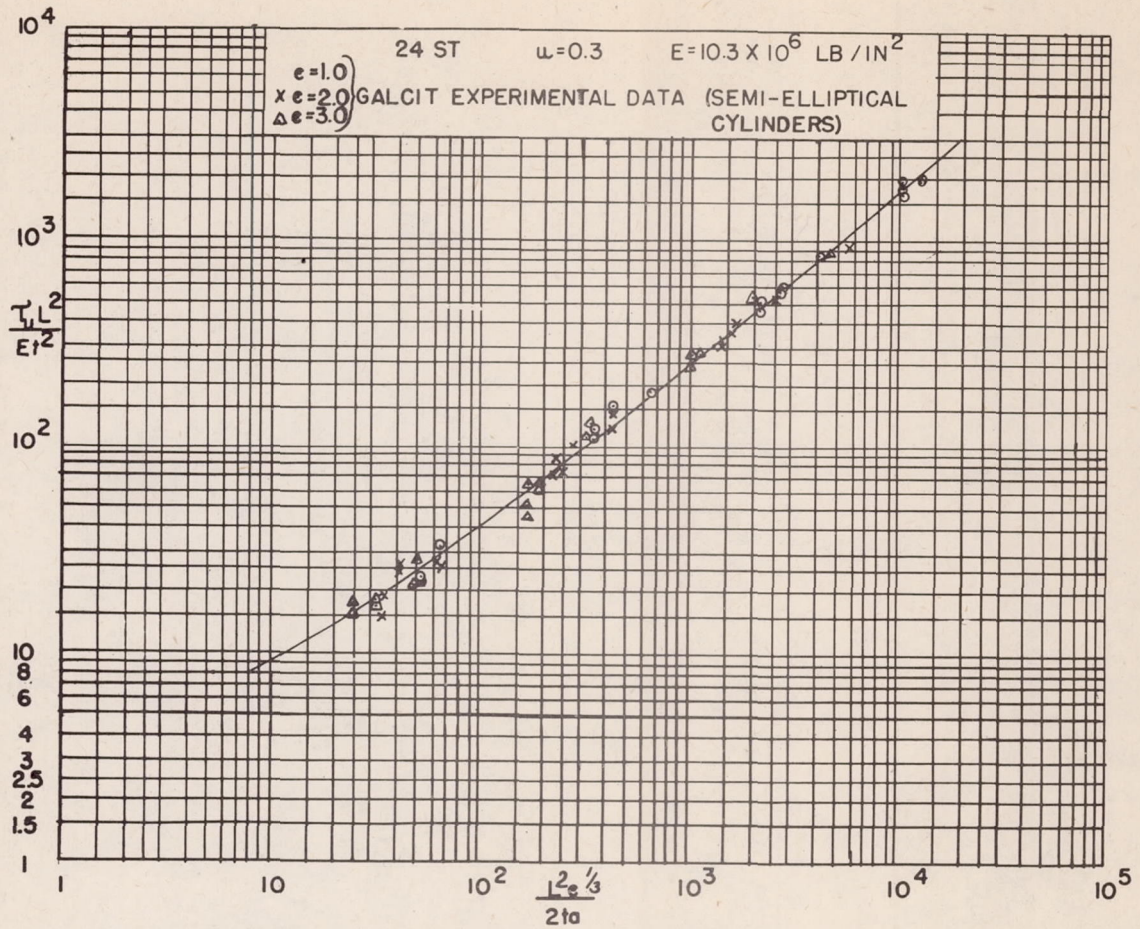


Figure 13.- Design curve of ultimate torsional strength of semi-elliptical cylinders.

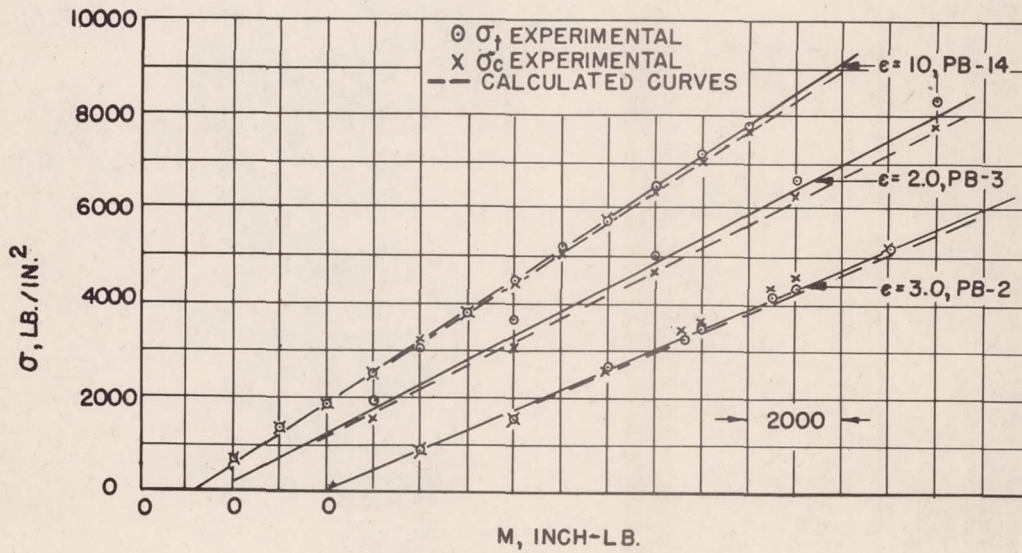


Figure 14.- Comparison of experimental and calculated normal stresses for pure bending (below buckling).

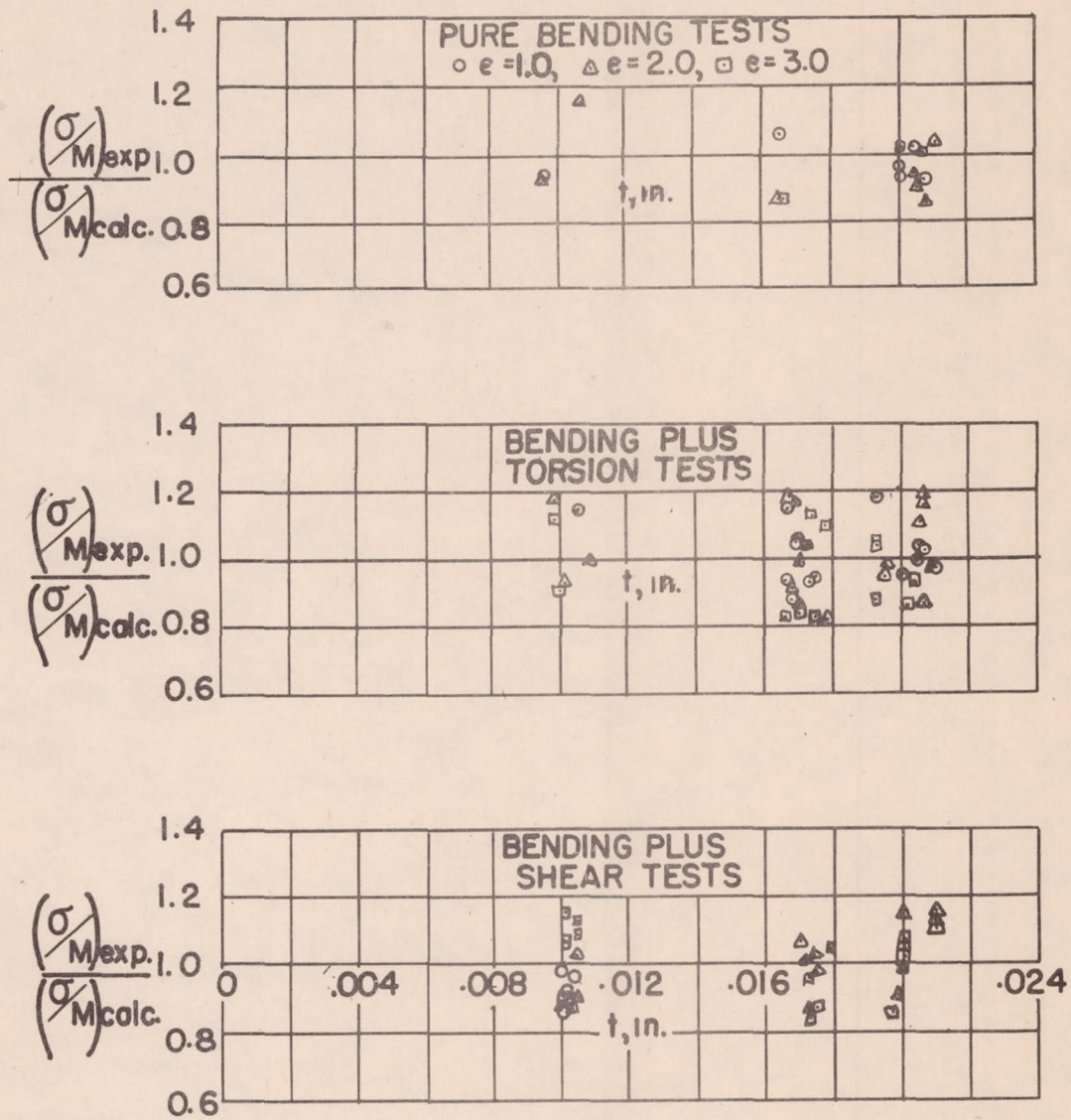


Figure 15.- Comparison of experimental and calculated normal stresses due to bending deformation taken just below the buckling load.

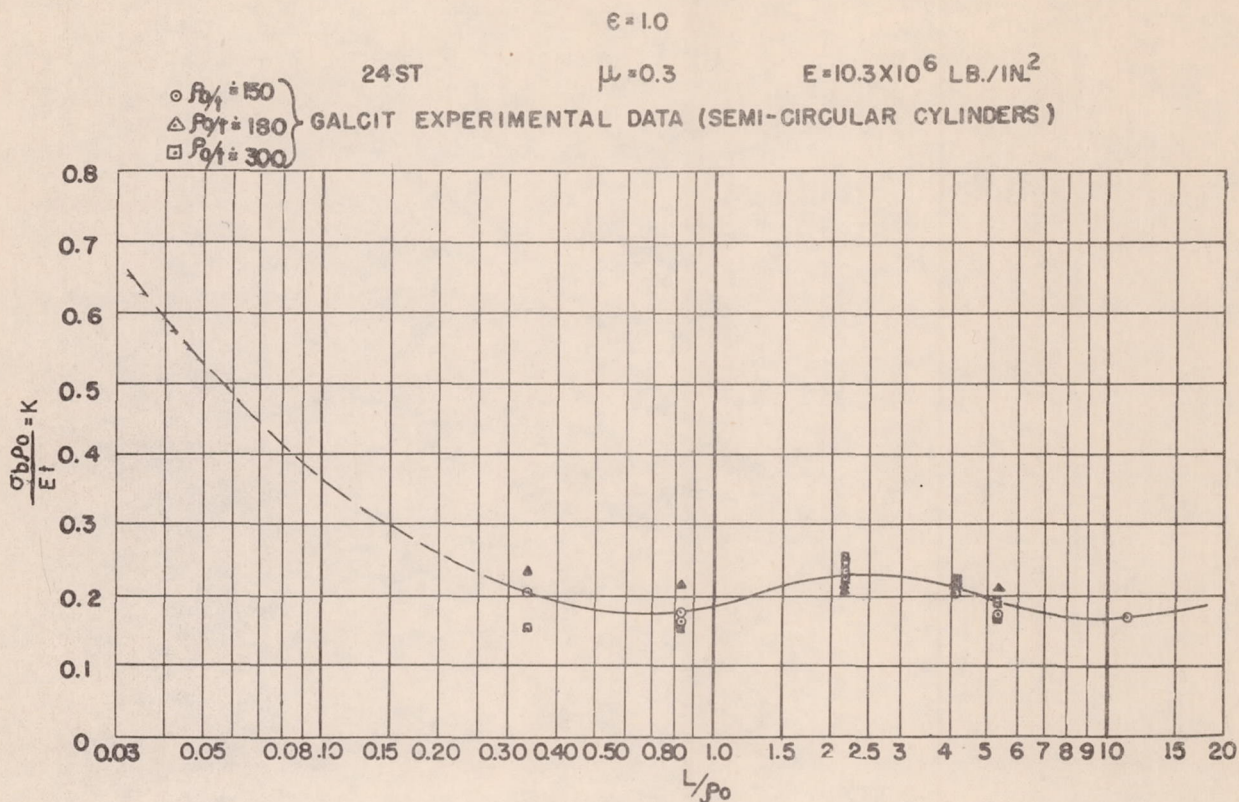


Figure 16.- Design curve of buckling (and ultimate) strength of semi-circular cylinders under pure bending.

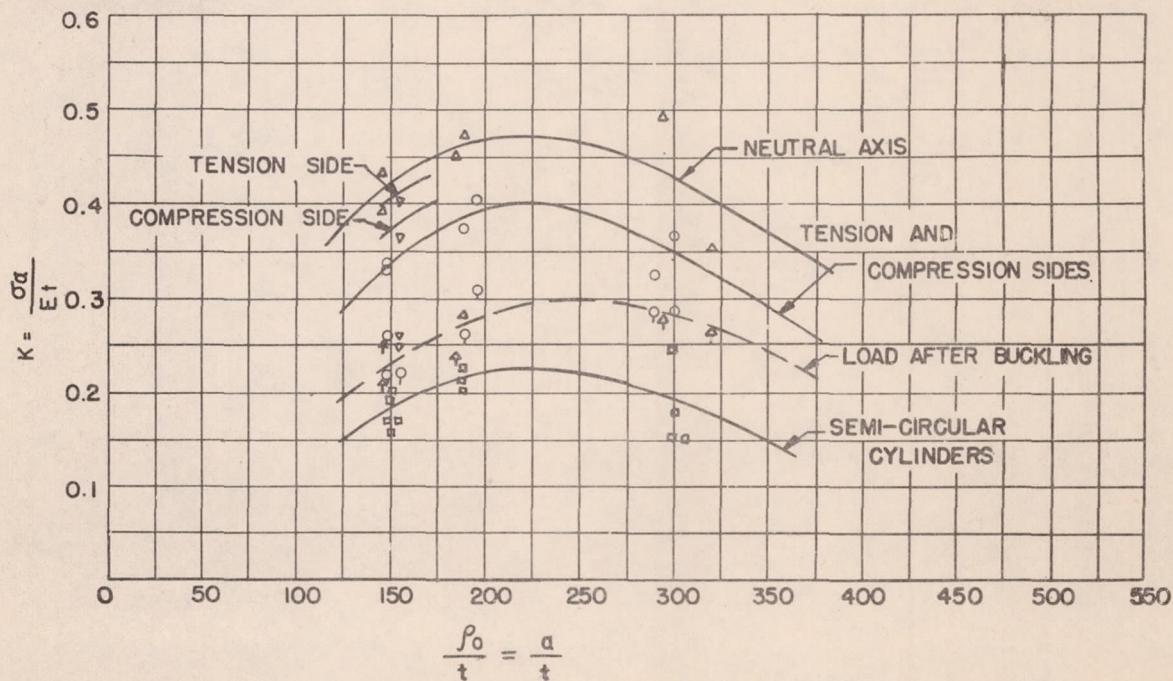


Figure 17.- Effect of seams on buckling strength of circular cylinders.

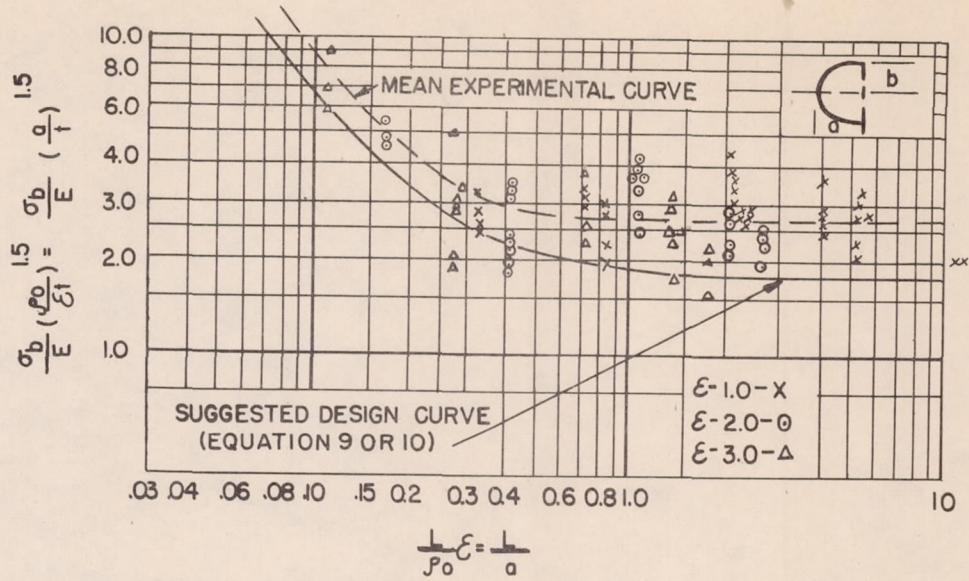


Figure 18.- Bending strength of semi-elliptical and semi-circular cylinders.

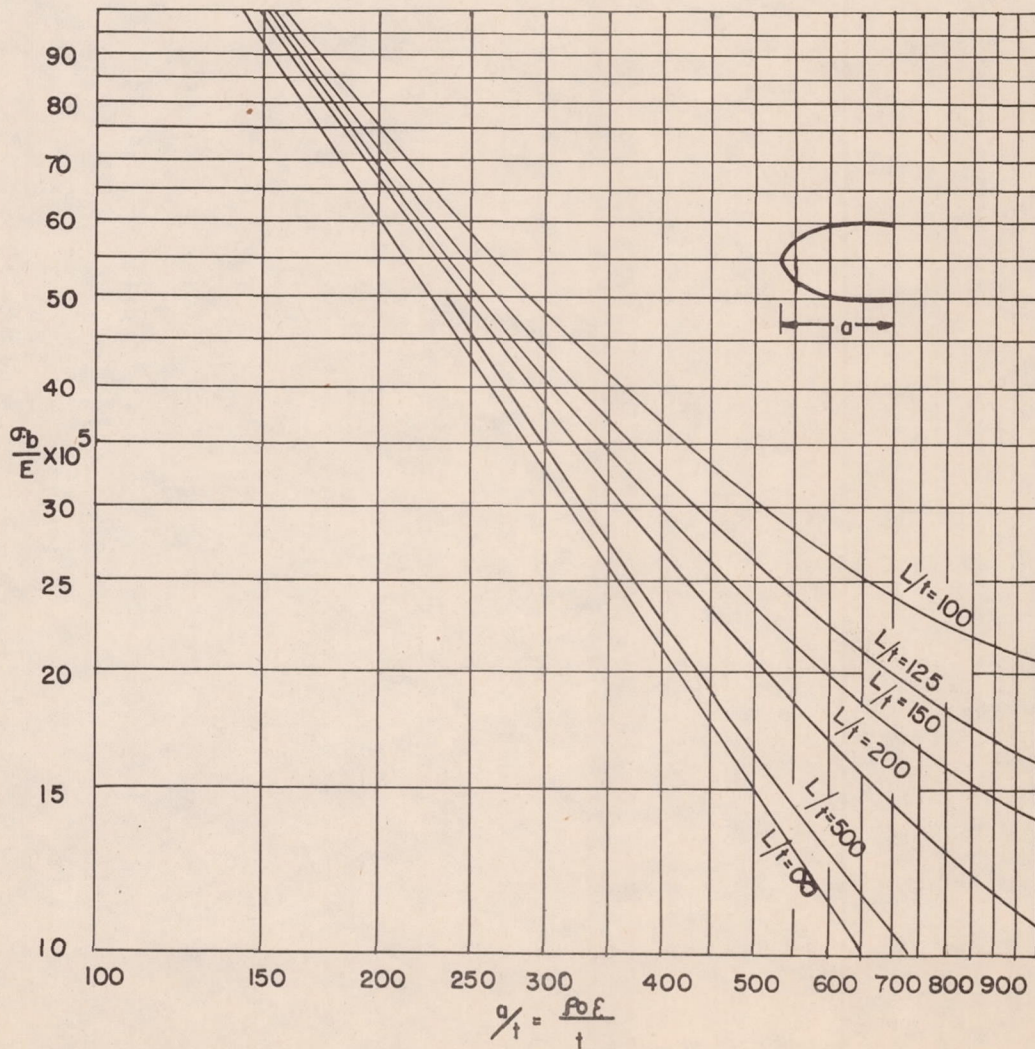


Figure 19.- Buckling stress for semi-elliptical cylinders under pure bending.

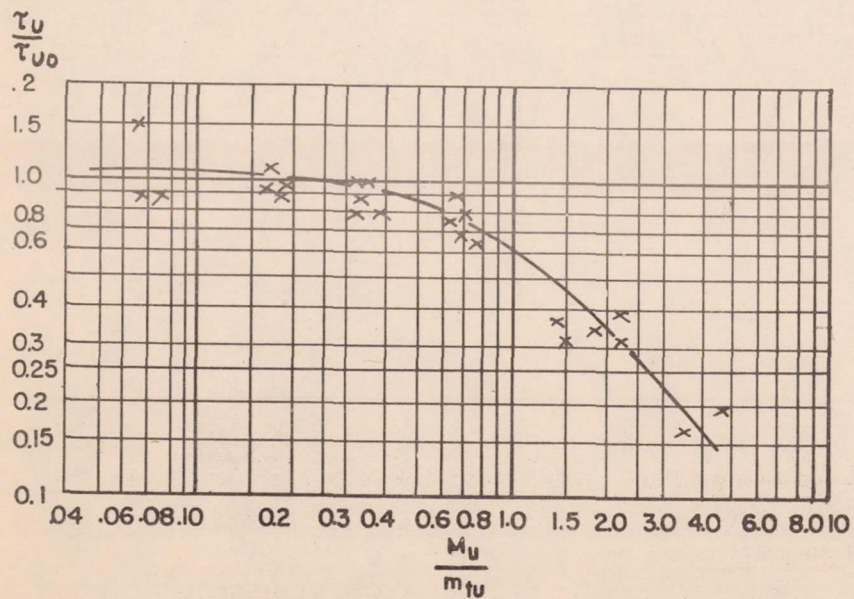
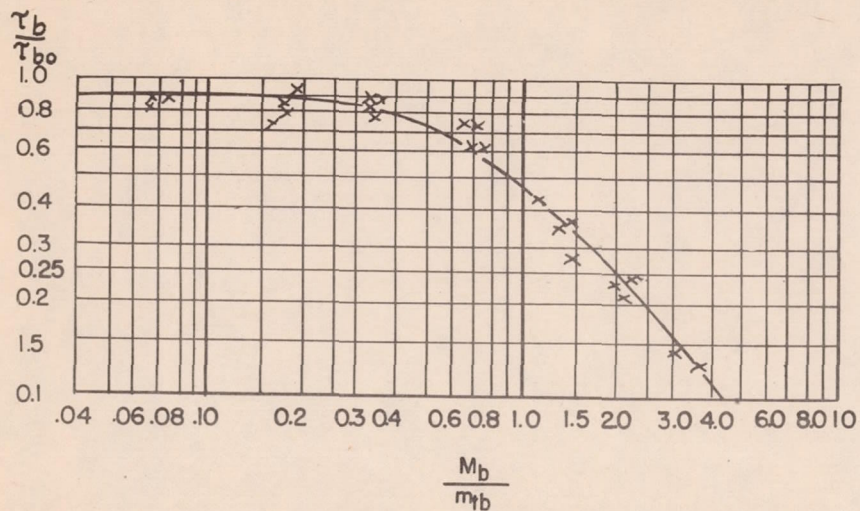


Figure 20.- Torsional stresses in semi-circular cylinders loaded in bending plus torsion for  $\epsilon = 1.0$ .

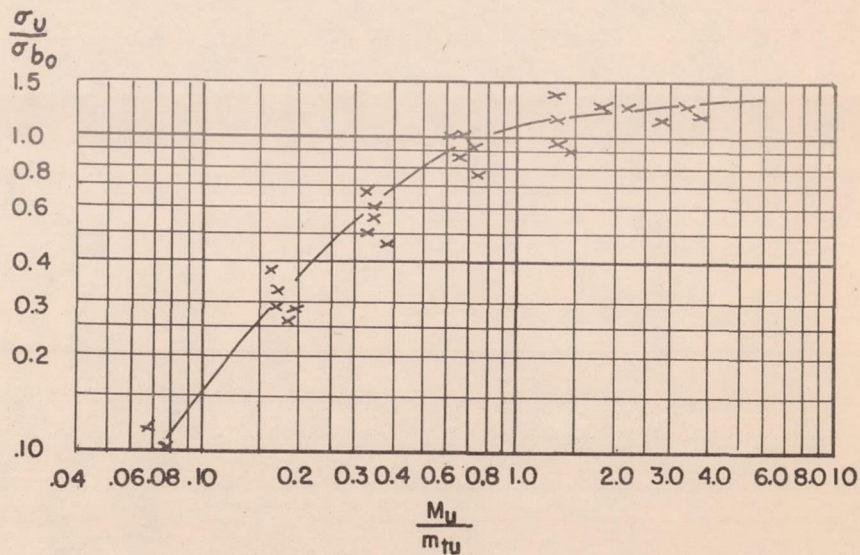
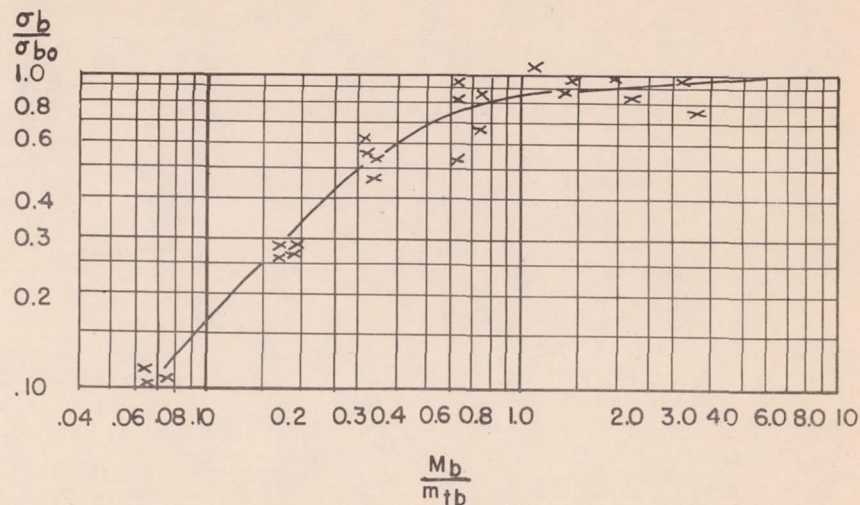


Figure 21.- Bending stresses in semi-circular cylinders loaded in bending plus torsion for  $\epsilon = 1.0$ .

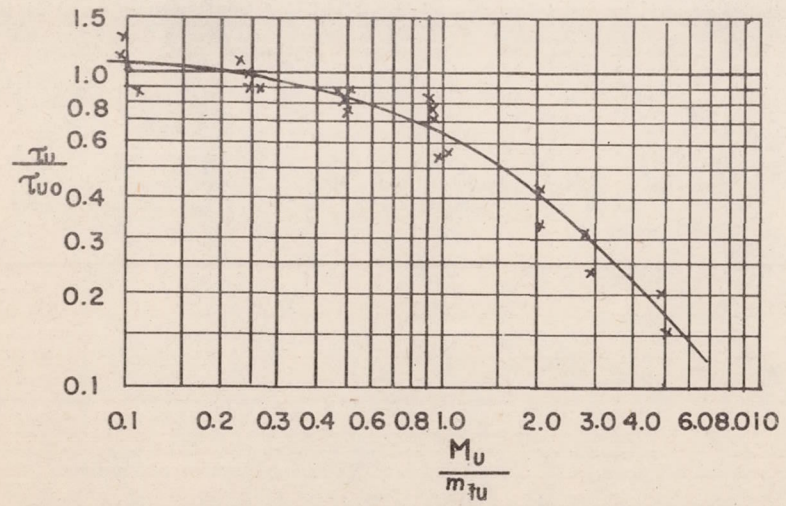
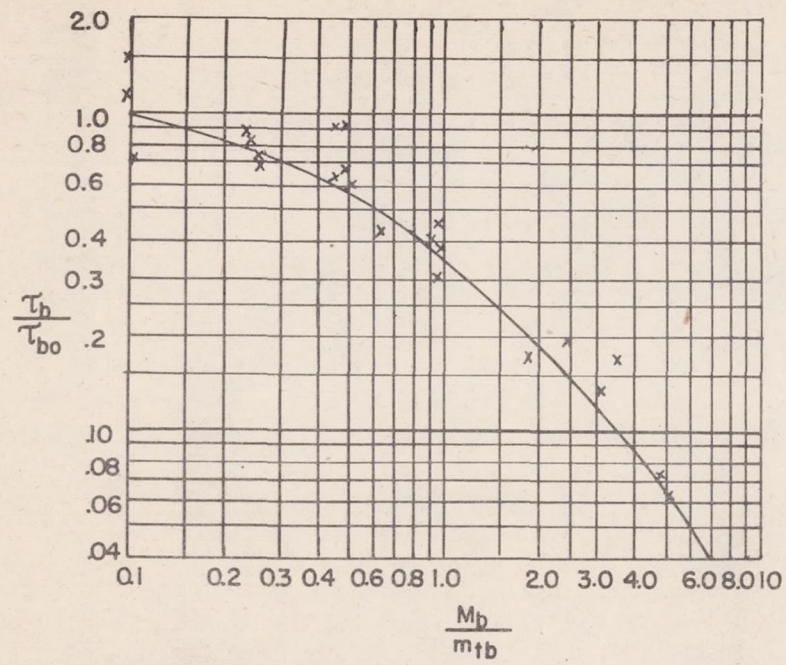


Figure 22.- Torsional stresses in semi-elliptical cylinders loaded in bending plus torsion for  $\epsilon = 2.0$ .

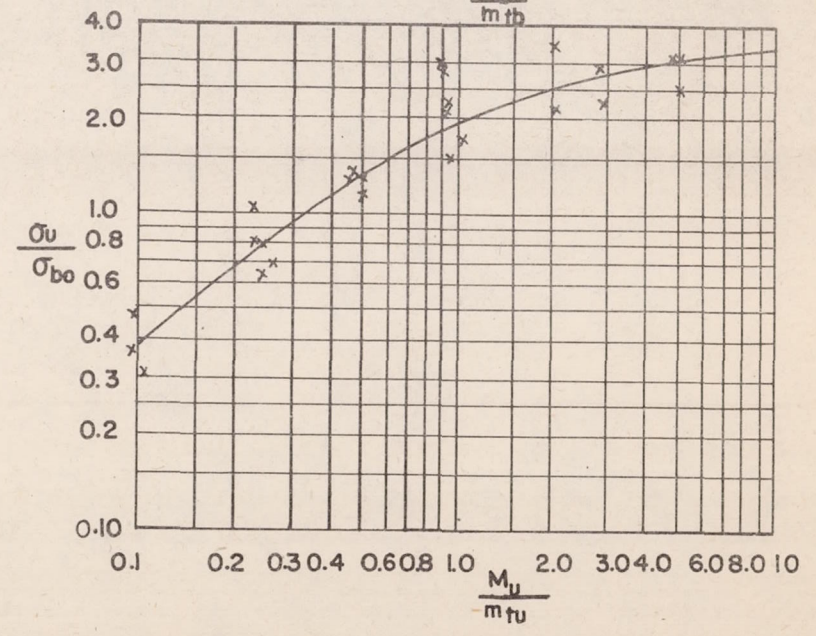
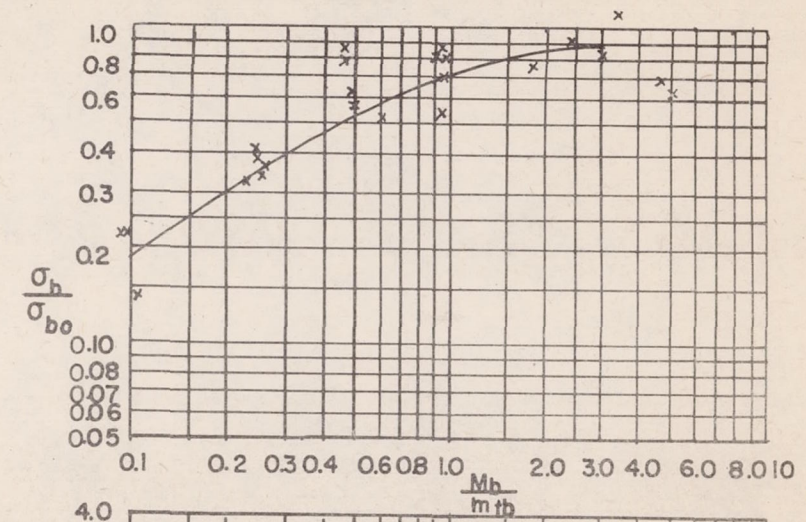


Figure 23.- Bending stresses in semi-elliptical cylinders loaded in bending plus torsion for  $\epsilon = 2.0$ .

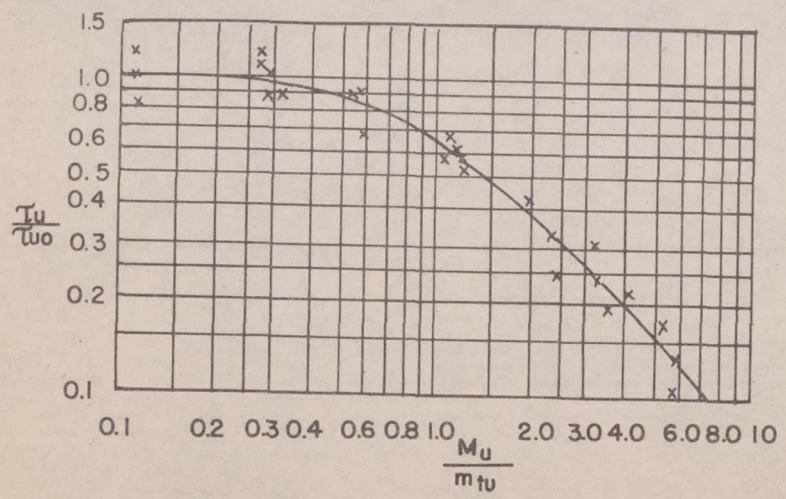
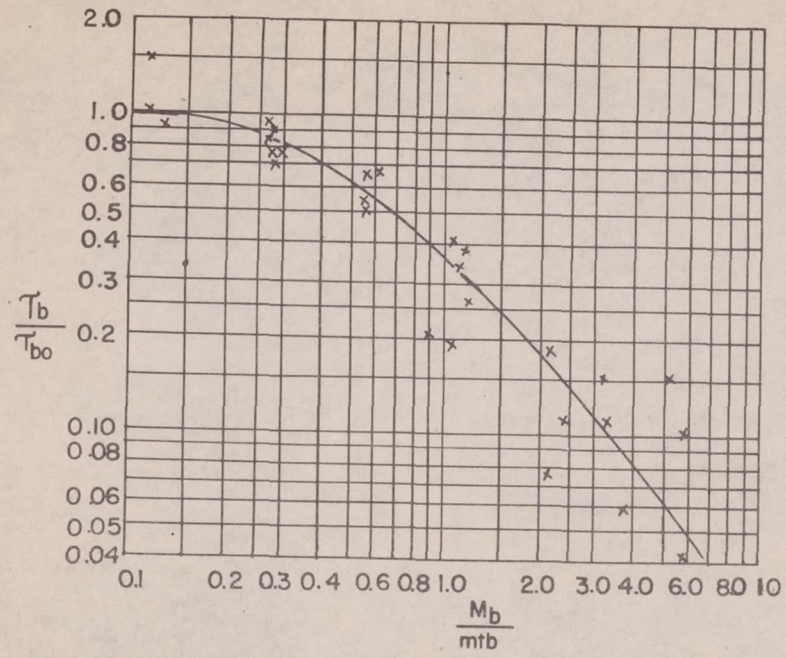


Figure 24.- Torsional stresses in semi-elliptical cylinders loaded in bending plus torsion for  $\epsilon = 3.0$ .

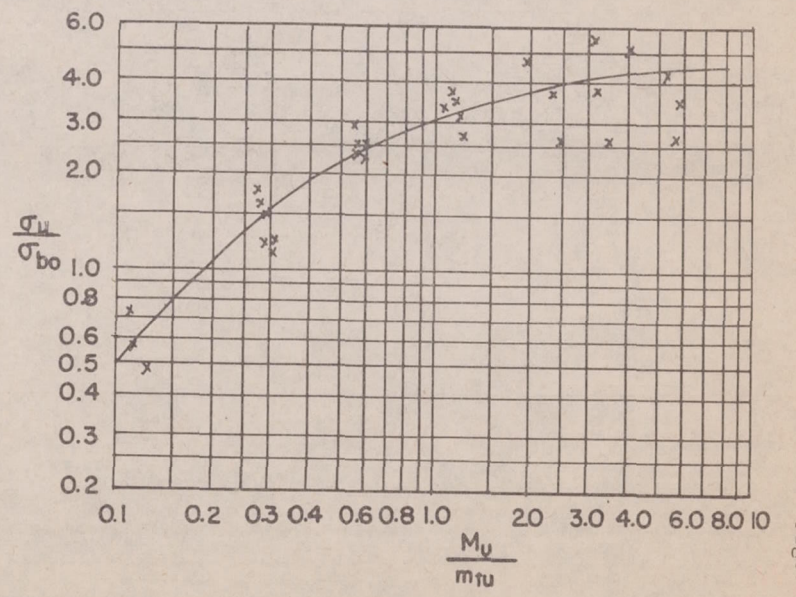
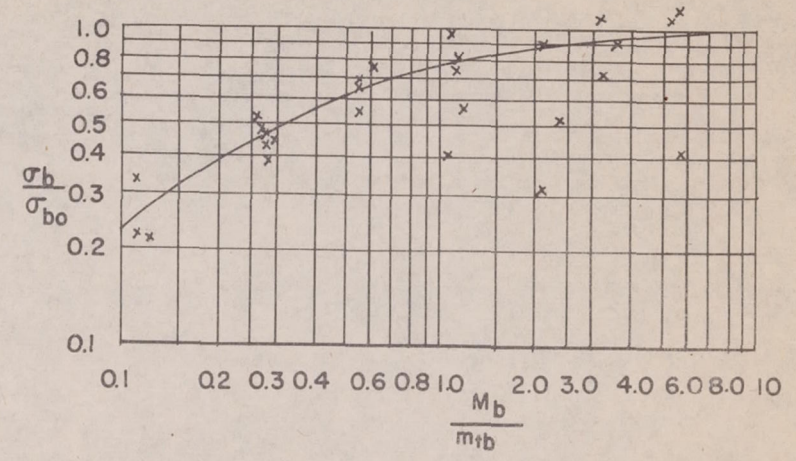


Figure 25.- Bending stresses in semi-circular cylinders loaded in bending plus torsion for  $\epsilon = 3.0$ .

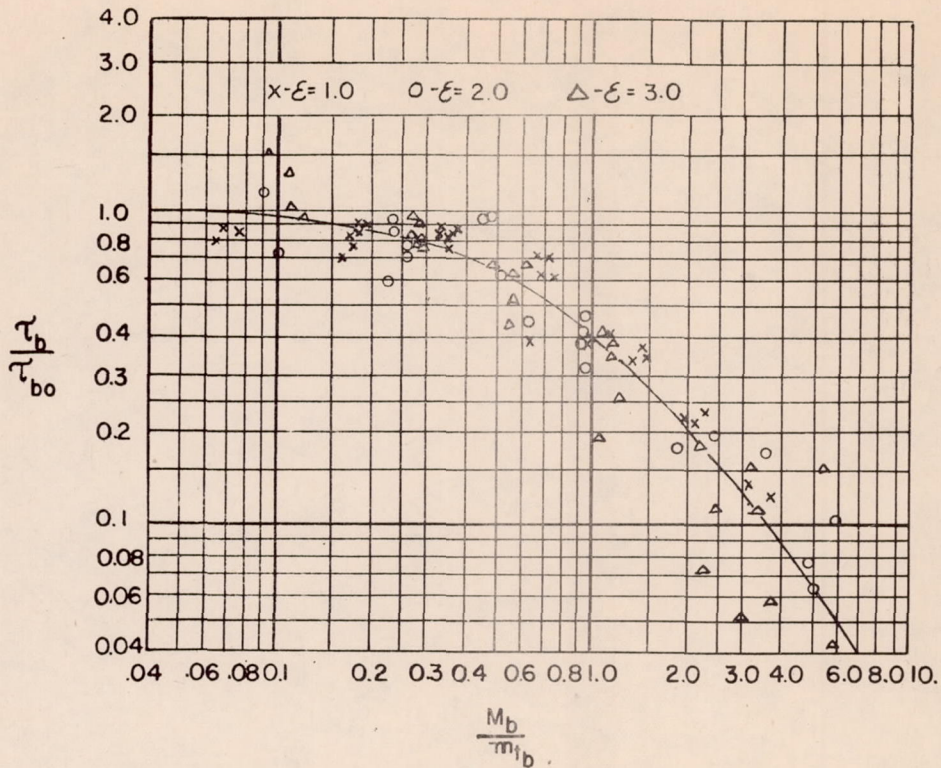


Figure 26.- Torsional buckling stress in semi-elliptical cylinders loaded in bending plus torsion.

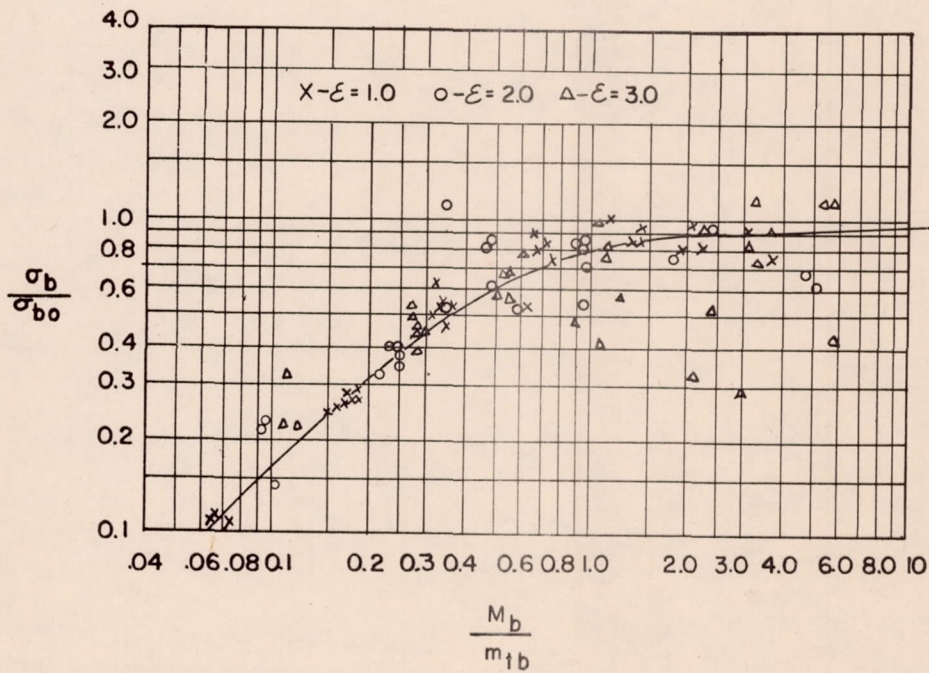


Figure 27.- Compression buckling stress in semi-elliptical cylinders loaded in bending plus torsion.

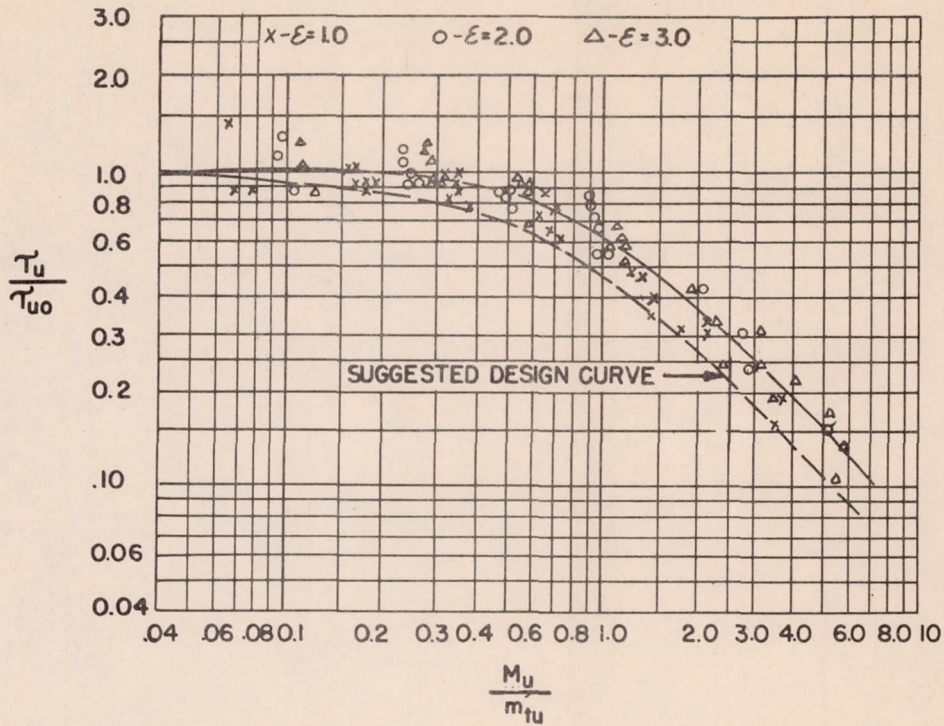


Figure 28.- Ultimate torsional stress in semi-elliptical cylinders loaded in bending plus torsion.

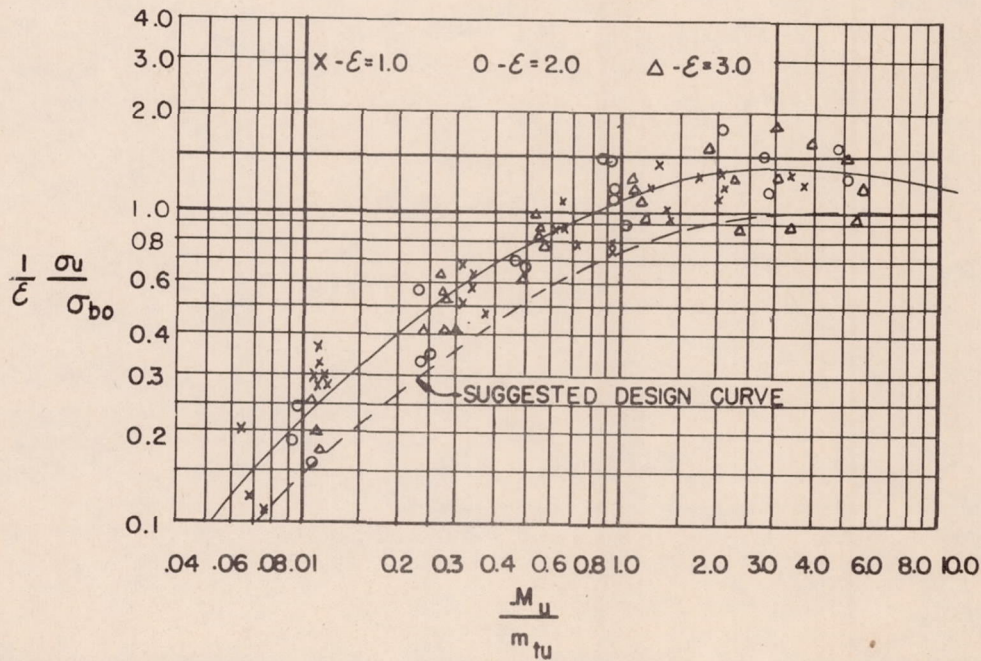


Figure 29.- Ultimate compression stress in semi-elliptical cylinders loaded in bending plus torsion.

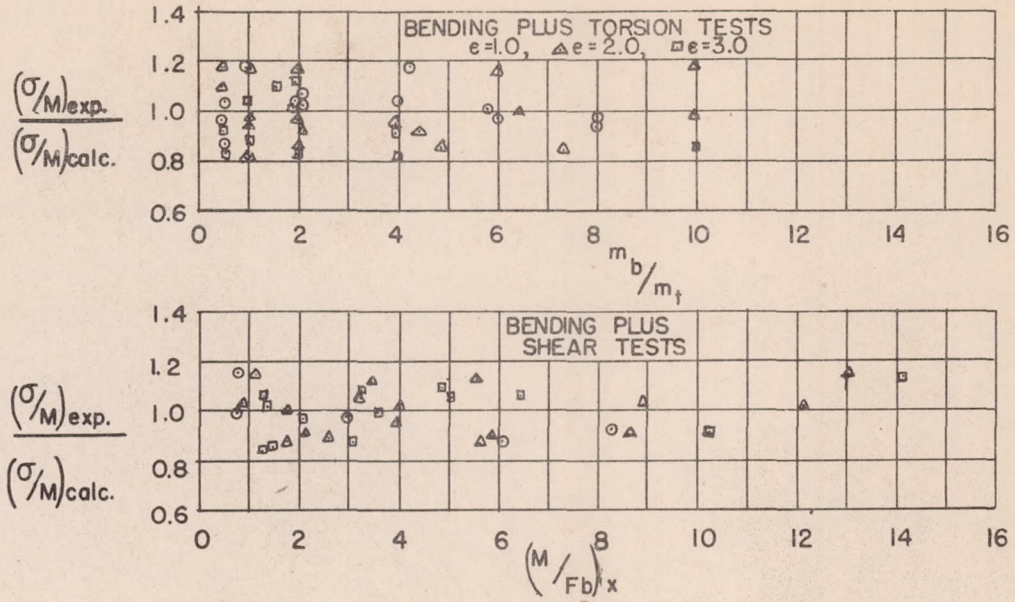


Figure 30.- Comparison of experimental and calculated bending stresses for combined loading conditions taken just below the buckling load.

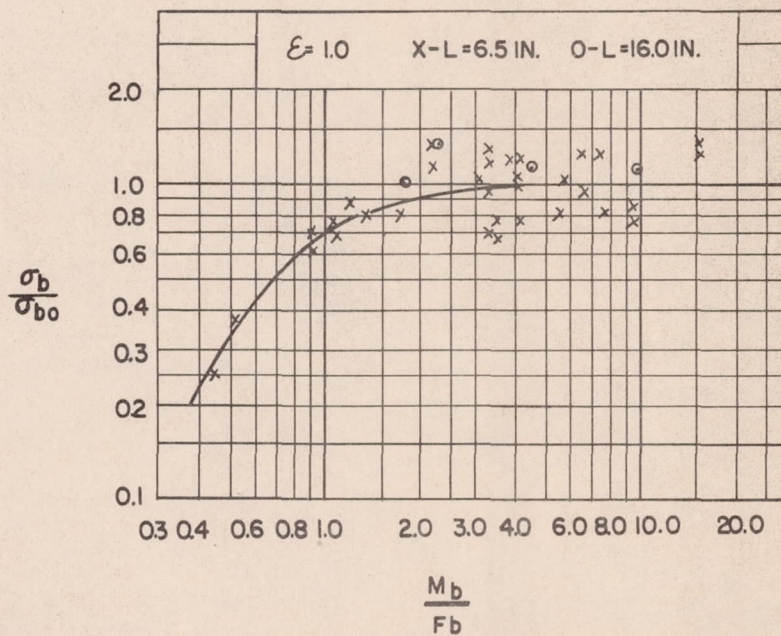


Figure 31.- Buckling stress in compression for bending plus shear tests.

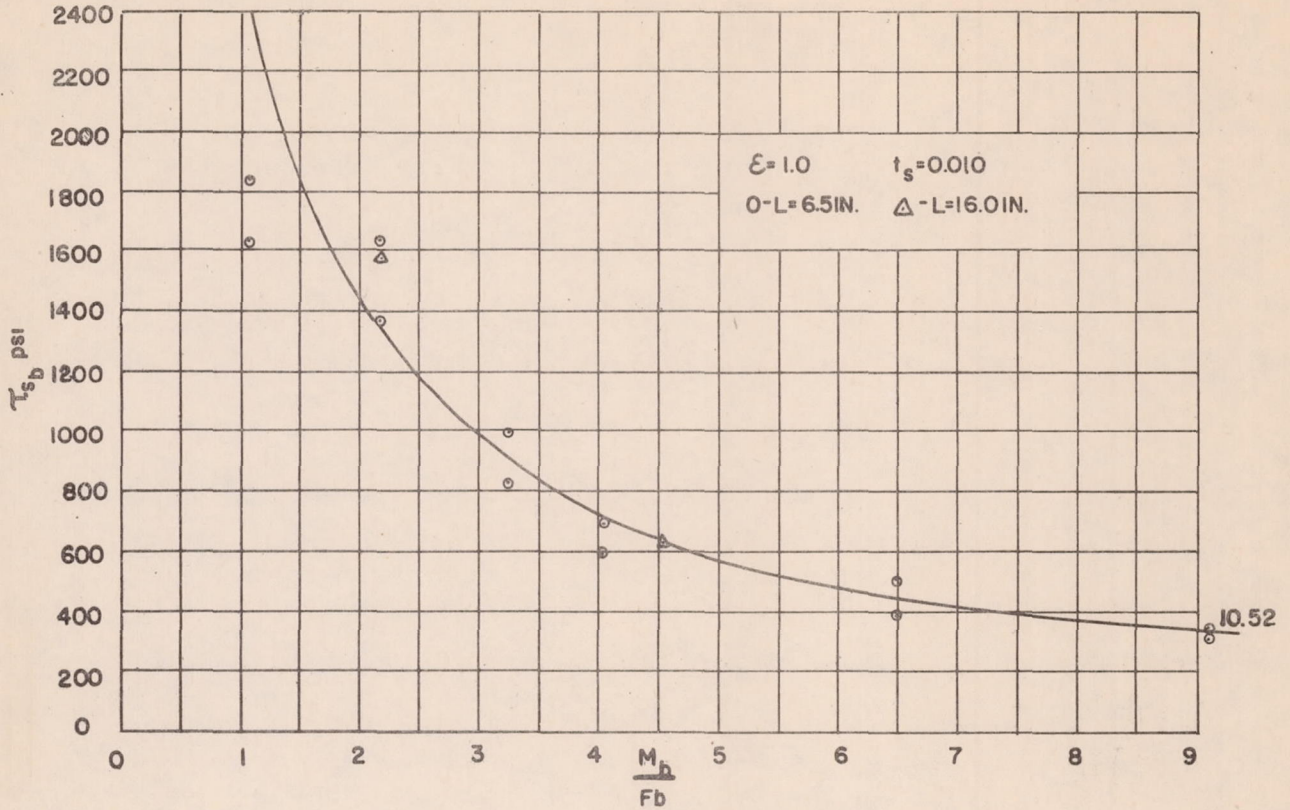


Figure 32.-  $\tau_{sb}$  for bending plus shear tests.

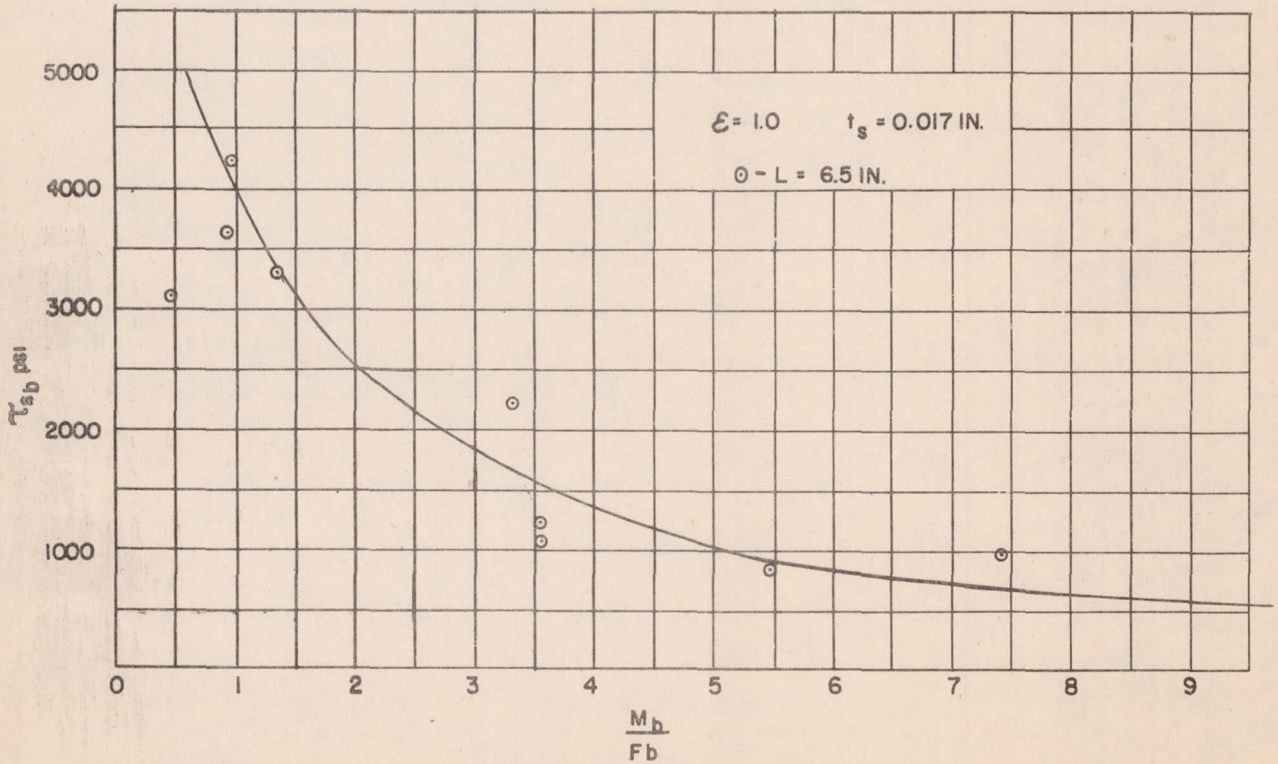
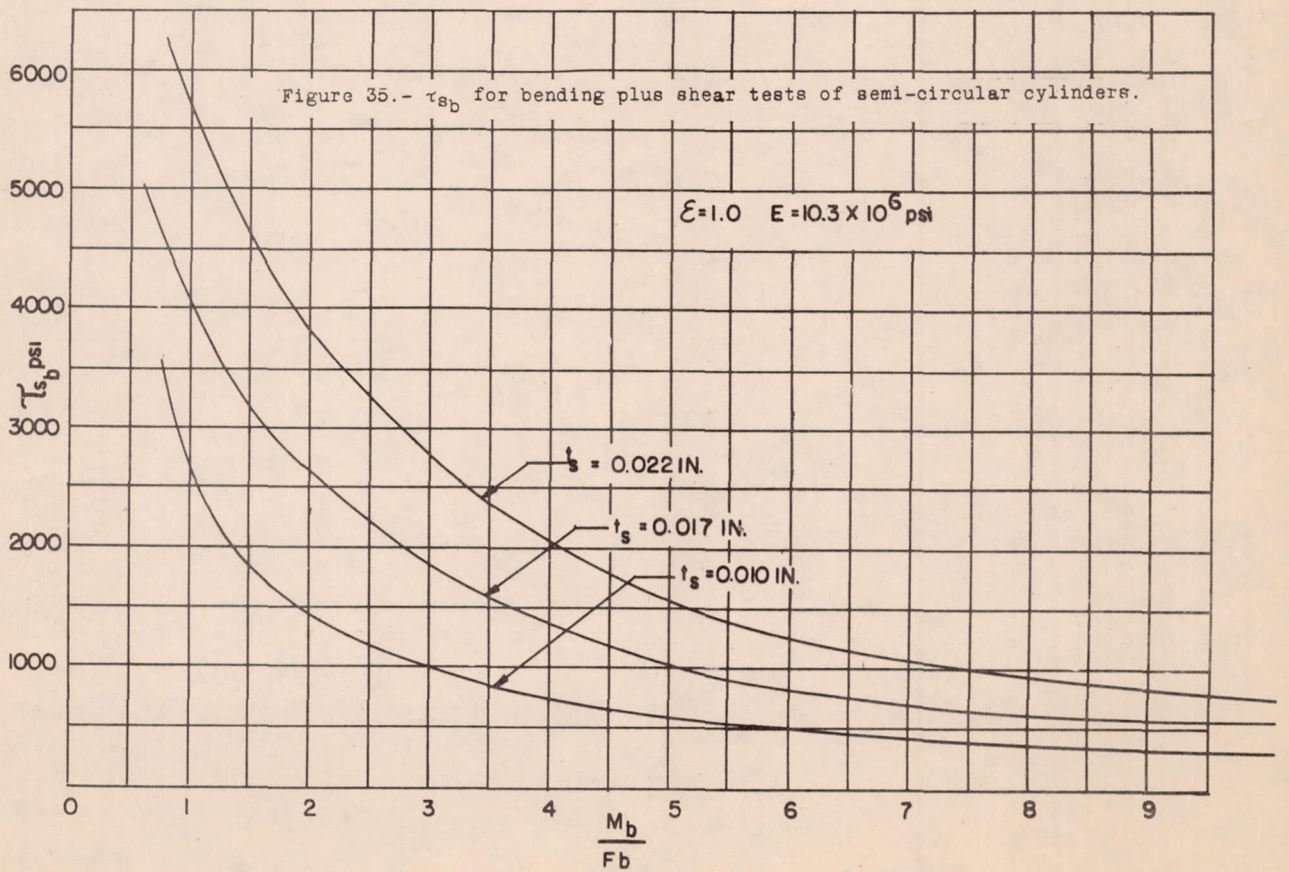
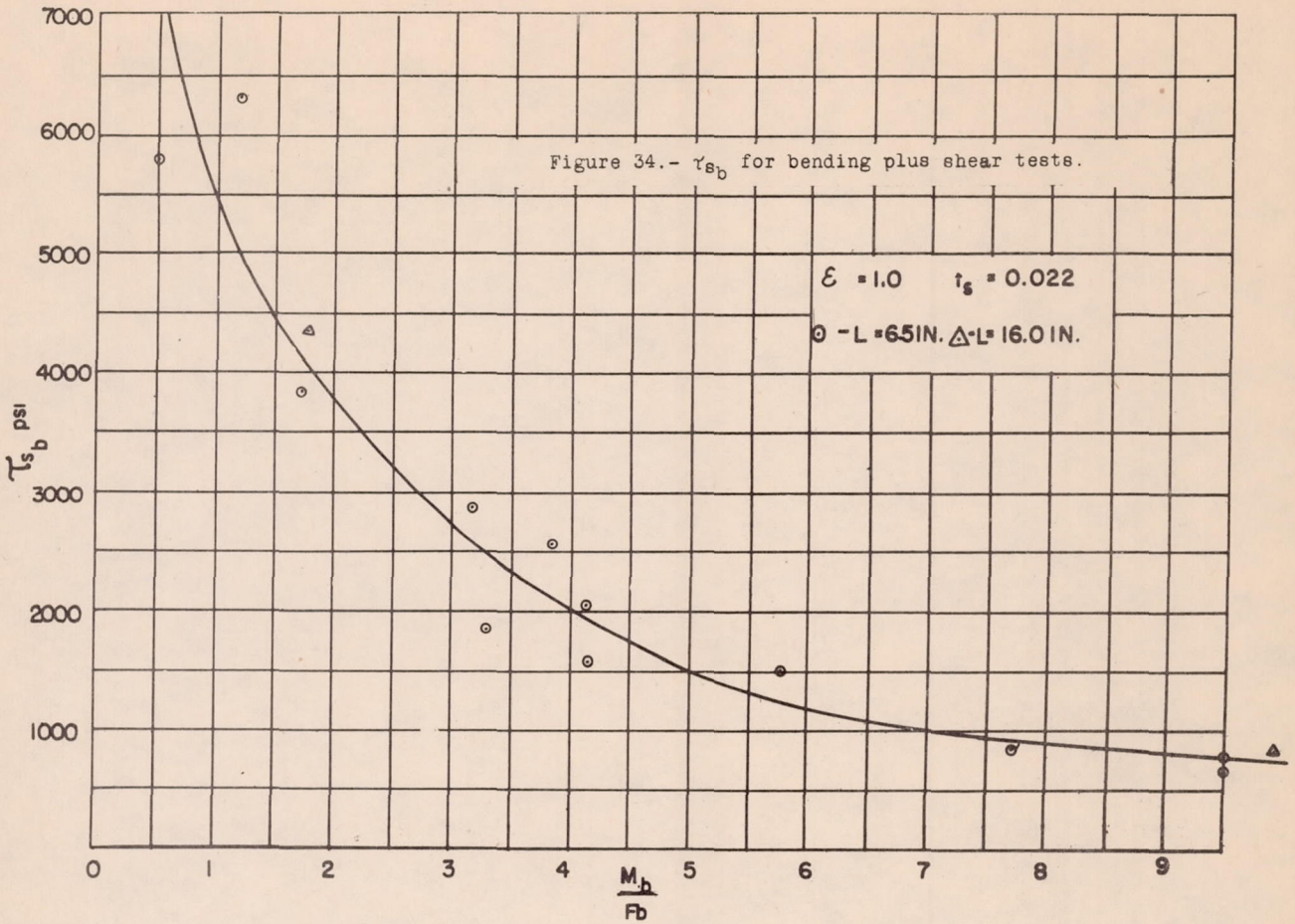


Figure 33 -  $\tau_{sb}$  for bending plus shear tests.



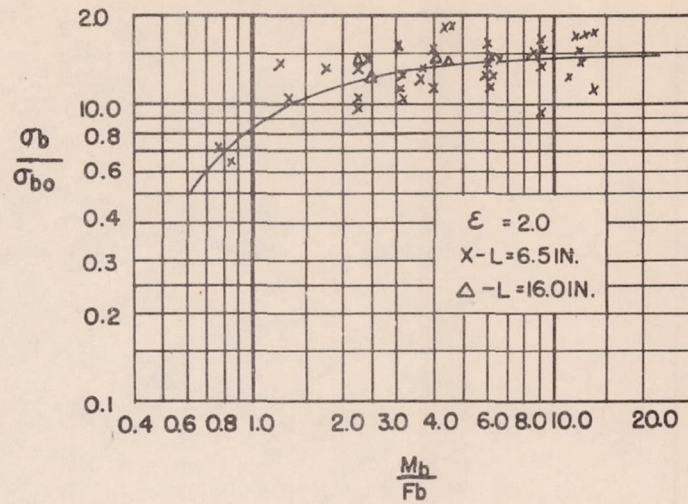


Figure 36.- Buckling stress in compression for bending plus shear tests.

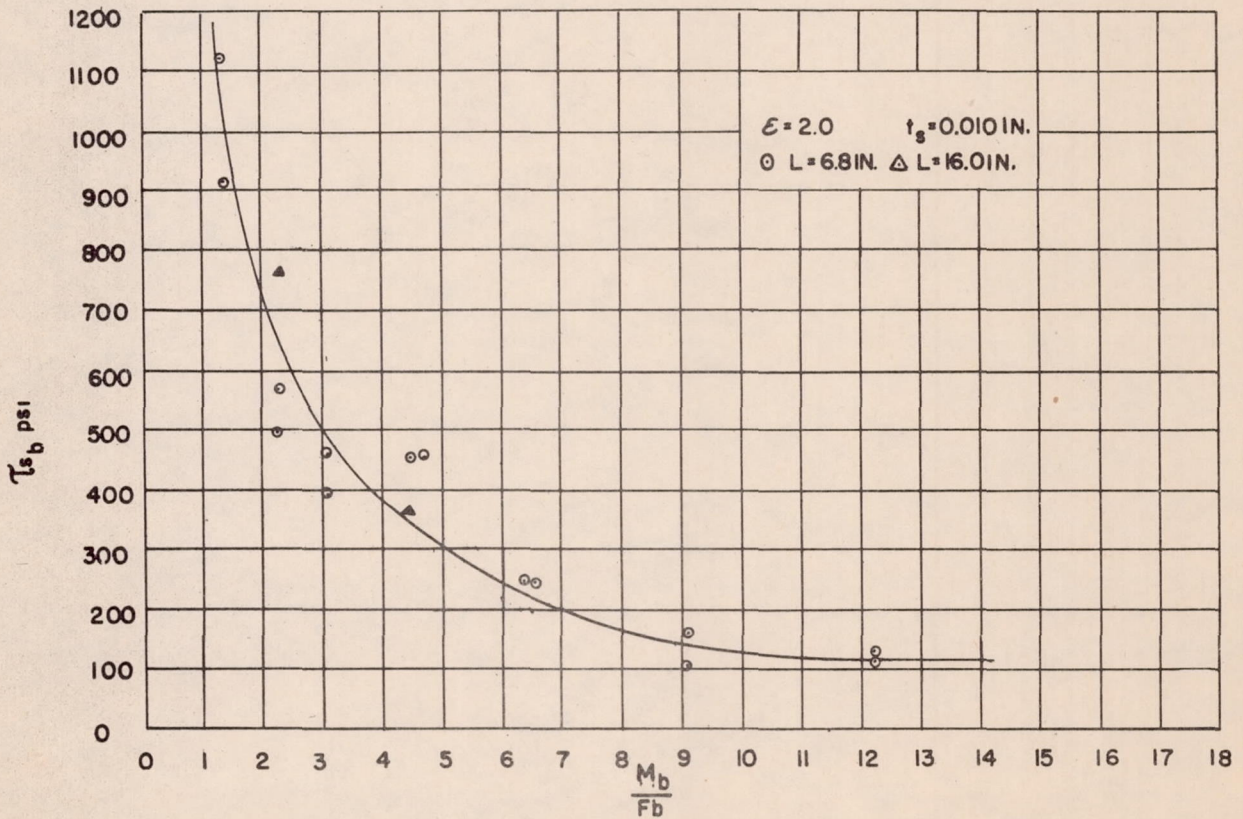
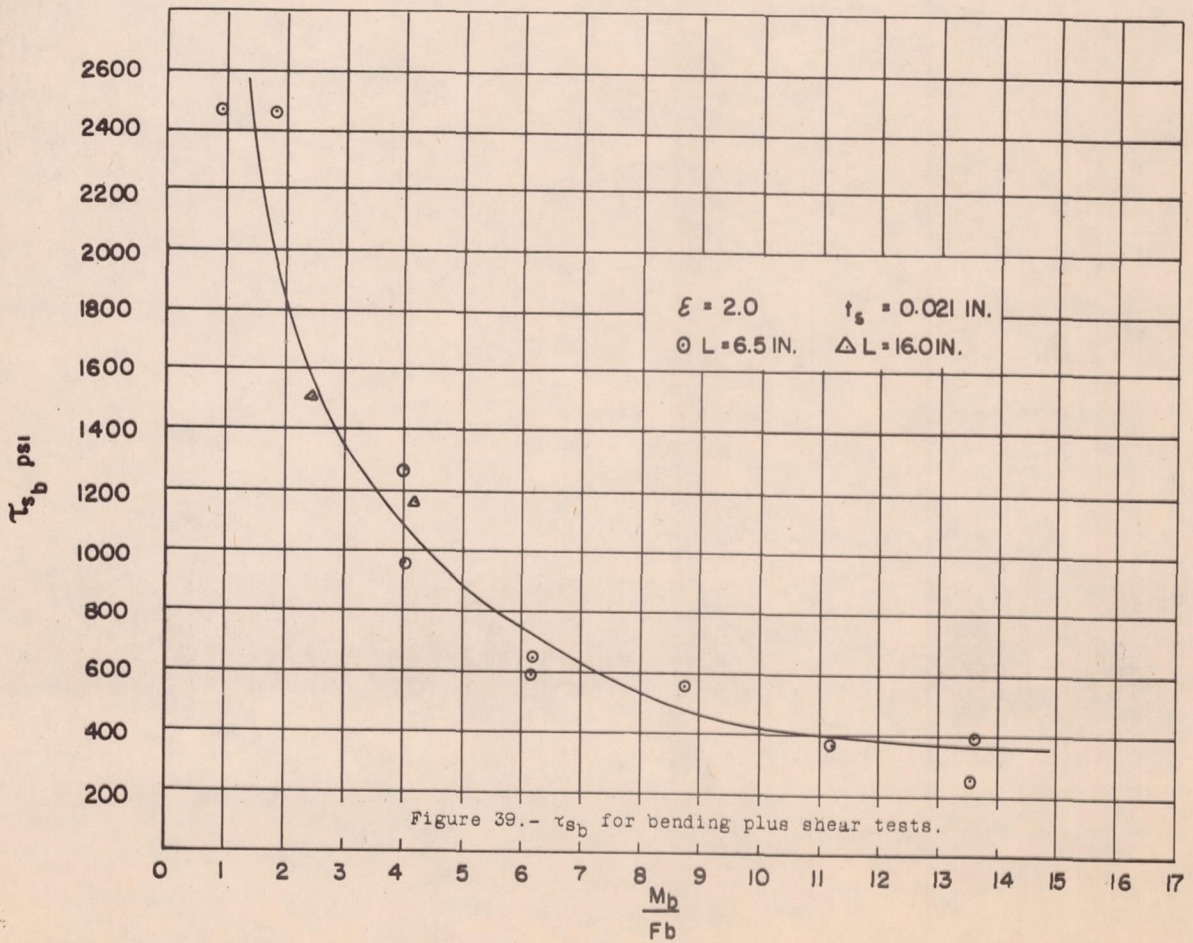
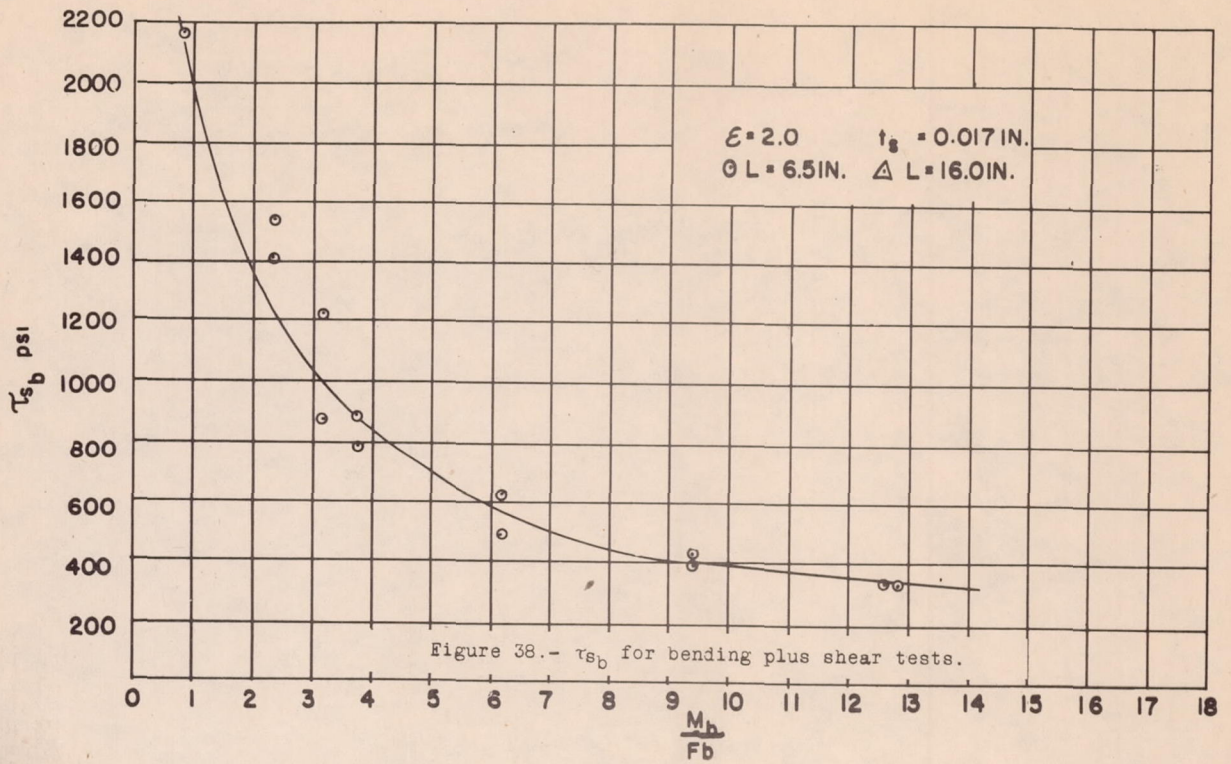


Figure 37.-  $\tau_{s_b}$  for bending plus shear tests.



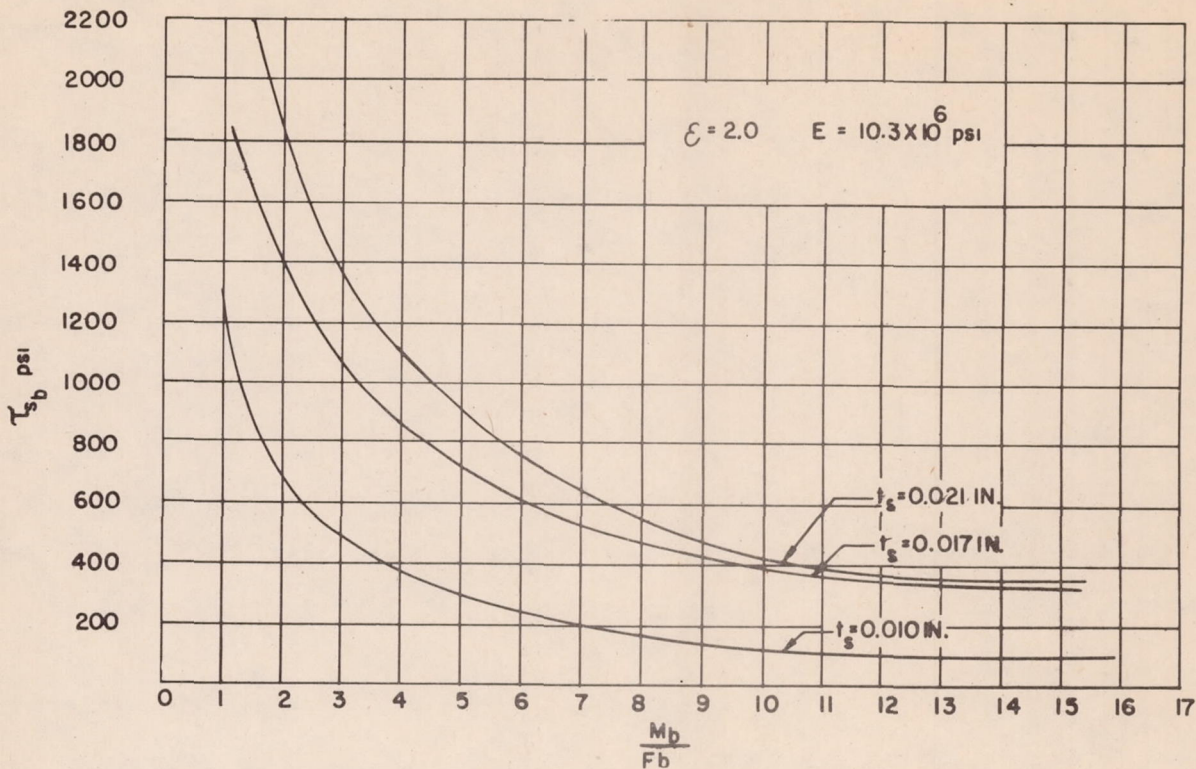


Figure 40.-  $\tau_{sb}$  for bending plus shear tests of semi-elliptical cylinders.

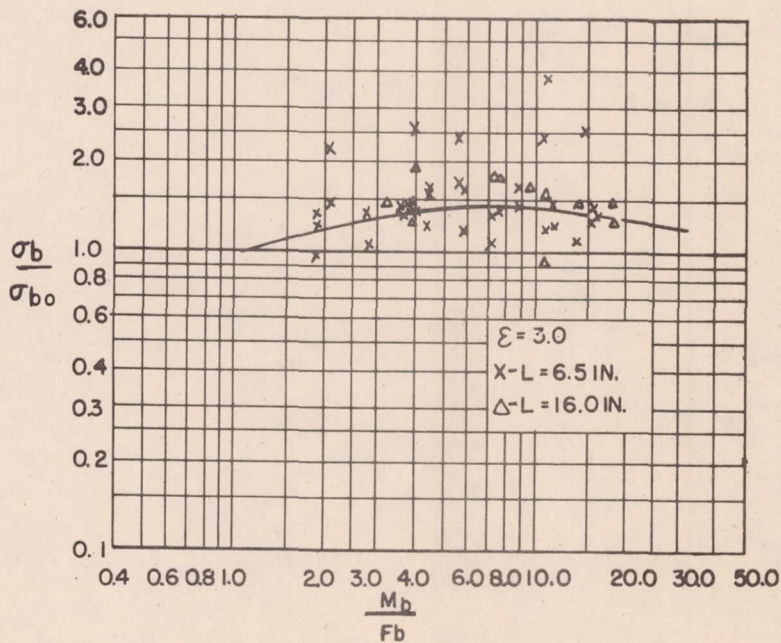


Figure 41.- Buckling stress in compression for bending plus shear tests.

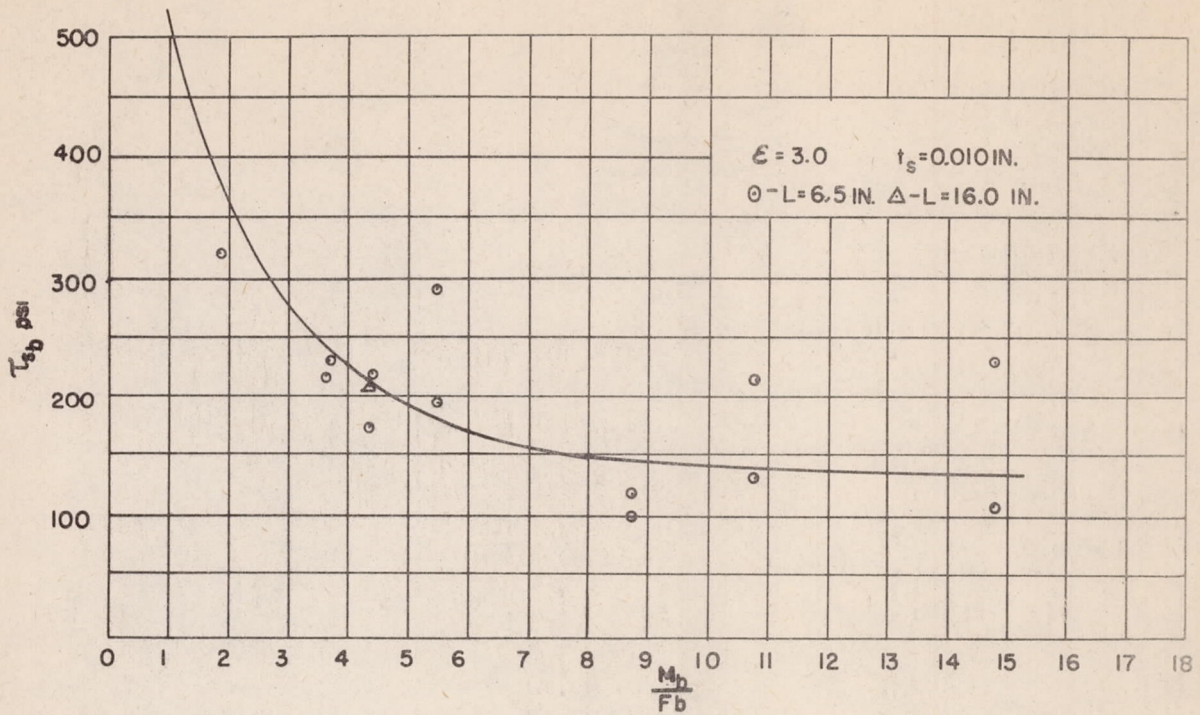


Figure 42.-  $\tau_{sb}$  for bending plus shear tests.

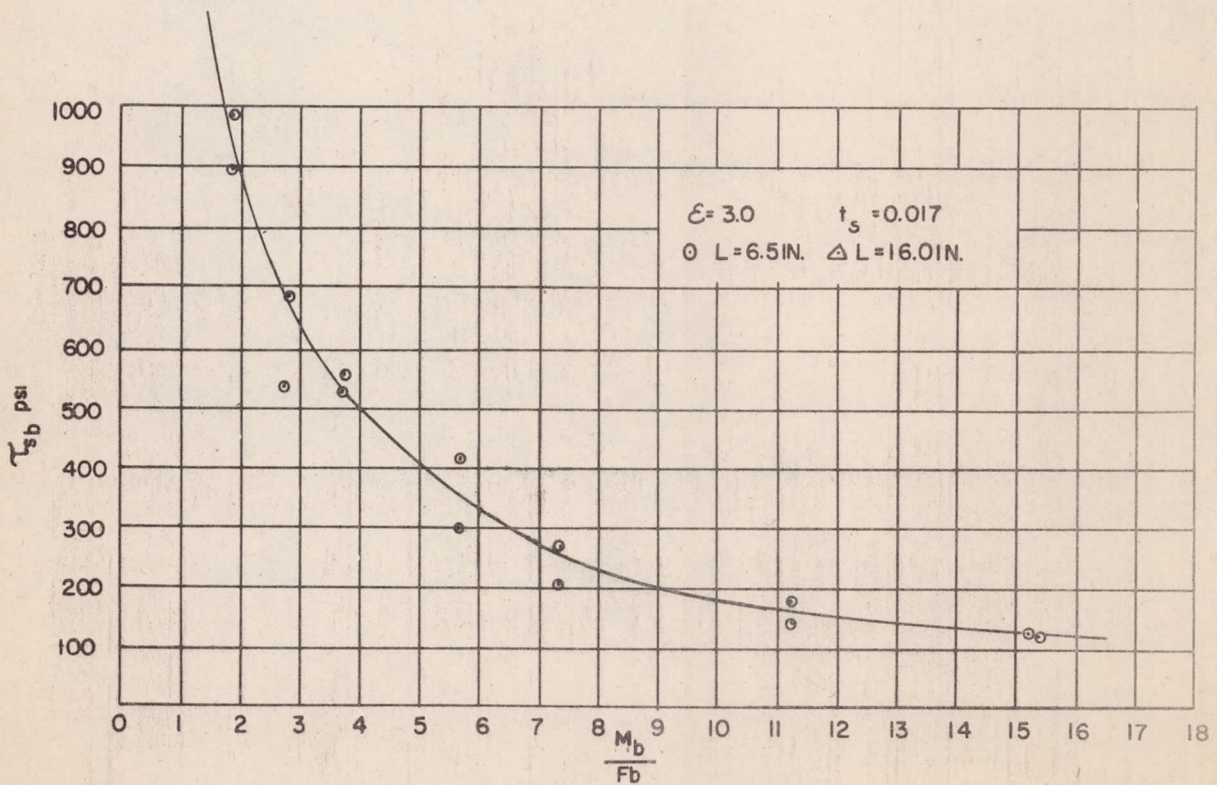


Figure 43.-  $\tau_{sb}$  for bending plus shear tests.

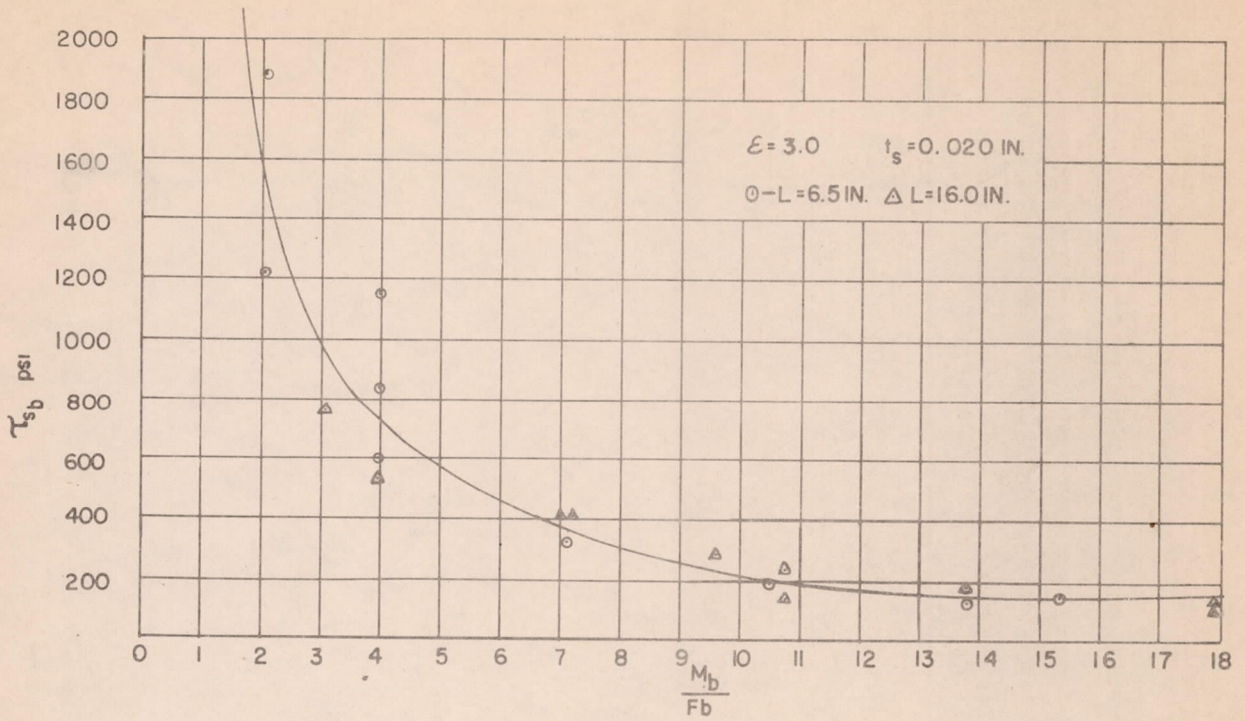


Figure 44 -  $\tau_{sb}$  for bending plus shear tests.

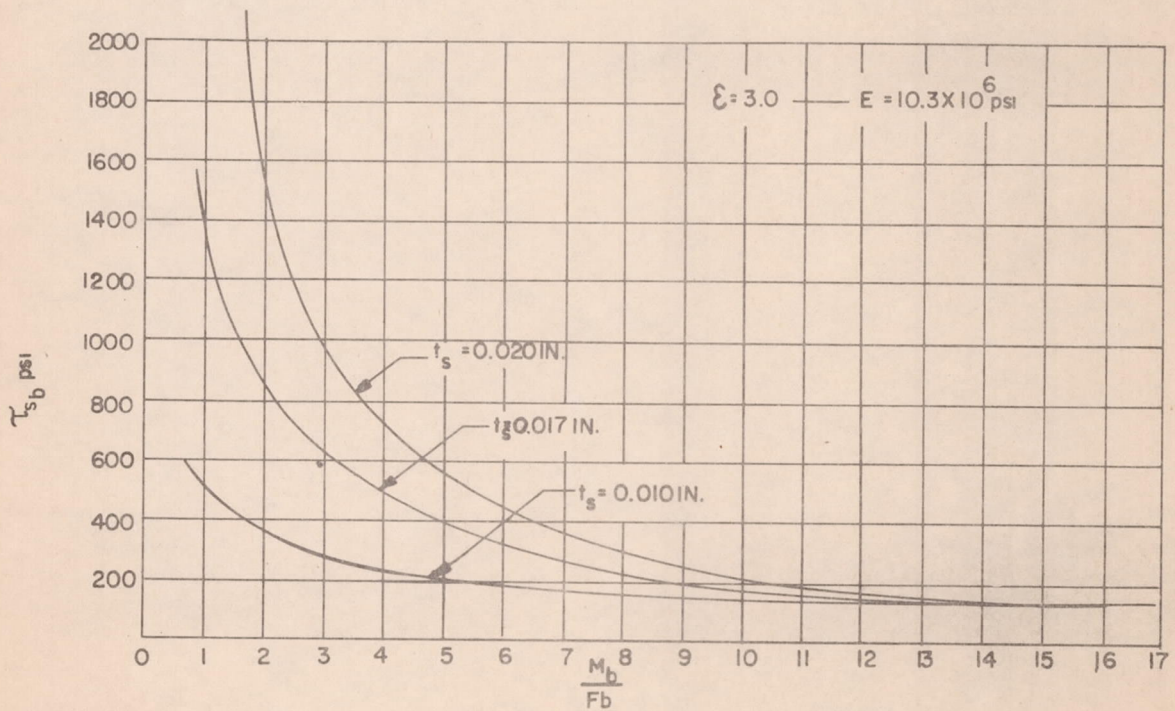


Figure 45.-  $\tau_{sb}$  for bending plus shear tests of semi-elliptical cylinders.